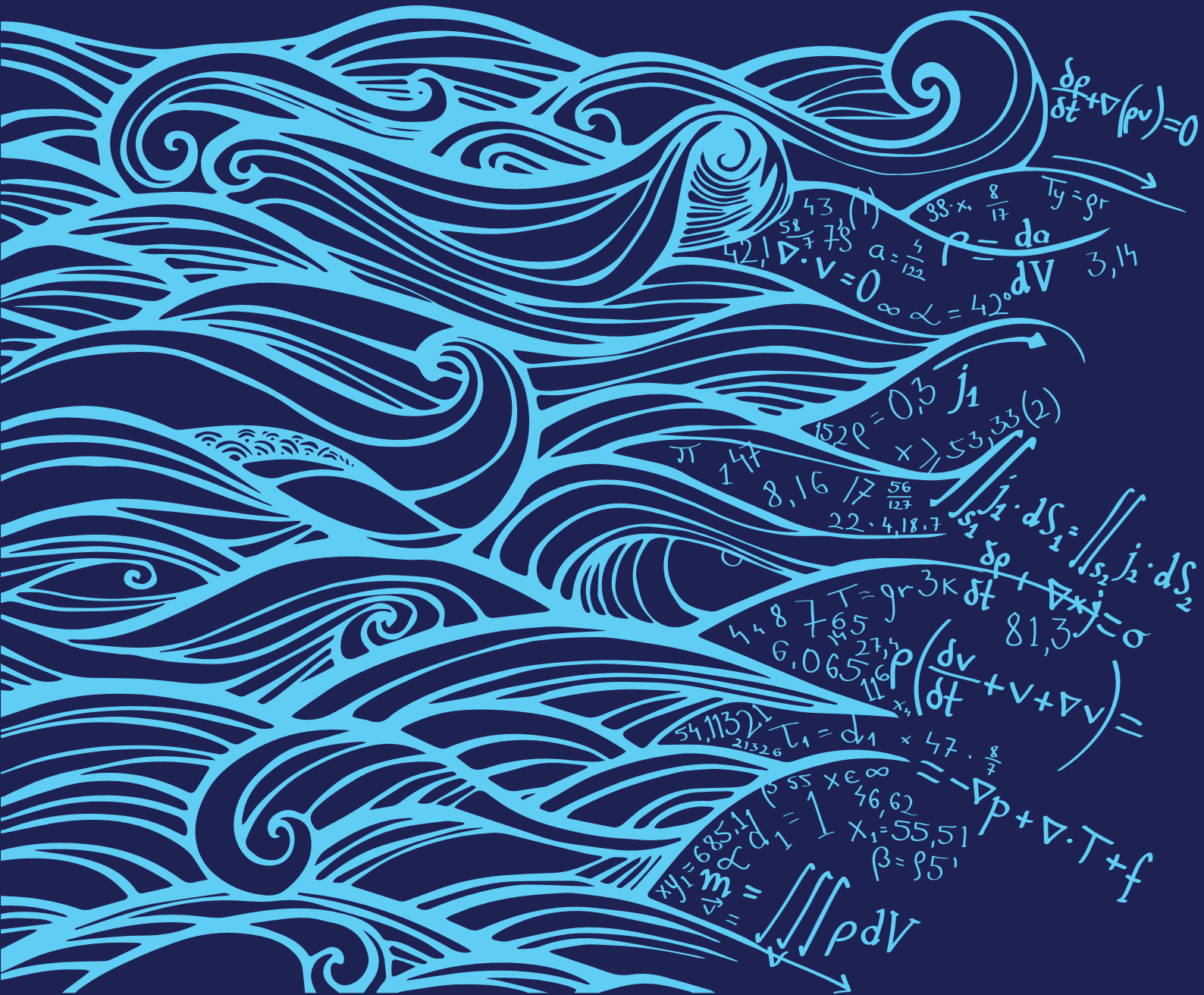


Application of numerical models and codes





Best practice report

Application of numerical models and codes

Task 3.4.4 of WP3 from the MERiFIC Project

**A report prepared as part of the MERiFIC Project
"Marine Energy in Far Peripheral and Island Communities"**

February 2014

Written by

Thomas Vyzikas (thomas.vyzikas@plymouth.ac.uk), University of Plymouth

With contributions from

Deborah Greaves (deborah.greaves@plymouth.ac.uk), University of Plymouth

Dave Simmonds (D.Simmonds@plymouth.ac.uk), University of Plymouth

Christophe Maisondieu (Christophe.Maisondieu@ifremer.fr), Ifremer

Helen Smith (H.C.M.Smith@exeter.ac.uk), University of Exeter

Lisa Radford, (Lisa.Radford@babcockinternational.com)



MERiFIC was selected under the European Cross-Border Cooperation Programme INTERREG IV A France (Channel) – England, co-funded by the ERDF.

The sole responsibility for the content of this report lies with the authors. It does not represent the opinion of the European Communities. The European Commission is not responsible for any use that may be made of the information contained therein.

The present report is intended for academic purposes only. It describes some of the numerical models for marine and ocean applications to the authors' best knowledge on the date of its publication. The authors thus bear no responsibility for any inaccuracies or omissions regarding the description of the models.

© University of Plymouth, February 2014

Contents

Introduction.....	9
<i>The MERiFIC Project.....</i>	<i>9</i>
<i>This report</i>	<i>9</i>
<i>Structure of the report.....</i>	<i>10</i>
<i>Scope of the report.....</i>	<i>11</i>
1. The Modelling Process	12
1.1 <i>Introduction to modelling</i>	<i>12</i>
1.2 <i>Physical and Numerical modelling</i>	<i>12</i>
1.2.1 <i>SWOT analysis of physical models</i>	<i>12</i>
1.2.1.1 <i>Strengths of physical models.....</i>	<i>12</i>
1.2.1.2 <i>Weaknesses of physical models</i>	<i>13</i>
1.2.1.3 <i>Opportunities for physical models</i>	<i>13</i>
1.2.1.4 <i>Threats to physical models.....</i>	<i>14</i>
1.2.2 <i>SWOT analysis of numerical models</i>	<i>14</i>
1.2.2.1 <i>Strengths of numerical models.....</i>	<i>14</i>
1.2.2.2 <i>Weaknesses of numerical models.....</i>	<i>15</i>
1.2.2.3 <i>Opportunities for numerical models.....</i>	<i>15</i>
1.2.2.4 <i>Threats to numerical models</i>	<i>15</i>
1.2.3 <i>Summary of SWOT analysis</i>	<i>16</i>
2. Fundamentals of Fluid Mechanics.....	17
2.1 <i>Governing equations of the fluid flow</i>	<i>17</i>
2.1.1 <i>Mass conservation in three dimensions</i>	<i>18</i>
2.1.2 <i>Momentum equation in three dimensions</i>	<i>19</i>
2.1.3 <i>Energy equation in three dimensions</i>	<i>22</i>
2.2 <i>Equation of state.....</i>	<i>24</i>
2.3 <i>Navier-Stokes equations</i>	<i>25</i>
2.4 <i>Summary of governing equations of fluid motion</i>	<i>28</i>
2.5 <i>Turbulence and its modelling.....</i>	<i>28</i>
2.5.1 <i>Introduction to turbulence</i>	<i>28</i>
2.5.2 <i>Characteristics of turbulence</i>	<i>30</i>
2.5.3 <i>Mathematical modelling of turbulence.....</i>	<i>30</i>
3. Fundamentals of Wave Mechanics.....	32
3.1 <i>Introduction.....</i>	<i>32</i>
3.2 <i>Characteristics of waves.....</i>	<i>33</i>
3.3 <i>Wave theories.....</i>	<i>34</i>
3.3.1 <i>Linear wave theory (Stokes 1st).....</i>	<i>34</i>
3.3.1.1 <i>The dispersion relationship.....</i>	<i>36</i>
3.3.1.2 <i>Deep water approximation.....</i>	<i>37</i>
3.3.1.3 <i>Shallow water approximation.....</i>	<i>37</i>
3.3.1.4 <i>Phase and group velocity</i>	<i>38</i>
3.3.1.5 <i>Wave energy.....</i>	<i>39</i>
3.3.2 <i>Nonlinear waves</i>	<i>41</i>

3.3.2.1	Introduction	41
3.3.2.2	Stokes theory of nonlinear waves.....	41
3.3.2.3	Stream function	42
3.3.2.4	Cnoidal and solitary wave theory.....	42
3.4	<i>Transformation of waves in near shore environment</i>	44
3.4.1	Shoaling.....	44
3.4.2	Refraction	44
3.4.3	Diffraction.....	45
3.4.4	Waves breaking in shallow water	46
3.4.5	Wave reflection.....	47
3.4.6	Wave-current interaction	48
3.5	<i>Wave-structure interaction</i>	49
3.5.1	Wave forces.....	49
3.5.2	From potential flow to Morison equation	49
3.5.3	Numerical methods for wave loading on large objects of arbitrary shapes.....	52
3.5.4	Spectral approach to wave force prediction	53
3.6	<i>Irregular waves</i>	53
3.6.1	Wind generated waves	53
3.6.2	Wave statistics.....	54
3.6.3	Wave spectrum.....	56
4.	Numerical Modelling	57
4.1	<i>Introduction</i>	57
4.2	<i>Pre-processing</i>	57
4.2.1	Definition of the problem.....	57
4.2.2	Boundary and initial conditions.....	58
4.2.3	Discretisation methods	58
4.2.3.1	Finite Difference Method	58
4.2.3.2	Finite Element Method.....	59
4.2.3.3	Finite Volume Method.....	60
4.2.3.4	Spectral Method	60
4.2.3.5	Boundary Element Method.....	62
4.2.3.6	Smooth Particle Hydrodynamics	62
4.3	<i>Solving</i>	65
4.3.1	Classification of physical behaviours.....	65
4.3.1.1	Equilibrium problems	65
4.3.1.2	Marching problems	66
4.3.2	Potential flow	68
4.3.3	Hydrostatic pressure models	68
4.3.4	Shallow water equations.....	68
4.3.5	Boussinesq equation	69
4.3.6	Mild-slope equation	70
4.3.7	Modelling of viscous turbulent flows.....	71
4.3.7.1	RANS equation for incompressible flow	71
The $\kappa - \epsilon$ model	74	
The $\kappa - \omega$ model	76	
4.3.7.2	Large Eddy Simulation (LES)	81
4.3.7.3	Direct Numerical Simulation (DNS)	83
4.4	<i>Post-processing</i>	84
4.5	<i>Errors and uncertainties</i>	84
4.5.1	Introduction.....	84
4.5.2	Model error and uncertainty.....	85

4.5.3	Discretisation or numerical error.....	85
4.5.4	Iteration or convergence error	85
4.5.5	Round-off errors	86
4.5.6	User errors.....	86
4.5.7	Code errors.....	86
4.5.8	Recommendations and guidelines	86
5.	Commonly Used Software	88
5.1	<i>Navier-Stokes solvers (CFD).....</i>	<i>88</i>
5.1.1	Introduction.....	88
5.1.2	OpenFOAM.....	89
5.1.3	ANSYS CFX	92
5.1.4	SPHysics & DualSPHysics	95
5.2	<i>Hydrostatic models</i>	<i>100</i>
5.2.1	POM.....	100
5.2.2	COHERENS	102
5.2.3	Delft3D.....	103
5.2.4	TELEMAC-MASCARET	108
5.2.5	MIKE 21	110
5.3	<i>Potential flow</i>	<i>114</i>
5.3.1	ANSYS AQWA.....	114
5.3.2	WAMIT.....	116
5.3.3	QALE-FEM	119
5.3.4	OrcaFlex	122
5.4	<i>Shallow Water Equations</i>	<i>126</i>
5.4.1	S.HY.F.E.M.....	126
5.5	<i>Boussinesq.....</i>	<i>128</i>
5.5.1	FUNWAVE.....	128
5.6	<i>Spectral.....</i>	<i>131</i>
5.6.1	WAM.....	131
5.6.2	WAVEWATCH III.....	133
5.6.3	SWAN.....	136
6.	Numerical Models: Overview and Applicability.....	141
6.1	<i>Introduction.....</i>	<i>141</i>
6.2	<i>Numerical models and physical processes</i>	<i>141</i>
6.3	<i>Numerical modelling for a MRE project.....</i>	<i>144</i>
6.4	<i>Conclusion.....</i>	<i>146</i>
7.	Bibliography.....	148

List of figures

Figure 2.1: Fluid particle showing the notation of the faces.....	17
Figure 2.2: Fluid particle showing the notation of stresses.....	20
Figure 3.1: Spectral categorization of surface water waves	32
Figure 3.2: Characteristics of a 2D linear water wave	33
Figure 3.3: Basic equations and boundary conditions for a wave according to linear wave theory, in terms of the velocity potential (Holthuijsen, 2007).....	35
Figure 3.4: Formation of wave groups	39
Figure 3.5: Surface elevation of cnoidal and solitary waves	43
Figure 3.6: Area of applicability of wave theories according to wave characteristics: height (H), period (T) and depth of water (d).....	43
Figure 3.7: Wave diffraction behind semi-infinitely long obstacles	46
Figure 4.1: The solving process in a SPH model	64
Figure 4.2: Typical measurement of the velocity in turbulent flows	72
Figure 5.1: Structure of OpenFOAM	90
Figure 5.2: GPU solving scheme	99
Figure 5.3: The sigma (σ) coordinate system.....	100
Figure 5.4: Modules of Delft3D	106
Figure 6.1: Technical aspects for a MRE project examined with numerical modelling.....	145

List of tables

Table 2.1: Surface and body forces	20
Table 2.2: Governing equation of fluid motion.....	28
Table 4.1: Classification of physical behaviours.....	67
Table 4.2: Values of $\kappa - \varepsilon$ model coefficients.....	75
Table 4.3: Boundary conditions for the $\kappa - \varepsilon$ model.....	76
Table 4.4: Values of $\kappa - \omega$ coefficients	77
Table 4.5: Boundary conditions for elliptic flows solved with RSM	81
Table 5.1: Capabilities of different ANSYS AQWA packages.....	115
Table 5.2: Applications of WAMIT.....	118
Table 6.1: Models presented in Chapter 5 classified according to the equations solved.....	142
Table 6.2: Suitability of wave models for simulation of different physical processes	143
Table 6.3: Efficiency of the numerical models.....	144
Table 6.4: Physical processes according to the depth of the sea.....	146
Table 6.5: Suitability of numerical models for different aspects of MRE projects.....	147

Introduction

The MERiFIC Project

MERiFIC is an EU project linking Cornwall and Finistère through the ERDF INTERREG IVa France (Manche) England programme. The project seeks to advance the adoption of marine energy in Cornwall and Finistère, with particular focus on the island communities of the Parc naturel marin d'Iroise and the Isles of Scilly. Project partners include Cornwall Council, University of Exeter, University of Plymouth and Cornwall Marine Network from the UK, and Conseil général du Finistère, Pôle Mer Bretagne, Technôpole Brest Iroise, IFREMER and Bretagne Développement Innovation from France.

MERiFIC was launched on 13th September at the National Maritime Museum Cornwall and runs until June 2014. During this time, the partners aim to

- Develop and share a common understanding of existing marine energy resource assessment techniques and terminology;
- Identify significant marine energy resource 'hot spots' across the common area, focussing on the island communities of the Isles of Scilly and Parc Naturel Marin d'Iroise;
- Define infrastructure issues and requirements for the deployment of marine energy technologies between island and mainland communities;
- Identify, share and implement best practice policies to encourage and support the deployment of marine renewables;
- Identify best practice case studies and opportunities for businesses across the two regions to participate in supply chains for the marine energy sector;
- Share best practices and trial new methods of stakeholder engagement, in order to secure wider understanding and acceptance of the marine renewables agenda;
- Develop and deliver a range of case studies, tool kits and resources that will assist other regions.

To facilitate this, the project is broken down into a series of work packages:

WP1: Project Preparation
WP2: Project Management
WP3: Technology Support
WP4: Policy Issues
WP5: Sustainable Economic Development
WP6: Stakeholder Engagement
WP7: Communication and Dissemination

This report

This report indicates the importance of numerical modelling in the modelling process, gradually builds the essential background theory in the fields of fluid mechanics, wave mechanics and numerical modelling, discusses a list of commonly used software and finally

recommends which models are more suitable for different engineering applications in a marine renewable energy project.

Structure of the report

The report contains six chapters that lead the reader from the simple principles of fluid mechanics to the complicated numerical modelling of free surface flows.

In chapter one, a definition for modelling is given and the two basic modelling techniques are briefly analysed. A thorough discussion of the strengths, weaknesses, opportunities and threats for physical and numerical modelling is presented. This first introductory chapter will help the reader to understand the importance of numerical modelling in engineering applications, but at the same time its limitations in order not to overestimate its power. The new concept of composite modelling is also introduced.

In chapter two, the fundamental principles and equations of Fluid Mechanics are presented that will help the reader advance to the next chapters. In chapter two, one can find the governing equations of a fluid flow, together with the derivation of the continuity, momentum and energy equations. The Navier-Stokes equations, which are the most commonly used equations in numerical modelling, are also included in this chapter. The chapter closes with an introduction to turbulence modelling.

Since the reader has become familiar with the fundamentals of fluid mechanics, the specific case of wave mechanics is discussed in chapter three. The fundamentals of wave mechanics include the characteristics of waves, wave theories, wave transformation in the near shore environment and the basics of wave-structure interaction. At the end of the chapter, the generation of irregular sea waves is discussed and the concept of the energy spectrum is introduced.

Numerical modelling is discussed in more detail in chapter four. This numerical modelling process is divided in three main parts: pre-processing, solving and post-processing. Pre-processing includes set-up of the numerical simulation, which refers to the definition of the problem, the specification of the boundary and initial conditions and the discretization method. The solving part discusses the classification of the physical behaviours (elliptic, parabolic and hyperbolic equations) and the different solvers, from potential flow to Navier-Stokes. The post-processing part contains the interpretation of the numerical results, in other words the extraction of data and their appropriate presentation with graphs and other media. At the end of this section, errors and uncertainties of numerical modelling is discussed and pitfalls that the modeller should be aware of.

Chapter five includes a presentation of the commonly used software for coastal hydrodynamics and free surface wave modelling. The most popular models, like OpenFOAM, ANSYS CFX, MIKE 21, Delft3D, SWAN etc, are described in this section. For each type of software, the description starts with a brief introduction about the model history, then the mathematical model is presented and it is followed by the assumptions and limitations of the software. At the end, some examples of applications are presented, that help the reader understand the use of models in practice.

The final chapter is an overview of the model's applicability. It concludes the report with some informative tables, which show the equations and the area of their application, the examined problem and the appropriate software to use, and a table that connects the

software with the resources needed to run it. The technical aspects of a marine renewable energy project that require numerical modelling are discussed at the end of the chapter.

Scope of the report

This report provides both the theoretical background and the software used for modelling of coastal processes and waves in general. The theoretical background consists of fluid and wave mechanics and basic principles of numerical modelling. The software is discussed in terms of areas of applicability and resources required.

This document aims to be a useful handbook which communicates the principles of numerical modelling techniques to early researchers and industrial modellers. It also presents the recent advances in wave modelling and CFD applications. However, since the field of numerical modelling and its applications is practically unlimited, this report attempts to provide only a starting point for research and not to analyse every model in depth. Therefore, it should be used as a reference guide for further bibliographic research through the extensive list of sources which is provided.

The thorough overview of the most commonly used software in chapter 5, is the most updated description of the most well-known numerical models to the authors' best knowledge. This is very handy guidance for someone that seeks a brief description and an awareness of the models' area of application. It also provides many references to websites, official documentation, scientific publications and technical reports.

In many parts of the report best practice advice is cited. This can be especially helpful for not experienced modellers who are likely to face some difficulties and fall into some pitfalls. One of the scopes of the report is to raise the awareness of the new modellers by providing information of the errors and uncertainties induced in the modelling process.

Last but not least, the report aims to be a decision making tool for new model users. This is achieved by the tables in chapter six, which link together the physical problem to be modelled, the appropriate software to use and the resources required. According to the available resources and the level of accuracy required, users can consult the report and choose the software that suits them best.

"Essentially, all models are wrong, but some are useful"

George E.P. Box (1919)

1. The Modelling Process

1.1 Introduction to modelling

The term modelling refers to the representation of a physical system, usually on a different scale. The purpose of modelling is the prediction of the behaviour of the system to a change of its conditions. Through modelling one can examine a system under extreme conditions, such as yielding load, storm etc, or estimate its long-term behaviour, such as the shoreline evolution over the years. Modelling is also extensively used to optimise a structure before building it at full-scale.

Modelling of systems can be done by physical or numerical models. The first refers to the physical representation of a natural phenomenon usually at a smaller scale, for example in laboratory tests. The second one aims to reproduce mathematically the physical processes which describe a natural phenomenon.

This report focuses on numerical modelling of hydraulic phenomena and coastal hydrodynamics, for example waves, tide currents, sediment transport, wave-structure interaction etc. Due to their complexity, hydraulic studies have traditionally been conducted with physical models. Physical hydraulic models are usually scaled models of the flow phenomena, which are reduced in scale using the laws of dynamic similarity (Payne, 2008). However, nowadays numerical models gain ground mainly because of the increasing processing power and their low cost. Numerical models are capable of describing very complex turbulent processes and can be very versatile thanks to the wide variety of boundary conditions that can be applied.

Focusing on coastal hydrodynamic processes, in addition to scaled laboratory physical models and the use of numerical models, a third modelling technique has emerged, namely composite modelling. It refers to the integrated and balanced use of physical and numerical modelling, which attempts to mitigate the weaknesses and make use of the advantages of the two classic modelling methods. Following the principles of composite modelling, physical and numerical modelling can improve further and broaden their range of applicability (Sutherland & Barfuss, 2011).

At this point, it should be noted that modelling might include many pitfalls and the final result might differ substantially from reality if the modeller is not aware of the uncertainties that each technique includes. The SWOT (Strengths Weaknesses Opportunities and Threats) analysis of the modelling techniques that follows, aims to provide a good overview of physical and numerical modelling.

1.2 Physical and Numerical modelling

1.2.1 SWOT analysis of physical models

1.2.1.1 Strengths of physical models

Since physical models are the natural reproduction of the physical processes, they do not include any parameterizations or assumptions and they are able to reproduce all the complex nonlinear physical phenomena accurately. Even more valuable is the fact that physical models can reproduce processes that are not fully understood so far and therefore cannot be sufficiently described mathematically. Such phenomena are breaking wave

impact forces, vortex generation and poor energy dissipation. These complex phenomena can be immediately apparent in a physical model.

Moreover, physical modelling is considered to be a very well established technique with a long tradition. The scientific community has built trust on physical modelling by performing physical tests for many centuries. For this reason, physical modelling is considered as the “gold standard” of almost all the modelling cases.

It is also important, that once the experimental set up has been prepared, it is fairly easy to perform many different tests in a very short time. For example, multiple flow rates or wave conditions can be implemented and examined quickly.

1.2.1.2 Weaknesses of physical models

Setting up a physical model is complex procedure and should be carried out by experienced modellers who understand the background and are familiar with the theory. The most important thing that limits the reliability of the physical models is the scale effects. This is because all the scaling criteria, such as Froude, Reynolds, Weber and Cauchy, cannot be satisfied simultaneously.

Apart from the scale effects, there are some unavoidable model effects that have a negative impact on the quality of the results. As an example, one can mention the reflections from the boundaries, the generation of spurious waves from the wave paddles and the imperfect absorption of the waves at the end of a flume or a tank.

Another very considerable limitation of physical models is the extraction of the data. Most of the time, the instrumentation provides only point measurements and multiple repetitions are necessary to provide the required coverage over the region of interest. At the same time, the instrumentation often interferes with the flow causing discrepancies at the measurements. On the other hand, more advanced techniques have been developed, which do not interfere with the flow and provide full coverage of the flow field. Particle Image Velocimetry is a relatively recent technique that is able to produce volume measurements without influencing the flow regime. Of course, the cost of such equipment is considerably high for the time being and the interpretation of the collected data requires advanced software and high computer power.

Last but not least, is the cost of physical modelling. It is perhaps the fundamental reason that has triggered the rapid evolution of the numerical models. The facilities and the personnel for physical experiments can be very costly, while constructing the model can be very time consuming. In many cases, significant adjustments to the model are impossible to be done due to the high cost and time needed. Another drawback, is the difficulty to return to a study after some time, because the models are often destroyed and the facilities are occupied by other users.

1.2.1.3 Opportunities for physical models

The development of sensor technology can seriously limit one of the greatest weaknesses of the physical models, which is the extraction of data. The measurement of distributed time series along a line, in a plane or over a 3D volume is currently under development and it is certain that the use of optical and acoustic technology will become broader and cheaper in

the near future. The development of computer power will facilitate the use of these new methods and the handling of the huge amount of data produced.

Furthermore, the construction of large-scale truly international testing facilities would allow some key studies with minor scale effects that can be used as the benchmarks for the smaller-scale studies.

International collaboration and the sharing of expertise and facilities is a key aspect that can help the further development of physical modelling. Projects like “Hydralab” and consortia like “MARINET” have proven this in practice. Each of the laboratories and research groups are specialized in particular areas and through international collaboration, experience can be built and the sharing of know-how can lead to better physical modelling practices.

As mentioned before, numerical modelling can also contribute to the development of physical modelling and vice versa. For this reason composite modelling can be a significant factor to the improvement of physical modelling.

1.2.1.4 Threats to physical models

As the processing power of the computers increases and the cost of commercial codes decreases or open source codes become available, the numerical models have started to dominate. In some areas, numerical models have rightfully replaced the physical models completely. Concurrently, the use of more sophisticated codes such as CFD, with the capability of describing very complex flows, has extended the use of numerical modelling in areas where physical modelling was traditionally applied.

However, the most serious threat is the almost unswerving acceptance of numerical results without validation with physical test series. These results can be in many cases quite misleading (Sutherland & Barfuss, 2011).

1.2.2 SWOT analysis of numerical models

1.2.2.1 Strengths of numerical models

Nowadays, most of the numerical models and codes have been validated for at least the most common cases of free surface flows. There is also extensive documentation (journal publications and reports) that confirm the fact that numerical models can represent adequately many physical processes (Sutherland & Barfuss, 2011).

The greatest advantage of numerical modelling is its low cost compared with physical model tests and the different configurations and options that it offers. All these options can be implemented relatively quickly and without additional cost. It is also important that repetition of the simulation is possible even a long time after the initial study. Return to the numerical experiment is much easier than in physical modelling. On the other hand, changes in some parts of the software or hardware might result in difficulty in rerunning the model. Moreover, numerical models can be operated anywhere on simple computers and even when high performance computer systems are necessary, the user can usually operate them remotely.

Numerical modelling can also mitigate two of the biggest weaknesses of physical modelling: a) extraction of data and b) scale effects. In numerical models, data of all kinds, such as velocity, pressure, surface elevation, turbulent kinetic energy etc. can be extracted from any

point and time in the simulation and of course the “virtual” probes do not interfere with the flow. Regarding scale effects, numerical models can be used for running full scale models. However, when validation is needed with laboratory scale models, extra care should be taken.

1.2.2.2 Weaknesses of numerical models

Some numerical models rely on parameterization of the physical processes. However, these parameterizations have often limited range of applicability and if the performance of the model is out of this range, the model might produce unrealistic results. At the same time, the final result is subject to assumptions that are made, such as turbulence models, boundary conditions, initial state etc., which are imperfect and sometimes far from reality.

The accuracy of a numerical model depends also on the fineness of the grid (see discretization of equations 4.2.3). So, the final result is grid-dependent. Usually, the finer the grid is, the more accurate the result becomes. However, refining the grid adds computational cost. For this reason, mesh convergence tests are required in order to achieve the level of accuracy wanted. One should take into account that no matter how fine a grid is, there are always sub-grid processes that cannot be simulated (e.g. molecular level processes).

Nowadays, sophisticated numerical models, like DNS (§ 4.3.7.3), that can handle very complex flows are available. However, the computational time is in many cases unrealistic and this prevents users from performing long-runs.

It should be pointed out again, that like in physical modelling, the best results are achieved by experienced modellers with a good understanding of the physics and the processes that take place in the simulation.

1.2.2.3 Opportunities for numerical models

One of the greatest weaknesses of numerical modelling is the high computational cost. However, the increasing computer power and the use of parallelised computation using High Performance Computer (HPC) units suggests a promising future in which numerical models will be able to handle long-runs and deal with larger/full-scale problems.

At the same time, validation is necessary to provide confidence from physical modelling and field studies. Numerical models can gain reliability by thorough validation with physical models with limited or known scale effects.

Last but not least, the sharing of knowledge and codes via open-source free distributed software can involve more people in the field making valuable contributions to code development and validation of models.

1.2.2.4 Threats to numerical models

There is not a real threat to numerical modelling, since the sector expands rapidly. A possible threat is to minimise the physical modelling in such a degree that will affect the

validation of numerical models. Misuse or overestimation of the capabilities of the models might result to loss of confidence and trust to the numerical modelling on its whole.

1.2.3 Summary of SWOT analysis

The SWOT analysis of the numerical and physical models indicates that both have their weaknesses and strengths and in most cases these are complementary. It is certain that each needs the other to develop and evolve further, but there is no doubt that they have improved significantly in the last few decades. Moreover, the new approach of composite modelling will improve the modelling process in general by mitigating the weaknesses and taking advantage of the strengths of each modelling technique (Sutherland & Barfuss, 2011).

2. Fundamentals of Fluid Mechanics

2.1 Governing equations of the fluid flow

Most of the definitions and equations that follow can be found in reference textbooks, such as that written by Versteeg & Malalasekera, 2007. Most of the books referring to CFD have similar structure and in general they provide the same theoretical background.

Any fluid flow is described by the governing equations of the fluid mechanics, which are the representation of the mathematical statements of the conservation laws of physics. The laws are described of the following statements:

- Conservation of mass: The mass of the fluid is conserved,
- Newton's 2nd law: The rate of change of momentum equals the total force on a fluid particle,
- First law of thermodynamics: The rate of change of energy equals the sum of heat addition to plus the rate of work done on a fluid particle.

It should be noted that the fluid is treated as a continuum, which has macroscopic properties, such as velocity, pressure, density and temperature, as well as their space and time derivatives, that are not influenced by the molecular dynamics. As a result, the analysis is considered to be macroscopic with length scales of $1\mu\text{m}$ or larger. Therefore the properties of the fluid can be assumed as averages over a sufficiently large number of molecules. At this point, the term fluid particle or element is introduced and it refers to the smallest possible element of fluid whose macroscopic properties are not influenced by individual molecules. A fluid particle is schematically presented in Fig. 2.1. The sketch will help the reader to follow the derivation and description of the fundamental equations.

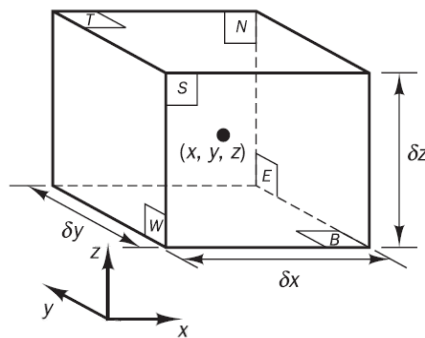


Figure 2.1: Fluid particle showing the notation of the faces

The fluid particle is represented here as a cuboid with sides of lengths δx , δy and δz . The six faces are labelled N , S , E , W , T and B , which stands for North, South, East, West, Top and Bottom. The element is represented by each centre, which is located at position (x, y, z) . Any fluid flow across the boundary faces of the fluid particle causes changes in the mass, momentum and energy to the particle. Same changes might occur due to the action

of source terms inside the element. The fluid flow equations will be derived by considering these changes on the fluid particle.

One should always keep in mind that all the fluid properties are functions of space and time. Therefore they all have arguments (x, y, z, t) . However, for the rest of the document, the notation will be simplified and the arguments will not be explicitly stated. For example, the velocity vector will be notated as \vec{u} instead of $\vec{u}(x, y, z, t)$, and its x -derivative at a certain time as $\partial\vec{u}/\partial x$. The same applies for the density ρ , pressure p and temperature T .

As the fluid particle is so small, the expression of the fluid properties by only the first two terms of the Taylor series expansion is considered to be accurate enough. For example faces W and E are equidistant from the centre of the element by $\frac{1}{2}\delta x$ and a property φ calculated on the faces using a Taylor expansion reads:

$$\varphi \pm \frac{\partial\varphi}{\partial x} \frac{(x - x_0)}{1!} = \varphi \pm \frac{\partial\varphi}{\partial x} \frac{1}{2} \delta x \quad (2.1)$$

2.1.1 Mass conservation in three dimensions

The first step in the derivation of any equation is to state the concept in words for better understanding. For the case of the mass conservation equation this is the mass balance for the fluid element:

Rate of increase of mass in a fluid element	=	Net rate of flow of mass into fluid element
---	---	---

Since the element volume is constant, the change of mass in the fluid element results to changes of the density:

$$\frac{\partial}{\partial t} (\rho \delta x \delta y \delta z) = \frac{\partial \rho}{\partial t} \delta x \delta y \delta z \quad (2.2)$$

The mass flow across a face of an element is a product of density, area and the velocity component normal to the face. Starting with the concept of the mass conservation stated before and after some algebra, this yields per unit volume:

$$\frac{\partial \rho}{\partial t} + \frac{\partial(\rho u)}{\partial t} + \frac{\partial(\rho v)}{\partial t} + \frac{\partial(\rho w)}{\partial t} = 0 \quad (2.3)$$

or in more compact vector notation

$$\frac{\partial \rho}{\partial t} + \text{div}(\rho \mathbf{u}) = 0 \quad (2.4)$$

where u, v, w refer to the velocity components in x, y, z direction respectively.

This equation is the most general and it describes the unsteady, three-dimensional mass conservation, else known as continuity equation, for a compressible fluid at a certain point. The first term refers to the time derivative of the density (mass per unit volume) and the second term to the net flow of mass out of the element across its boundaries, else known as convective term.

The basic assumption for the most common applications is the assumption of incompressibility. An incompressible fluid (i.e. a liquid) has a constant density. Therefore the derivative of density is zero and the continuity equation reads:

$$\text{div } \mathbf{u} = 0 \quad (2.5)$$

or in longhand notation

$$\frac{\partial u}{\partial x} + \frac{\partial v}{\partial y} + \frac{\partial w}{\partial z} = 0 \quad (2.6)$$

2.1.2 Momentum equation in three dimensions

As mentioned before the momentum equation comes from Newton's second law, which states that the sum of the forces acting on a fluid particle equals the rate of change of its momentum. The simplest mathematical expression found in textbooks is: $\Sigma F = \frac{d(mu)}{dt}$. In words, it is stated bellow:

Rate of increase of momentum of fluid particle	=	Sum of forces on fluid particle
--	---	---------------------------------------

The rates of increase of x -, y - and z -momentum per unit volume of a fluid particle are given by the derivatives of the corresponding velocities:

$$\rho \frac{Du}{Dt} \quad \rho \frac{Dv}{Dt} \quad \rho \frac{Dw}{Dt}$$

At this point it is important to know which forces might act on a fluid particle. For the sake of clarity these forces are divided into two types: surface and body forces.

Table 2.1: Surface and body forces

Surface Forces	Body Forces
Pressure forces	Centrifugal force
Viscous forces	Coriolis force
Gravity force	Electromagnetic force

According to the common practice, the body forces work as source terms in the momentum equation, while surface forces are included as distinguished terms.

The forces acting on a fluid particle result to stresses on its surface. The state of stress of a fluid element is defined in terms of the pressure and the nine viscous stress components. Pressure is considered to be a normal stress and it is denoted by p . Viscous stresses are denoted by τ and they have three components on every surface of the element. Their direction is indicated when by usual suffix notation τ_{ij} . The suffices i and j in τ_{ij} indicate that the stress component acts in the j -direction on a surface normal to the i -direction. The schematic that follows (Fig. 2.2) depicts the direction that each component act on.

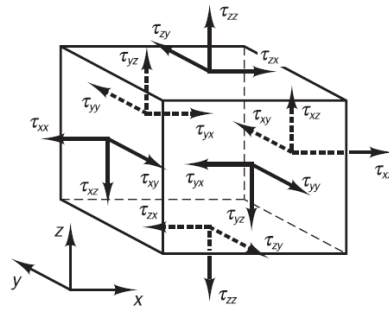


Figure 2.2: Fluid particle showing the notation of stresses

In order to derive the momentum equation in all three dimensions, first the x-components will be considered and then according to them the y- and z-components will be written. The x-components include the forces due to pressure p and stress components τ_{xx} , τ_{yx} and τ_{zx} . The force due to a stress acting on a surface is given by the product of stress and the surface area. According to their orientation, the forces get either a positive or a negative sign. Positive when they are aligned with the direction of the corresponding co-ordinate axis and negative when they have opposite to the axis direction. The sum of the force components acting in the same direction yields the net force in the corresponding direction. For the x-direction, the sum of the net forces in the x-direction on the pair faces, i.e. *E-W*, *N-S* and *T-B*, divided by the volume of the element ($\delta x \delta y \delta z$) reveals the total force per unit volume. The force in x-direction is expressed by the following sum:

$$\frac{\partial(-p + \tau_{xx})}{\partial x} + \frac{\partial\tau_{yx}}{\partial y} + \frac{\partial\tau_{zx}}{\partial z} \quad (2.7)$$

The effect of body forces is not included in the previous sum. As mentioned before, the effect of the body forces can be included by defining a source term. For the momentum in x -direction the source term per unit volume per unit time reads: S_{Mx} .

The next step is to write the x -component of the momentum equation. In order to achieve that the sum of forces and the source term in x -direction is written on the right side and it equals the rate of change of the x -momentum of the fluid:

$$\rho \frac{Du}{Dt} = \frac{\partial(-p + \tau_{xx})}{\partial x} + \frac{\partial\tau_{yx}}{\partial y} + \frac{\partial\tau_{zx}}{\partial z} + S_{Mx} \quad (2.8a)$$

Similarly, the other two components of the momentum can be found.

The y -component of the momentum equation is given by

$$\rho \frac{Dv}{Dt} = \frac{\partial\tau_{xy}}{\partial x} + \frac{\partial(-p + \tau_{yy})}{\partial y} + \frac{\partial\tau_{zy}}{\partial z} + S_{My} \quad (2.8b)$$

and the z -component of the momentum equation by

$$\rho \frac{Dw}{Dt} = \frac{\partial\tau_{xz}}{\partial x} + \frac{\partial\tau_{yz}}{\partial y} + \frac{\partial(-p + \tau_{zz})}{\partial z} + S_{Mz} \quad (2.8c)$$

Attention should be paid to the signs of the terms in the equations. The sign of the pressure is negative, because by definition pressure is a compressive normal stress. At the same time, according to the usual convention, tensile stresses are positive normal stresses.

The source terms S_{Mx} , S_{My} and S_{Mz} include contributions due to body forces only. As an example, the force due to gravity results the following source terms: $S_{Mx} = 0$, $S_{My} = 0$ and $S_{Mz} = -\rho g$.

2.1.3 Energy equation in three dimensions

As stated previously, the energy equation is derived from the first law of thermodynamics. According to which the rate of change of energy of a fluid particle is equal to the rate of heat addition to the fluid particle plus the rate of work done on the particle.

Rate of increase of energy of fluid particle	=	Net rate of heat added to fluid particle	+	Net rate of work done on fluid particle
--	---	--	---	---

The rate of energy change of energy of a fluid particle per unit volume is given by:

$$\rho \frac{DE}{Dt}$$

To begin with, the work done by surface forces will be examined. When a force acts on the surface, the product of the force and the velocity component in the direction of the force yields the rate of work done on a fluid particle. After some algebra, the net rate of work can be found in each direction. For the x-direction the net rate of work reads:

$$\left[\frac{\partial(u(-p + \tau_{xx}))}{\partial x} + \frac{\partial(u\tau_{yx})}{\partial y} + \frac{\partial(u\tau_{zx})}{\partial z} \right] \delta x \delta y \delta z \quad (2.9a)$$

And for the y- and z-direction the net rate of work is given respectively:

$$\left[\frac{\partial(v\tau_{xy})}{\partial x} + \frac{\partial(v(-p + \tau_{yy}))}{\partial y} + \frac{\partial(v\tau_{zy})}{\partial z} \right] \delta x \delta y \delta z \quad (2.9b)$$

and

$$\left[\frac{\partial(w\tau_{xz})}{\partial x} + \frac{\partial(w\tau_{yz})}{\partial y} + \frac{\partial(w(-p + \tau_{zz}))}{\partial z} \right] \delta x \delta y \delta z \quad (2.9c)$$

The total rate of work done per unit volume on the fluid particle by all the surface forces is given by the sum of the net rate of work in each direction divided by the volume $\delta x \delta y \delta z$. By gathering the pressure terms together and writing in the compact vector form that follows:

$$-\frac{\partial(Up)}{\partial x} - \frac{\partial(vp)}{\partial y} - \frac{\partial(wp)}{\partial z} = -div(p\mathbf{u}) \quad (2.10)$$

the sum the previous equations can be written in more convenient way:

$$[-div(p\mathbf{u})] + \left[\frac{\partial(u\tau_{xx})}{\partial x} + \frac{\partial(u\tau_{yx})}{\partial y} + \frac{\partial(u\tau_{zx})}{\partial z} + \frac{\partial(v\tau_{xy})}{\partial x} + \frac{\partial(v\tau_{yy})}{\partial y} + \frac{\partial(v\tau_{zy})}{\partial z} + \frac{\partial(w\tau_{xz})}{\partial x} + \frac{\partial(w\tau_{yz})}{\partial y} + \frac{\partial(w\tau_{zz})}{\partial z} \right] \quad (2.11)$$

which expresses the total rate of work done on the fluid particle by surface stresses.

Next, the energy equation must be derived. The energy of a fluid particle comprises of three terms: the internal (thermal) energy i , kinetic energy $\frac{1}{2}(u^2 + v^2 + w^2)$ and gravitational potential energy. In this context, the fluid element is considered to store gravitational potential energy. The gravitational force can be also regarded as a body force that acts on the fluid particle as it moves in the gravity field. By considering the latter view, the effects of the potential energy changes can be included as a source term. Therefore, S_E is defined as the source energy term per unit volume per unit time.

In order to derive the conservation of energy equation, the rate of change of energy of a fluid particle needs to be equated to the sum of the net rate of work done on the fluid particle, the net rate of heat addition to the fluid and the rate of increase of energy due to sources. The equation reads:

$$\rho \frac{DE}{Dt} = -div(p\mathbf{u}) + \left[\frac{\partial(u\tau_{xx})}{\partial x} + \frac{\partial(u\tau_{yx})}{\partial y} + \frac{\partial(u\tau_{zx})}{\partial z} + \frac{\partial(v\tau_{xy})}{\partial x} + \frac{\partial(v\tau_{yy})}{\partial y} + \frac{\partial(v\tau_{zy})}{\partial z} + \frac{\partial(w\tau_{xz})}{\partial x} + \frac{\partial(w\tau_{yz})}{\partial y} + \frac{\partial(w\tau_{zz})}{\partial z} \right] + div(k \text{ grad}T) + S_E \quad (2.12)$$

where $E = i + \frac{1}{2}(u^2 + v^2 + w^2)$.

The previous energy equation describes the rate of the energy change adequately. However, in practical applications it is often desirable to separate the changes of the (mechanical) kinetic energy in order to obtain an equation for internal energy i or temperature T only. The kinetic energy contribution to the total energy can be found by multiplying the x-momentum equation by velocity component u , the y-momentum equation by v and the z-momentum equation by w and adding the results together.

For the common case of an incompressible fluid the internal energy equals the product of the specific heat c and the temperature T : $i = cT$. At the same time, according to the continuity equation for an incompressible fluid: $\text{div } u = 0$.

For compressible fluids, the interest might be in the enthalpy equation. This equation is derived by the energy equation by rearranging the terms. The specific enthalpy h and the specific total enthalpy h_0 of a fluid are defined as

$$h = i + \frac{p}{\rho} \quad \text{and} \quad h_0 = h + \frac{1}{2}(u^2 + v^2 + w^2) \quad (2.13)$$

By merging the previous definitions with the one for specific energy E , the specific total enthalpy is found:

$$h_0 = i + \frac{p}{\rho} + \frac{1}{2}(u^2 + v^2 + w^2) = E + \frac{p}{\rho} \quad (2.14)$$

2.2 Equation of state

So far five equations have been presented: 1) the mass conservation; 2) x -, 3) y -, 4) z -momentum equation; and 5) energy equation. These fundamental equations contain four unknowns: density (ρ), pressure (p), internal energy (i) and temperature (T). There is a linkage between these variables. This linkage is the equations of state.

In order to derive a relation that connects ρ, p, i, T , an assumption needs to be considered: thermodynamic equilibrium. This means that the fluid can adjust its properties so rapidly that the changes are practically instantaneous. That means that these changes occur much faster than the flow velocities and the fluid remains in thermodynamic equilibrium. This assumption is valid for most of the flows, apart for some particular exceptions like strong shockwaves. Even in these cases, the equilibrium assumption gives close approximations.

The state of a fluid in thermodynamic equilibrium can be described by just two state variables. Therefore the equations of state relate the two variables to the two other variables. Most commonly ρ and T are used as state variables, while p and i are given by the following state equations:

$$p = p(\rho, T) \quad \text{and} \quad i = i(\rho, T) \quad (2.15)$$

For example, for a perfect gas the equations of state read:

$$p = \rho RT \quad \text{and} \quad i = C_v T$$

where R is the universal gas constant and C_v is the specific heat capacity.

It can be easily seen that the equations of state can eliminate all but two thermodynamic state variables. For compressible fluids, the equations of state are necessary to provide the linkage between the energy equation and the other four equations (continuity, x -, y -, z -momentum equations). In compressible flows, density changes might result to pressure and temperature variations in the flow field.

On the other hand, if the fluid is moving at a low speed, most of the times the assumption of incompressibility is valid. In this case, there are no density variations and no connection between the energy equation and continuity and momentum equations. Therefore the flow field can be calculated by solving the continuity and momentum equations only. However, if heat transfer is involved in the problem, the energy equation needs to be solved alongside.

2.3 Navier-Stokes equations

The Navier-Stokes equations are able to describe any fluid flow. In this chapter, a description of the derivation of the N-S equations for a Newtonian fluid will be presented. In Newtonian fluids the viscous stresses are proportional to the rates of deformation.

By looking back to the transport equations, there are further unknowns, i.e. the viscous stress components τ_{ij} . In order to define these unknowns and solve the equations, a model is necessary. The most common way to do this is to associate the viscous stresses with the local deformation rate or strain rate of the fluid element. In the case of three-dimensional flows, the local rate of deformation is composed of the linear deformation rate and the volumetric deformation rate.

All gases and many liquids are isotropic. This means that the fluid has the same behaviour in any point and in any direction at the area that it covers. On the other hand, there are certain liquids with polymer molecules that have anisotropic behaviour, but they are not considered here.

For isotropic fluids, the rate of linear deformation of a fluid element involves nine components, six of which are independent. They are denoted by s_{ij} , following the same suffix system to the stress components. The deformation components are divided in linear elongating and shearing linear deformation components. The three linear elongating components are:

$$s_{xx} = \frac{\partial u}{\partial x} \quad s_{yy} = \frac{\partial v}{\partial y} \quad s_{zz} = \frac{\partial w}{\partial z} \quad (2.16a, b, c)$$

and the six shearing linear deformation components:

$$s_{xy} = s_{yx} = \frac{1}{2} \left(\frac{\partial u}{\partial y} + \frac{\partial v}{\partial x} \right) \quad s_{xz} = s_{zx} = \frac{1}{2} \left(\frac{\partial u}{\partial z} + \frac{\partial w}{\partial x} \right) \quad (2.17a, b)$$

$$S_{yz} = S_{zy} = \frac{1}{2} \left(\frac{\partial v}{\partial z} + \frac{\partial w}{\partial y} \right) \quad (2.17c)$$

So far, the linear deformation components have been presented. What is left is the volumetric deformation given by:

$$\frac{\partial u}{\partial x} + \frac{\partial v}{\partial y} + \frac{\partial w}{\partial z} = \text{div } \mathbf{u} \quad (2.18)$$

At this point, the Newtonian fluid principle will be used to define the viscous stresses. According to the three-dimensional form of Newton's law of viscosity for compressible flows, two constants of proportionality between the viscous stresses and the rates of deformation are defined. The first one is the dynamic viscosity, denoted by μ , which relates the stresses to the linear deformations. The second one is the viscosity, λ , which relates the stresses to the volumetric deformation. The nine viscous stress components are given by the relations below. Only six of the components are independent.

$$\tau_{xx} = 2\mu \frac{\partial u}{\partial x} + \lambda \text{div } \mathbf{u} \quad \tau_{yy} = 2\mu \frac{\partial v}{\partial y} + \lambda \text{div } \mathbf{u} \quad \tau_{zz} = 2\mu \frac{\partial w}{\partial z} + \lambda \text{div } \mathbf{u} \quad (2.19a, b, c)$$

$$\tau_{xy} = \tau_{yx} = \mu \left(\frac{\partial u}{\partial y} + \frac{\partial v}{\partial x} \right) \quad \tau_{xz} = \tau_{zx} = \mu \left(\frac{\partial u}{\partial z} + \frac{\partial w}{\partial x} \right) \quad (2.19d, e)$$

$$\tau_{yz} = \tau_{zy} = \mu \left(\frac{\partial v}{\partial z} + \frac{\partial w}{\partial y} \right) \quad (2.19f)$$

The effect of the viscosity λ is practically small. More specifically, if the fluid is incompressible, the mass conservation equation is simplified to $\text{div } \mathbf{u} = 0$. By substituting this into the viscous stresses, the effect of λ is eliminated and the viscous stresses are twice the local rate of linear deformation multiplied by the dynamic viscosity μ .

Substitution of the shear stresses into the momentum equations yields the so-called Navier–Stokes equations, named after the two nineteenth-century scientists who derived them independently:

$$\rho \frac{Du}{Dt} = -\frac{\partial p}{\partial x} + \frac{\partial}{\partial x} \left[2\mu \frac{\partial u}{\partial x} + \lambda \text{div}u \right] + \frac{\partial}{\partial y} \left[\mu \left(\frac{\partial u}{\partial y} + \frac{\partial v}{\partial x} \right) \right] + \frac{\partial}{\partial z} \left[\mu \left(\frac{\partial u}{\partial z} + \frac{\partial w}{\partial x} \right) \right] + S_{Mx} \quad (2.20a)$$

$$\rho \frac{Dv}{Dt} = -\frac{\partial p}{\partial y} + \frac{\partial}{\partial x} \left[\mu \left(\frac{\partial u}{\partial y} + \frac{\partial v}{\partial x} \right) \right] + \frac{\partial}{\partial y} \left[2\mu \frac{\partial v}{\partial y} + \lambda \text{div}v \right] + \frac{\partial}{\partial z} \left[\mu \left(\frac{\partial v}{\partial z} + \frac{\partial w}{\partial y} \right) \right] + S_{My} \quad (2.20b)$$

$$\rho \frac{Dw}{Dt} = -\frac{\partial p}{\partial z} + \frac{\partial}{\partial x} \left[\mu \left(\frac{\partial u}{\partial z} + \frac{\partial w}{\partial x} \right) \right] + \frac{\partial}{\partial y} \left[\mu \left(\frac{\partial v}{\partial z} + \frac{\partial w}{\partial y} \right) \right] + \frac{\partial}{\partial z} \left[2\mu \frac{\partial w}{\partial z} + \lambda \text{div}w \right] + S_{Mz} \quad (2.20c)$$

The Navier–Stokes equations can be written in the most useful form for the development of the numerical methods, by rearranging the viscous stress terms:

$$\rho \frac{Du}{Dt} = -\frac{\partial p}{\partial x} + \text{div}(\mu \text{grad} u) + S_{Mx} \quad (2.21a)$$

$$\rho \frac{Dv}{Dt} = -\frac{\partial p}{\partial y} + \text{div}(\mu \text{grad} v) + S_{My} \quad (2.21b)$$

$$\rho \frac{Dw}{Dt} = -\frac{\partial p}{\partial z} + \text{div}(\mu \text{grad} w) + S_{Mz} \quad (2.21c)$$

The internal energy equation using the Newtonian model for viscous stresses yields:

$$\rho \frac{Di}{Dt} = -p \text{div}u + \text{div}(k \text{grad}T) + \Phi + S_i \quad (2.22)$$

where Φ represents a dissipation function, which describes all the effects due to viscous stresses in this internal energy equation. It can be shown after considerable algebra that Φ is given by the following equation:

$$\Phi = \mu \left\{ 2 \left[\left(\frac{\partial u}{\partial x} \right)^2 + \left(\frac{\partial v}{\partial y} \right)^2 + \left(\frac{\partial w}{\partial z} \right)^2 \right] + \left(\frac{\partial u}{\partial y} + \frac{\partial v}{\partial x} \right)^2 + \left(\frac{\partial u}{\partial z} + \frac{\partial w}{\partial x} \right)^2 + \left(\frac{\partial v}{\partial z} + \frac{\partial w}{\partial y} \right)^2 \right\} + \lambda (\text{div}u)^2 \quad (2.23)$$

It should be pointed out that the dissipation function contains only squared terms and therefore is always positive. The physical meaning of this is that Φ represents a source of internal energy due to deformation work on the fluid particle. By extracting this work from the mechanical energy, which is related the motion, the conversion to internal energy or heat can be found.

2.4 Summary of governing equations of fluid motion

Table 2.2: Governing equation of fluid motion

Continuity	$\frac{\partial \rho}{\partial t} + \text{div}(\rho \mathbf{u}) = 0$
x-momentum	$\rho \frac{Du}{Dt} = \frac{\partial(-p + \tau_{xx})}{\partial x} + \frac{\partial \tau_{yx}}{\partial y} + \frac{\partial \tau_{zx}}{\partial z} + S_{Mx}$
y-momentum	$\rho \frac{Dv}{Dt} = \frac{\partial \tau_{xy}}{\partial x} + \frac{\partial(-p + \tau_{yy})}{\partial y} + \frac{\partial \tau_{zy}}{\partial z} + S_{My}$
z-momentum	$\rho \frac{Dw}{Dt} = \frac{\partial \tau_{xz}}{\partial x} + \frac{\partial \tau_{yz}}{\partial y} + \frac{\partial(-p + \tau_{zz})}{\partial z} + S_{Mz}$
Energy	$\rho \frac{Di}{Dt} = -p \text{div} \mathbf{u} + \text{div}(k \text{grad} T) + \Phi + S_i$
Equations of state	$p = p(\rho, T) \quad \text{and} \quad i = i(\rho, T)$

2.5 Turbulence and its modelling

2.5.1 Introduction to turbulence

Osborne Reynolds in 1883 demonstrated experimentally that two entirely different types of fluid flow exist. In his experiment, he used a water tank, a glass tube and some dye. Water was discharged from the tank through the glass tube and a fine filament of dye was injected at the entrance to the tube.

At low velocities, the dye filament remained undisturbed, indicating that the particles of the water moved in parallel lines. This type of flow is called laminar, viscous or streamline flow. In the laminar regime, fluid particles move in an orderly fashion and retain their relative positions in successive cross-sections of the flow field.

As the velocity in the tube was gradually increased, the dye filament at first started to oscillate and then broke up. The visual result was that the colour was diffused over the whole cross-section proving that the fluid particles were not moving in an orderly manner. This type of flow is called turbulent and it is characterized by continuous small fluctuations in the magnitude and direction of the velocity of the fluid particles. The velocity fluctuations cause pressure fluctuations as well.

Whether a flow is laminar or turbulent can be determined from its physical characteristics. As with all physical bodies in motion, there are forces acting on the fluid particles in a disturbed stream, which tend to keep them in the same direction and other forces that push them in different directions. For the fluid particles in motion, the force that tends to lead the

particles in the new direction is the inertial force. On the contrary, the surrounding fluid particles will pose viscous forces on the disturbed particle, which tend to restrain it to move with the stream. In laminar flows, the viscous shear stresses prevail and they eliminate the effects of any deviation in the fluid flow. On the other hand, in turbulent flows, the viscous shear stresses cannot overcome the inertial forces and the total flow is disturbed. Therefore, a criterion that can describe when a flow is laminar or turbulent is the ratio of the inertial force to the viscous force acting on the fluid particles. This ratio is called the “Reynolds number” after Osborne Reynolds (Douglas, Gasiorek, Swaffield, & Jack, 2005).

Similar experiments on fluid flows showed that there is a certain value of Reynolds number that defines the flow regime. This is called the critical Reynolds number Re_{crit} . If Re is below Re_{crit} , the flow is laminar. If Re is above Re_{crit} the flow starts to become turbulent. The transition from laminar to turbulent flow includes a series of complicated events that gradually transform an undisturbed flow to a random and chaotic one. Turbulent flows include different scales of eddies incorporated in the flow.

According to their magnitude, the behaviour of eddies is dominated by different factors. Large eddies are dominated by inertia effects and viscous effects can be neglected. As a result, large eddies are practically inviscid. Moreover, large eddies interact with the mean flow and extract energy. This process is known as “vortex stretching”. This is explained as follows: the mean flow velocity gradients in sheared flows distort the rotational turbulent eddies. When eddies are suitably aligned, the different ends of the vortex are forced to move with different velocities. The latter results in vortex stretching. It is important to note that angular momentum is conserved during this process. The consequence of this is an increase in the rotation rate and a decrease in the radius of the vortex cross-section.

The case is different for the smaller eddies. These eddies are stretched mainly by the larger eddies and less by the mean flow. Via this interaction, energy exchange takes place. Kinetic energy is transferred from large eddies to smaller and smaller eddies in a process called “energy cascade”. As mentioned, the energy is acquired from the interactions with the mean flow. In further detail, the smallest scales of motion in turbulent flows, in typical engineering problems, have lengths of order between 0.1 and 0.01mm and frequencies around 10 kHz. In these scales, viscous effects dominate. The smallest eddies have a Reynolds number Re_η based on their characteristic velocity u and characteristic length η equal to 1 ($Re_\eta = u\eta/\nu = 1$). Therefore, the smallest scales in a turbulent flow are those for which the inertia and viscous effects are of equal strength. These micro scales are termed after a Russian scientist named Kolmogorov, who performed innovative research on turbulence structures in the 1940s. In Kolmogorov microscales energy losses occur. This is because, at these scales work is done against the action of viscous stresses and energy is dissipated and converted into thermal internal energy.

It has become clear up to this point that turbulence is generated and maintained by shear stresses in the mean flow. Large shear causes high and anisotropic fluctuations in turbulence properties and high interaction with the mean flow. Without shear or any other alternative energy source, turbulence gradually decays and becomes more isotropic. Therefore, even in relative simple thin shear layers, the turbulence structure basically depends on the flow itself.

As becomes apparent, the study of turbulence is a very complicated topic. Most of the engineering applications include interaction between the flow and structures, which in general are turbulent flows. The structures are often treated like solid walls, which cause shear stresses due to wall friction. Solid walls cause damping of the turbulent velocity

fluctuations perpendicular to them. In the region adjacent to the wall, a complex flow with rapid changes in the mean and fluctuating velocity takes place. The turbulence structure is very dependent on the geometrical features of the walls.

In conclusion, when performing flow calculations, it is important to describe turbulence sufficiently in order to capture all the above effects and even further interactions of turbulence and body forces (Versteeg & Malalasekera, 2007).

2.5.2 Characteristics of turbulence

After the introduction to the generic principles of turbulence, it is important to point out some characteristics of turbulent flows. In practice, most engineering problems include turbulent flows, which are characterised by the following properties (Ferziger & Peric, 2002):

- Turbulent flows are highly unsteady, which is their basic characteristic resulting to a chaotic behaviour.
- Turbulent flows are three-dimensional. Even though the time-averaged velocity is a function of two coordinates in the end, the real flow field includes velocities in all three spatial dimensions that fluctuate in smaller scales.
- Turbulence flows have different vortex structures spanning in a broad range of length scales.
- Turbulent flows contain an important amount of vorticity. The turbulence is maintained and increased by extracting energy from the main flow through the process of vortex stretching.
- Turbulence results in turbulent diffusion in the flow. This is a process that tends to increase the rate at which conserved quantities are mixed. When fluid elements with different concentrations of a conserved property are brought into contact, mixing by turbulent diffusion takes place and the concentrations change.
- Turbulence causes energy dissipation to the flow. When fluid elements of different momentum are brought in contact, the action of viscosity reduces the kinetic energy of the flow, due to reduction of the velocity gradients. The energy is converted to internal fluid energy or heat.
- Despite the fact that turbulent flows have coherent structures and most of the events that take place in these flows are repeatable and deterministically defined, turbulent flows include a strong element of randomness. This is the reason that makes turbulent flows to differ in size, strength and temporal characteristics.

The complexity of turbulent flows has its source to the spatial and temporal variations in the flow field. Understanding and predicting turbulence is a demanding task. Even more challenging is the mathematical description and numerical modelling of turbulent flows.

2.5.3 Mathematical modelling of turbulence

The complexity of turbulent flows precludes any easy and economical mathematical description of the motion of the fluid particles. A suggested practice is to treat the total velocity as a summation of a mean and a fluctuating component. Therefore the velocity is decomposed into a mean value U with a superimposed fluctuating component $u'(t)$, thus $u(t) = U + u'(t)$. This interpretation method is called Reynolds decomposition and applies

to all flow properties, which are characterized in terms of mean values (U, V, W, P etc.) and their fluctuations (u', v', w', p' etc) (Versteeg & Malalasekera, 2007).

The numerical modelling of turbulent flows is based on different approaches, which can be allocated in six distinguished categories, most of them further divided in sub-categories. The categories are presented in the list below. This classification scheme was first introduced by Bardina *et al.* (1980). Different models have been developed for each category following different concepts to predict turbulence.

It will be apparent that as one progresses down the following list, more and more of the turbulent properties are computed and fewer are approximated by models. Therefore, the models close to the bottom of the list become more complicated and computationally expensive, as well as being more accurate.

According to Ferziger & Peric (2002) the six groups are:

1. In the first approach, correlations are included. For example these correlations relate the friction with the Reynolds number or give the Nusselt number, which is the ratio of convective over the conductive heat transfer, as a function of Reynolds and Prandtl numbers, which are the ratio of inertia over the viscous forces and the ratio of the viscous over the thermal diffusion rate respectively. This method can be very useful for simple types of flows that can be described by a few parameters only. This simple approach is often taught in introductory courses.
2. The second approach employs integral equations that are derived from the equations of motion by interpolating over one or more coordinates. This method simplifies the problem to one or more ordinary differential equations, which are easily solved using solving techniques for ordinary differential equations.
3. The third method is called one-point closure and it is based on the averaging of the equations of motion. The averaging can be performed a) over time, b) over a coordinate in which the mean flow remains steady or c) over ensemble of realizations. This is possible if the flow is assumed to stay statistically steady, not to vary or to keep fixed all the controllable factors respectively. This interpretation leads to a set of partial differential equations, namely RANS, which is not "closed" and it requires extra approximations, namely turbulence models.
4. The fourth method is called two-point closure, because it correlates the velocity components at two spatial points. This is achieved by the use of correlation equations or commonly the Fourier transform of these equations. The two-point closure is mainly used for homogeneous turbulence cases.
5. The fifth method is called Large Eddy simulation (LES) and it accounts for the largest scale motions in the flow. At the same time it approximates smaller scale motions using a sub grid scale model. LES can be considered as a compromise between the simpler one-point closure models and the much more complicated DNS method that follows.
6. The sixth and most advanced method of describing turbulence is the Direct Numerical Simulation (DNS). This method does not include any approximation or models and solves the Navier-Stokes equations for all the motions in a turbulent flow. All scales of turbulence are properly described.

Even though a lot of work has been done in the field of the modelling of turbulent flows, it still remains a challenging topic and new more accurate and economical models continue to appear.

3. Fundamentals of Wave Mechanics

3.1 Introduction

In chapter two the basics of fluid dynamics were presented. This chapter focuses on water wave mechanics useful in marine and ocean engineering applications. Wave mechanics is a specific domain of fluid mechanics. Many of the mathematical descriptions include important simplifications and some others are based on empirical formulas.

When a fluid is in a stationary state, the forces of gravity and surface tension act on it, tending to maintain it in this state and keep the level of the free surface constant. However, the fluid might be excited by some external forces and when this happens waves are created on its free surface. Once a wave is created, the same gravitational and surface tension forces will allow the wave to propagate (Dean & Dalrymple, 1991).

There are many different types of waves, characterised by different sizes and speeds of propagation. Different stimulation forces result in different types of waves. The size and the form of the wave that will be created depends on the magnitude of the force that will excite the water, as well as from the way that this force will act on the fluid body. In other words, how strong the force is and how quickly it is applied on the fluid mass. The magnitude of the force is related to the displaced volume of water, while the speed of action of the force is related to the pressure field that will be created. The schematic below shows in a quasi-spectral representation the wide span of the water waves in nature (Holthuijsen, 2007). The terms frequency and period will be explained later.

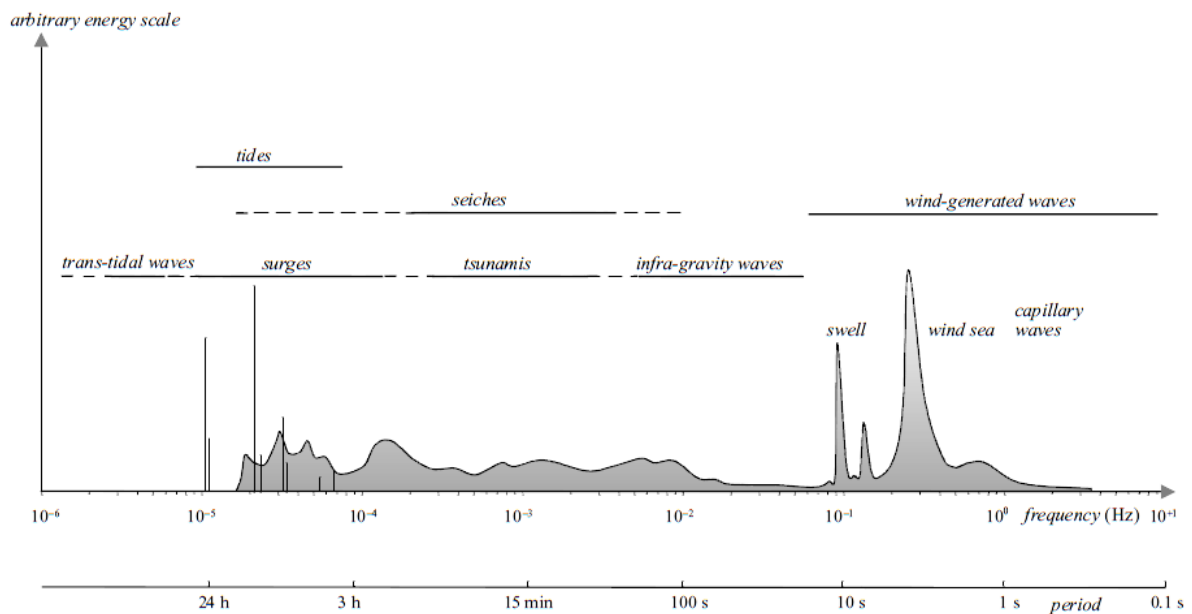


Figure 3.1: Spectral categorization of surface water waves

It can be seen that the longest waves, those with the lowest frequency, are the tidal waves or simply the tides. These are the longest known waves circling halfway the earth from end to end propagating with significant speeds. Tides are caused by the gravitational forces from the moon, sun and other astronomical bodies. On the other hand, there are very short waves in scales of a centimetre or less. These waves are high frequency waves and they

are controlled by the surface tension forces. Extrapolating, the length of the wave gives an important information on the type of the forces that created it. The longer the wave is, the more dominant the gravitational forces are in comparison to surface tension and vice versa.

There are hardly any fluids with free surface in nature that include no wave motion. A body that is near or in the water experiences the forces of the wave action. Therefore, study of wave modelling is of great importance in order to predict correctly the wave forces. In practice, these forces cause morphological change to the coastline by moving tremendous amounts of sediments along the shore or create “freak” waves up to 34m in height, which are great threat to the survivability of ships or offshore structures, such as oil platforms and wave energy converters. Moreover, when a ship moves, the forces of waves pose an important portion of resistance to their motion, causing delays or increased fuel consumption. Thus, it is clear that the study of waves and their numerical modelling has not only an academic interest, but is also of considerable economic importance.

3.2 Characteristics of waves

At this point it is important to introduce some basic terminology regarding the physical features of the waves. The water waves are described by their length (L), height (H), and the water depth (h) over which they are propagating. Other variables, such as particle velocities, pressures and accelerations can be explicitly mathematically calculated from the basic three quantities. The following schematic is a “snapshot” of a two-dimensional wave propagating in the x direction (Dean & Dalrymple, 1991).

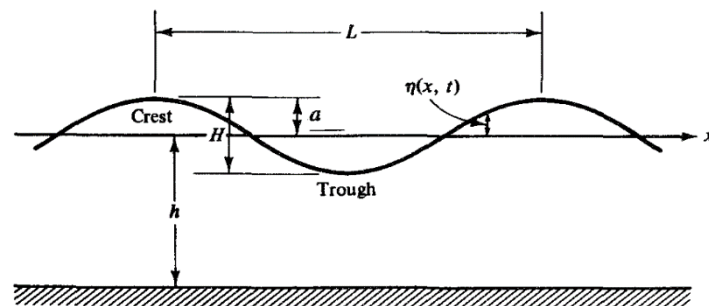


Figure 3.2: Characteristics of a 2D linear water wave

This is the most simplistic representation of a sinusoidal wave, where a represents the wave amplitude, i.e. the vertical distance between the mean water level and the crest height and $\eta(x, t)$ represents the vertical position of the free surface at a specific location and time. L, H and h have been mentioned previously. The coordinate axis that will be used to describe wave motion will be located at the still water line, $z = 0$. The bottom of the water body will be at $z = -h$.

The wavelength L is defined as the horizontal distance between two successive wave crests or troughs. The wave length is related with the wave period and water depth through the dispersion relation, which will be discussed later. The wave period T is the required time for two successive crests or troughs to pass from a fixed point in space. Eventually, in time T ,

the wave moves distance equal to L . Therefore the speed of the wave, namely wave celerity C , can be defined as $C = L/T$. It is important to point out that as the wave propagates, the water mass that comprises the wave does not translate in the direction of the wave. The particles move in orbital trajectories and practically the wave is a transfer of energy.

Waves in nature rarely appear to look exactly the same from wave to wave, nor do they always propagate in the same direction. This sea state can be seen to be a superposition of a large number of sinusoids going in different directions. It is this superposition of sinusoids that permits the use of Fourier analysis and spectral techniques in order to describe a sea state. There is a great amount of randomness in a sea, and statistical techniques need to be brought to bear. Fortunately, very large waves or waves in shallow water appear to be more regular than smaller waves and not so random. Therefore, in these cases, each wave is more readily described by one sinusoid, which repeats itself periodically.

3.3 Wave theories

3.3.1 Linear wave theory (Stokes 1st)

As mentioned in the previous paragraph, random ocean waves are assumed to be a summation of independent harmonic waves. Therefore, the understanding of these harmonic waves is necessary for understanding random waves. Harmonic waves can be described in detail with linear theory for surface gravity waves. Linear theory is only valid for small amplitude waves; small compared to the wave length and the depth. Linear theory is also called Airy theory and linear waves, Airy waves.

Linear theory is based on two fundamental equations: the mass balance equation and the momentum balance equation. These equations can be expressed in terms of an auxiliary function Φ , namely the velocity potential function, which results in Laplace and Bernoulli equations. When combined with appropriate boundary conditions, which account for the kinematic and dynamic nature of the waves, these equations describe harmonic waves. The boundary conditions need to be applied on the lateral boundaries of the domain, i.e. the upstream and downstream sides of the virtual wave tank, and the water surface and bottom. The assumption for reducing the waves into two dimensions is that the wave has infinitely long crests in the y -direction (see Figure 3.2).

At the water surface, the main restriction that defines the boundary conditions is that water particles are not allowed to leave the surface. Therefore, the velocity of the water particles normal to the surface equals the speed of the surface in the corresponding direction. At the same time, the kinematic boundary condition for the bottom does not allow the particles to penetrate the seabed. These two boundary conditions are expressed mathematically as follows:

$$u_z = \frac{\partial \eta}{\partial t} \quad \text{at } z = 0 \quad \text{and} \quad u_z = 0 \quad \text{at } z = -d \quad (3.1a, b)$$

where η is the surface elevation, measured vertically and being positive when moving upwards from still-water level.

Gravity waves, also named free waves, are subject only to gravity force and only atmospheric pressure is applied at the water surface. Atmospheric pressure is assumed to be constant and for simplification it is taken as zero:

$$p = 0 \quad \text{at} \quad z = 0 \quad (3.2)$$

In order to find analytical solutions for the energy balance equations and boundary conditions, it is necessary to consider an abstract function. In this case, the velocity potential function $\Phi = \Phi(x, y, z, t)$ is employed, for which the spatial derivatives are equal to the velocities of the water particles. Assuming that the flow is irrotational, Φ reads:

$$\Phi(x, y, z, t) \quad \text{defined such that} \quad u_x = \frac{\partial \Phi}{\partial x}, \quad u_y = \frac{\partial \Phi}{\partial y}, \quad u_z = \frac{\partial \Phi}{\partial z} \quad (3.3a, b, c)$$

If the continuity equation is written in terms of the function Φ , the well known Laplace equation is derived. Similarly, the linearised Bernoulli equation for unsteady flow is derived from the momentum equations.

Regarding the dynamic boundary conditions, they can be expressed using the velocity potential and the linearised Bernoulli equation at the free surface. The free surface is assumed to be at $z = 0$ instead of $z = \eta$, since small amplitude theory is used, and pressure equals zero ($p = 0$).

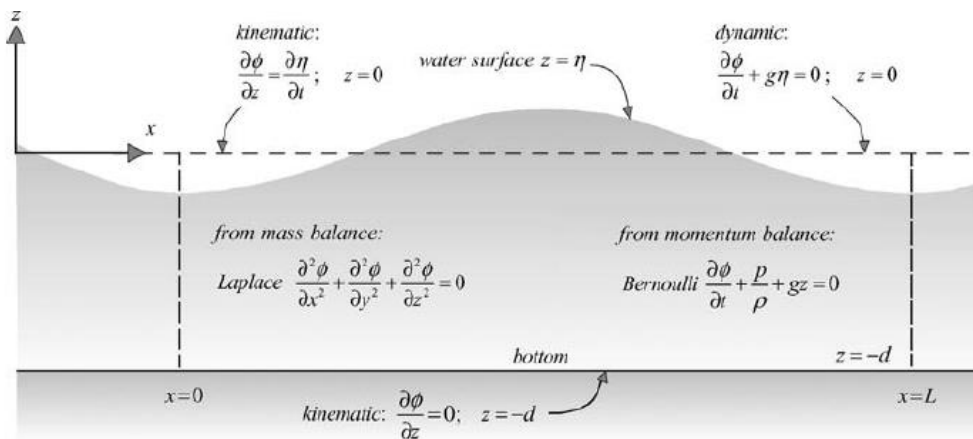


Figure 3.3: Basic equations and boundary conditions for a wave according to linear wave theory, in terms of the velocity potential (Holthuijsen, 2007)

Combining Laplace's equation with the kinematic boundary conditions mentioned before gives the solution of a long-crested harmonic propagating wave in the x-direction, which reads:

$$\eta(x, t) = a \sin(\omega t - kx) \quad (3.4)$$

The corresponding velocity potential function is given by:

$$\Phi = \hat{\Phi} \cos(\omega t - kx) \quad \text{with} \quad \hat{\Phi} = \frac{\omega \alpha \cosh[k(d+z)]}{k \sinh(kd)} \quad (3.5)$$

Using the definition of Φ and the previous equation, the particle velocities can be obtained. The velocity components are the spatial derivatives of Φ : $\partial\Phi/\partial x = u_x$ and $\partial\Phi/\partial z = u_z$. Therefore, the particle velocities are given by:

$$u_x = \omega \alpha \frac{\cosh[k(d+z)]}{\sinh(kd)} \sin(\omega t - kx) \quad \text{and} \quad u_z = \omega \alpha \frac{\sinh[k(d+z)]}{\sinh(kd)} \cos(\omega t - kx) \quad (3.6\alpha, \beta)$$

The velocity in the y-direction is zero since the wave is propagating in the x-direction only: $u_y = 0$.

Substitution of the velocity potential into the Bernoulli equation reveals the analytical expression for the pressure, which is the sum of the hydrostatic pressure under the wave and the hydrodynamic pressure. The pressure equation reads:

$$p = -\rho g z + \rho g \alpha \frac{\cosh[k(d+z)]}{\cosh(kd)} \sin(\omega t - kx) \quad (3.7)$$

3.3.1.1 The dispersion relationship

So far, the boundary conditions and velocity potential function have been stated for a free travelling wave, subject only to gravitational force. The surface profile is expressed by the harmonic function, which can be substituted, together with the velocity potential, in the zero atmospheric pressure condition on the free surface. This reveals a relationship between the angular frequency ω and wavenumber $k = 2\pi/L$.

$$\omega^2 = gk \tanh(kd) \quad \text{or} \quad L = \frac{gT^2}{2\pi} \tanh\left(\frac{2\pi d}{L}\right) \quad (3.8)$$

Equation 3.8 is called the dispersion relationship, which is an implicit expression of the wave number. This means that an iteration process is required to calculate the wave number for a given for a specific frequency and depth.

3.3.1.2 Deep water approximation

Deep water is considered when $kd \rightarrow \infty$. This results to the reduction the amplitudes of the velocity components to an exponential function:

$$\frac{\cosh[k(d+z)]}{\sinh(kd)} = \frac{\sinh[k(d+z)]}{\sinh(kd)} = e^{kz} \quad (3.9)$$

In practice, these expressions imply that the wave-induced velocities decrease exponentially with increasing distance from the surface. Water particles move in circles of decreasing radius towards the sea bottom. Eventually, the amplitude of the wave is equal to the radius of the biggest circle on the free surface.

A practical way to check if the wave propagates in deep water is to compare the depth with the wave length. If $d > 0.5L$, the deep water approximation is valid. The wave length in deep water can be calculated explicitly and the celerity of the wave is given only a function of the period only (Koutitas, 1988):

$$L_0 = \frac{gT^2}{2\pi} \quad \text{and} \quad C_0 = \frac{gT}{2\pi} \quad (3.10)$$

3.3.1.3 Shallow water approximation

For shallow waters, $kd \rightarrow 0$ and the amplitudes of the wave-induced velocities can be simplified to:

$$\frac{\cosh[k(d+z)]}{\sinh(kd)} = \frac{1}{kd} \quad \text{and} \quad \frac{\sinh[k(d+z)]}{\sinh(kd)} = 1 + \frac{z}{d} \quad (3.11)$$

Two important conclusions regarding the particle kinematics can be drawn from the previous expressions. The first one shows that the amplitude of the horizontal velocity is constant over the vertical axis and it does not depend on the depth. The second one shows

that the amplitude of the vertical velocity increases linearly from the seabed to the surface. The orbits of the particles in shallow waters are elliptic.

Shallow water approximation can be considered when $d < 0.05L$. In a shallow water regime, the celerity is calculated only by the depth and the wave length is proportional to the wave period (Koutitas, 1988):

$$C = \sqrt{gd} \quad \text{and} \quad L = CT = T\sqrt{gd} \quad (3.12)$$

3.3.1.4 Phase and group velocity

The dispersion relationship can be used to calculate the propagation speed of the wave at any depth, given only the wave period: $c = L/T = \omega/k$. c is also known as phase speed and it is calculated by:

$$c = \frac{g}{\omega} \tanh(kd) = \sqrt{\frac{g}{k} \tanh(kd)} \quad (3.13)$$

It should be pointed out that the phase speed depends on the wave number, which is a function of the frequency. As a result, long waves travel faster compared to short waves. These waves, whose propagation speed depends on the wave length and frequency, are called dispersive waves.

When waves travel in the ocean, they form groups comprising of different components. Assuming that the difference between the frequencies is infinitely small, the difference between the wave numbers is also infinitely small and the velocity of the group can be calculated from the phase velocity as shown below:

$$c_{group} = \frac{\partial \omega}{\partial k} = nc \quad (3.14)$$

where c is the phase speed of the wave and n is calculated from the dispersion relationship as a function of the wave number and the depth:

$$n = \frac{1}{2} \left(1 + \frac{2kd}{\sinh(2kd)} \right) \quad (3.15)$$

As shown previously, kd varies between zero and infinite and therefore $2kd/\sinh(2kd)$ varies between zero and one. As a result, $0.5 \leq n \leq 1$; $n = 0.5$ for deep water and $n = 1$

for shallow water. This indicates that the phase speed (speed of an individual wave) is always equal or greater than the speed of the group: $c \geq c_g$. More specifically, in shallow waters, the individual components travel at the same speed of the group, maintaining their position in the group. On the other hand, in deep and intermediate waters, the individual waves of the group travel faster than the group and the consequence of this is that each wave seems to be born at the tail of the group, travel forward in the group and disappear at the front of the group. This is only a visual effect, since it is not the waves that propagate, but the wave energy that keeps the group alive.

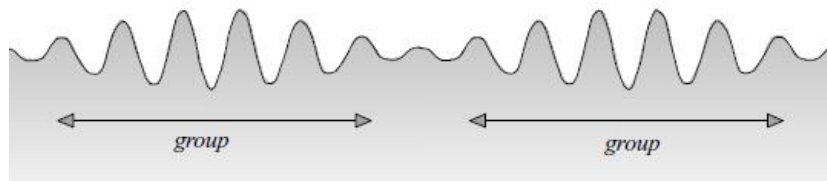


Figure 3.4: Formation of wave groups

Since ocean waves propagate in groups, their travel times should be calculated from the group velocity and not the phase velocity. At the same time, the dependence of the group velocity on frequency results to the disintegration of the wave groups. Longer waves travel faster ahead of the shorter waves and wave energy disperses across the ocean. A consequence of that is the transformation of an irregular sea created by a storm into regular swells.

3.3.1.5 Wave energy

It can be easily perceived that since the water particles move when a wave passes, there is a transfer of energy in the water. The total energy of the particles is the sum of the potential and the kinetic energy. The first is calculated from the work done against gravitation to change the position of the particles, and as water particles move continuously, they also have kinetic energy.

Potential energy can be calculated in a small water element of thickness Δz covering an horizontal surface area $\Delta x \Delta y$. Considering a reference level of $z = 0$, the instantaneous potential energy is given by the product of mass and elevation from $z = 0$: $\rho g \Delta x \Delta y \Delta z \times z$. The wave-induced potential energy is then calculated by the difference of the potential energy between the presence and absence of the wave. Integrating to the water column from bottom to surface and averaging over one wave period, the potential energy is given by:

$$E_{potential} = \overline{\int_{-d}^{\eta} \rho g z dz} - \overline{\int_{-d}^0 \rho g z dz} = \overline{\int_0^{\eta} \rho g z dz} \quad (3.16)$$

where the overbar represents time-averaging.

For a linear wave with amplitude α , the previous integral yields:

$$E_{potential} = \overline{\frac{1}{2} \rho g n^2} = \frac{1}{4} \rho g \alpha^2 \quad (3.17)$$

The instantaneous value of kinetic energy is given by: $\frac{1}{2} \rho \Delta x \Delta y \Delta z u^2$ (where $u^2 = u_x^2 + u_z^2$), for the same water particle as above. Time averaging over the wave period and integration in the entire water column results to the following expression:

$$E_{kinetic} = \overline{\int_{-d}^{\eta} \frac{1}{2} \rho u^2 dz} \quad (3.18)$$

Considering a harmonic wave of amplitude a and using the expressions for u_x and u_z from the linear theory, the kinetic energy is given by:

$$E_{kinetic} = \frac{1}{4} \rho g \alpha^2 \quad (3.19)$$

Comparing the expressions of potential and kinetic energy for a linear wave it is easily noticeable that $E_{potential} = E_{kinetic}$. The total time-averaged wave-induced energy density $E = E_{potential} + E_{kinetic}$ is then:

$$E = \frac{1}{2} \rho g \alpha^2 = \frac{1}{8} \rho g H^2 \quad (3.20)$$

It should be pointed out that the expression of wave energy has been derived according to linear theory assumptions, which is based on the small-amplitude approximation. As discussed before, linear theory matches the spectral description of ocean waves perfectly and the propagation speed of wave energy equals the group velocity of the waves. In many cases though, waves turn out to be very steep or the water is too shallow for linear theory to be valid. The description of such waves is feasible through nonlinear wave theories that are presented in the next paragraphs.

3.3.2 Nonlinear waves

3.3.2.1 Introduction

Nonlinear wave theories describe a wave of constant shape, amplitude and length, similarly to linear theory. The nonlinear theories have analytical expressions (Holthuijsen, 2007). Additionally, more recent theories are based on partial differential equations and allow waves to evolve, as they propagate from deeper to shallower waters. These extended theories can account for complex phenomena such as mass transport caused by the small net forward movement of water caused by the wave (CEM, 2002).

For complex sea states, the conventional approach treats each wave individually and independently, meaning that the wave characteristics are computed for each wave separately according to the chosen nonlinear theory. A large number of waves is then superimposed in order to replicate the sea state, whose statistical characteristics are calculated from the total number of waves.

3.3.2.2 Stokes theory of nonlinear waves

In 1847, Stokes published his work for nonlinear waves, according to which a wave can be approximated by adding extra harmonic waves to the basic harmonic. Each time a harmonic is added, the order of the wave increases by order of one. Every higher order correction is calculated by the previously obtained lower order correction, so that the process is successive. Stokes theory is based on the velocity potential (Dean & Dalrymple, 1991).

Some of the major differences between linear wave theory and high-order theories are that linear theory predicts a harmonic wave which is symmetrical about the still water level (SWL) and that water particles move in closed paths. On the other hand, even though high order waves are symmetrical about the vertical axis, they are asymmetrical about the SWL, having steeper crests and flatter troughs compared to linear waves. At the same time, some high order theories can predict open water particle orbits (CEM, 2002).

The easiest example to understand the formulation of higher order waves is the second-order Stokes wave. By adding the second harmonic to the linear basic harmonic, the surface elevation is given by:

$$\eta(x, t) = \alpha \cos(\omega t - kx) + ka^2 \frac{\cosh(kd)}{4 \sinh^3(kd)} [2 + \cosh(2kd)] \cos[2(\omega t - kx)] \quad (3.21)$$

A relatively new and practical wave theory covering applications from deep to shallow waters is fifth-order Stokes finite-amplitude wave theory (Fenton, 1985). Stokes fifth order wave theory has many advantages as it shows good convergence properties and it is computationally efficient. It also includes closed-form asymptotic expressions for both deep and shallow wave limits. One of the most important aspects of Stokes fifth order theory is that it can account for open orbits of water particles, which result in the description of a drift or mass transport in the direction of wave propagation. Additionally, this expansion shows a secondary crest in the wave trough for waves with high amplitudes (Peregrine 1972; Fenton 1985).

3.3.2.3 Stream function

Another theory based on similar principles to Stokes' high order theories has been developed by Dean in 1965. It is called Stream function theory and is computationally simpler and orientated to computer applications. Instead of adding harmonics through successive corrections, Dean's corrections are obtained simultaneously and they satisfy the dynamic boundary condition exactly. The second difference is that instead of forming the waves in terms of the velocity potential, Dean employed another equivalent function, i.e. the Stream function (Dean & Dalrymple, 1991).

The linear form of the stream function for water waves is

$$\psi(x, z, t) = -\frac{H g \sinh[k(d+z)]}{2 \sigma \cosh(kd)} \cos(kx - \sigma t) \quad (3.22)$$

In analogy to Stoke's theory, the N^{th} - order Stream function has the following form:

$$\psi(x, z) = \sum_1^N X(n) \sinh[nk(d+z)] \cos nkx \quad (3.23)$$

It should be noted that none of the previous wave theories is able to perform well in very shallow water, where the water depth is of the same order of the wave height or even less. For such conditions, other wave theories should be considered, namely Cnoidal and solitary wave theory.

3.3.2.4 Cnoidal and solitary wave theory

A shallow water wave theory was developed in 1895 by Korteweg and Devries, allowing periodic waves to exist even in very shallow waters. This theory is called Cnoidal theory and it is based on the Boussinesq equations, restricted though to wave propagation in one direction only. The wave profile is computed by Jacobian elliptic integral. The theory was named Cnoidal to be consonant with the sinusoidal and Airy theory, since the water profile is expressed in terms of cosines, at least to one of its limits. At the other limit, waves reduce to the solitary wave. Therefore, Cnoidal theory spans from linear to solitary waves. According to any given wave amplitude, wave length and water depth; the velocity potential and hence all the wave characteristics are computed through Cnoidal theory.

It is interesting to see how Cnoidal theory behaves in shallow water. As the water depth decreases, the profile of the wave changes shape developing sharper crests and flatter troughs. This effect is equivalent to the nonlinear effect of water steepness. In the specific case that water depth approaches zero ($L/d \rightarrow \infty$), the wave length and period become infinite. In this case, the wave lies entirely above the SWL and it is not periodic anymore. This wave is named solitary wave or soliton. In a solitary wave the water particles are

transferred in the direction of the wave propagation, as the crest passes and therefore, the solitary wave is considered as a wave of translation.

It is not common to observe solitary waves in the sea, mainly because small dispersive waves exist at the trailing edge of the main wave. In some cases though, there are waves, such as tsunamis and other waves generated by large displacements of water like landslides and earthquakes, which can be sufficiently described via solitary wave theory. The same applies for oscillatory waves moving into shallow water and becoming steeper with longer and flatted troughs (CEM, 2002).

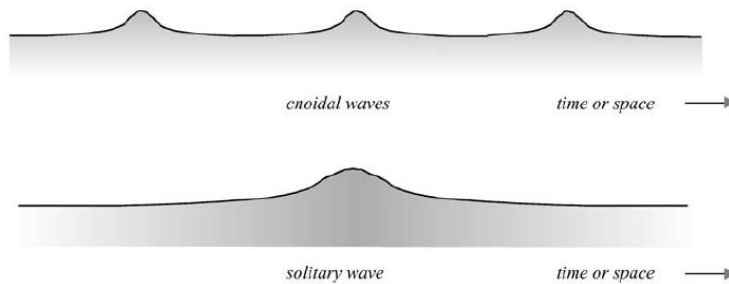


Figure 3.5: Surface elevation of cnoidal and solitary waves

The diagram depicted in Figure 3.6 (CEM, 2002) is one of the most classic in water wave mechanics. It is a handy guide for engineers that can be easily used to find which wave theory describes a wave with given characteristics.

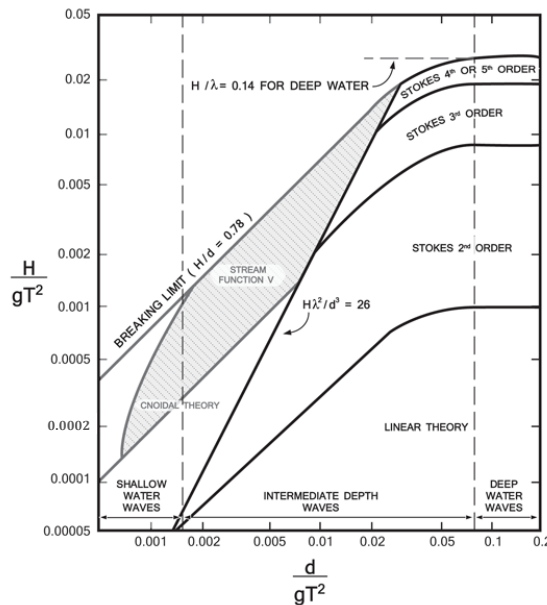


Figure 3.6: Area of applicability of wave theories according to wave characteristics: height (H), period (T) and depth of water (d)

3.4 Transformation of waves in near shore environment

3.4.1 Shoaling

Shoaling is one of the most easily recognisable processes happening in the near shore areas. For the sake of simplicity, a harmonic wave passing over a mild slope fixed seabed in the absence of currents is considered. It is easy to observe that as the wave approaches the coastline, it slows down, thus maintaining its frequency. According to the dispersion relationship, the wave length will decrease and the phase speed will correspondingly decrease as well, approaching the group celerity. In other words, in shallow waters, waves become less and less dispersive, meaning that the phase speed is less dependent on the wave frequency. However, as the wave approaches the waterline, the applicability of linear theory becomes less valid. This is because, the phase and group velocities approach zero, causing the wave amplitude to approach infinity (Holthuijsen, 2007).

The change in the wave height due to shoaling can be easily estimated from the following relationship:

$$H_2 = H_1 \sqrt{\frac{C_{g1}}{C_{g2}}} = H_1 K_s \quad (3.24)$$

where K_s is the shoaling coefficient.

This simple relationship is derived by considering the conservation of energy in a steady state case. The phenomenon is examined in a control volume, where no energy generation or dissipation is allowed. Since, there are no source terms in the control volume, wave energy can only enter the control volume via plane 1 and leave via plane 2. The rate at which energy enters and leaves the control volume per unit time is $P_1 b$ and $P_2 b$ respectively, where $P = EC_g$ is the energy transport per unit crest length and b is the distance between the two lateral sides. According to the conservation of energy, $P_1 b = P_2 b$. Replacing P with EC_g in the equality and doing the same for E , which is proportional to the square of the wave height, the previous equation is readily obtained.

When the wave passes over an arbitrary seabed topography other processes, such as refraction and wave breaking, are dominant. These processes are discussed in the following paragraphs.

3.4.2 Refraction

The refraction of water waves refers to the change of the direction of propagation of the waves, due to change on the wave velocity. Wave refraction is analogous to the optic refraction and it satisfies Snell's law:

$$\frac{\sin \theta}{C} = \frac{\sin \theta_0}{C_0} \quad (3.25)$$

The result of refraction is the gradual change in the direction of the waves when they approach a coastline at an angle, known as oblique incidence. As waves propagate towards a coast, wave crests tend to become parallel to the coastline. The principle of refraction can be explained simply: since phase velocity is related to the water depth via the dispersion relationship $c = \sqrt{\frac{g}{k} \tanh(kd)}$, the depth variation will cause different propagation velocities. It is readily seen that the wave crest moves faster in deeper water than in shallower water. Considering a cross section along a wave crest of an oblique wave, one part of a wave will move faster than the other one. If the crest moves over a large distance, the result will be to turn the wave towards the region with shallow water, i.e. the coast. A general rule to remember is that a wave always turns towards the region with lower propagation speed. On the other hand, if a wave is parallel to the shoreline, it is not refracted (see Snell's law for $\theta = \theta_0$) (Dean & Dalrymple, 1991).

Moreover, refraction has an effect on the wave height. To derive the relationship that accounts for that effect, the conservation of energy in a steady-state case has to be employed. Considering a control volume with no energy losses or sources, the energy that enters the control volume through plane 1 ($P_1 b_1$) is equal to the energy leaving the control volume at plane 2 ($P_2 b_2$), where P is the energy transport per unit crest length and b is the distance between the two wave rays. Substituting the energy with its expression (see paragraph 3.3.1.5), the height of the wave in plane 2 can be obtained from the wave height in plane 1 (Holthuijsen, 2007):

$$H_2 = H_1 \sqrt{\frac{C_{g1}}{C_{g2}}} \sqrt{\frac{b_1}{b_2}} = H_1 K_s K_r \quad (3.26)$$

where K_s is the shoaling coefficient and K_r the refraction coefficient.

3.4.3 Diffraction

Wave diffraction is defined as the spreading of energy laterally perpendicular to the dominant direction of wave propagation. The result is that wave energy spreads behind obstacles and waves appear in sheltered areas. If diffraction would not exist, no wave disturbance would appear in the "geometric shadow zone" of physical obstacles and waves would propagate along straight wave rays, assuming that refraction is absent (Dean & Dalrymple, 1991).

The simple schematic in Figure 3.7 illustrates the circular pattern of wave crests as they penetrate in the shadow zone of obstacles. The left one shows the transmission of disturbance behind a pier head, while the right one shows the penetration of waves from a small opening between two successive breakwaters.

The wave height diminishes rapidly as waves are diffracted further behind the obstacles. Analytical solutions to estimate the wave height for simple cases of refraction are available. For the case of a straight, semi-infinite breakwater located at constant depth, with reflections coming off only by the breakwater itself, Sommerfield developed an analytical

solution for light waves in 1896 (Holthuijsen, 2007). If reflected waves are ignored, graphical methods can be used to approximate the diffraction coefficient K_D and through it the wave height. K_D is a function of the wave length, the angle of incidence between the breakwater and the wave and the distance between the head of the breakwater and the point of calculation (Koutitas, 1988). For more complicated cases, the utilization of numerical models is necessary.



Figure 3.7: Wave diffraction behind semi-infinitely long obstacles

3.4.4 Waves breaking in shallow water

Wave breaking is one of the most complicated phenomena that take place in coastal waters and there is still a lot of on-going research related to the effects of wave breaking in shallow waters.

Looking back to shoaling (§ 3.4.1), the shoaling coefficients suggests that the wave height will increase to infinity in very shallow water, which is clearly unrealistic. Observing the waves propagating in shallow water, they become steeper and after some depth they become unstable and break. Wave breaking is related to energy dissipation in the form of turbulence and work against the bottom friction.

There are different types of wave breaking that depend on the characteristics of the wave and the bottom topography: a) Spilling breaking is common for mild-slope beaches and it spans within the whole surf zone, which is defined as the area extending from the coastline to the seaward limit of the breaking; b) Plunging breaking is easy to spot, since waves curls forward and impinges onto part of the preceding trough. A formation of tube, caused by the wave crest takes place, making the phenomenon very spectacular and violent since the trapped air escapes by bursting through the back of the wave or by blowing out at a nonbreaking section of wave crest; c) Surging breaking occurs on very steep beaches forming a very narrow or even non-existing surf zone. The reflection in this case is quite high; d) Collapsing breaking is the fourth classification for breaking suggested by Galvin (1968) and it comprises of a combination of plunging and surging breaking (Dean & Dalrymple, 1991).

The depth at which wave breaking starts was estimated by McCowan in 1984 and it is the simplest and earliest breaker criterion. The breaking height of the wave is H_b is equal to a fraction of the water depth h_b :

$$H_b = kh_b \quad (3.27)$$

where $k = 0.78$ and the subscript b denotes the value at breaking.

Weggel (1972) performed many laboratory tests showing the association of the breaker height to the beach slope, denoted as m .

Wave breaking still remains one of the most challenging areas of research, and can cause large wave impacts on coastal structures. When designing a structure inside the surf zone it is necessary to be able to predict the location of the breaker line and the beach topography in order to identify the type of wave loading.

3.4.5 Wave reflection

Wave reflection occurs when a wave hits an obstacle and wave energy travels back into the open sea. A vertical frictionless wall may reflect 100% of the incoming wave energy. However, there are not only vertical walls or cliffs that reflect the waves, and even mild slopes reflect some amount of wave energy. For very mild-slope sandy beaches, reflection might be deemed insignificant and it is often ignored. In more complicated situations, such as rocky coasts, reflection is very hard to estimate. Between these two limiting cases, there are many less intricate, but variable cases of reflection, where numerical models can be applied. Wave diffraction models can give accurate results in most of the cases. In the specific situation that reflection is fairly homogenous, spectral models based on energy balanced equation and combined with appropriate reflective boundary conditions can also perform well.

The mathematical description of wave reflection lies in the concept of calculating the wave motion as a sum of the incident wave and the reflected wave. If the physical phenomenon of reflection has sufficient time to develop, a kind of standing wave shape will start forming. The simplest case is a wave reflecting on a vertical wall located at $x = 0$ and forming a standing wave. The wave profile is then the summation of the incident and reflected wave given by:

$$\eta(x, t) = a_i \sin(\omega t - kx) + a_r \sin(\omega t + kx) \quad (3.28)$$

where a_i and a_r are the amplitudes of the incident and reflected wave respectively.

As mentioned before, more commonly, reflection is far less than 100% and therefore $a_r < a_i$. The wave field formed is not a fully standing wave, but a partially standing wave. In these cases, it is important to determine the reflection coefficient $K_{refl} = a_r/a_i$. In the laboratory it can be calculated by measuring the maximum and minimum amplitudes along the flume. In real coasts and structures the situation is more complicated, because there are other phenomena, such as wave breaking included and determination of the reflection coefficient cannot be done theoretically. A parameter called the Iribarren number is employed for these complex cases. The Iribarren number is based on observation and it is defined as a function of the bottom gradient and wave steepness as:

$$\xi = \tan \alpha / \sqrt{H/L_0} \quad (3.29)$$

where α is the bottom slope, H is the incident wave height and L_0 is the deep-water wave length.

The reflection coefficient can be calculated in terms of the Iribarren number for some simple cases like: a) gentle slopes or steep waves on flat, smooth, impermeable, inclined surfaces, observations show that $K_{refl} \approx 0.1\xi^2$ with $\xi < 2.5$; b) For the same conditions ($\xi < 2.5$), but for rough or permeable surfaces the reflection is less down to 50%; c) For different conditions, such as steep slopes or lower wave steepness, waves tend not to break and reflect with higher reflection coefficient: $K_{refl} > 0.1\xi^2$ with $\xi > 2.5$.

3.4.6 Wave-current interaction

So far, waves have been examined independently from tides and currents. In real seas though, the presence of currents has important consequences on the propagation of waves. Time-varying water depths and ambient currents might be generated due to tides, storm surges or river discharges. They result to changes in the amplitude, frequency and direction of the incident waves (Dean & Dalrymple, 1991).

Changes in amplitude might occur due to several causes like energy bunching from shoaling, current-induced refraction and energy exchange between the current and the wave.

Changes in frequency are closely associated to the Doppler effect. When a harmonic wave propagates at a constant depth across an ambient current, which is constant in space and time, it can be considered as propagating on a moving plate without “realizing” the existence of the current. Linear theory is still valid and its results can be applied in a frame of reference of the moving current. Two frequencies can be defined: a relative or intrinsic frequency, which is the frequency of the wave in the moving frame of reference, denoted as σ and the absolute frequency, which refers to a fixed frame of reference, such as the stationery seabed, denoted as ω (Peregrine, 1976). Absolute frequency is related to the relative frequency by the following relationship, which is derived directly from the bodily transport of the wave by the current:

$$\omega = \sigma + kU_n \quad (3.30)$$

where U_n is the component of the current in the wave direction.

Wave energy propagates in a fixed frame of reference with velocity $c_{g,absolute}$, which is computed by adding as vectors the current velocity \vec{U} and the group velocity relative to the current, $c_{g,relative}$. For the case of constant water depth and current ω and σ are constant. In any other case, they might vary.

Changes in the direction of wave propagation, i.e. refraction, are induced by current-related changes in propagation speed. Current-induced refraction is a phenomenon caused by the bodily transport of the wave by the ambient current with a varying speed, assuming that the changes occur horizontally and in time only. The result is that the direction of the wave energy is not normal to the wave crest when an ambient current is present. It is readily seen

that current-induced refraction is analogous to depth-induced refraction. As a result, waves turn towards the area with lower absolute propagation speed.

Interaction between waves and currents also leads to the exchange of energy between the two. The result is that wave energy is not conserved as the wave propagates through a current field. On the other hand, another quantity is conserved, which is the energy divided by relative frequency: $A = E/\sigma$. Wave models that account for wave–current interactions are therefore often based on an action balance equation rather than an energy balance equation (Holthuijsen, 2007).

3.5 Wave-structure interaction

3.5.1 Wave forces

The engineering interest of water wave mechanics lies basically on the determination of wave-induced forces on structures in the sea. The structures can be fixed, compliant or floating; attached to the bottom, moored or freely floating. All structures in the sea are subjected to wave forces and their accurate calculation is of great interest for the designers.

Research into wave forces is well established and has been carried out for a considerable time (Dean & Dalrymple, 1991). The most common case, which is used as a reference point is the case of wave forces on a vertical pile. This case might be one of the simplest; however a generally accepted calculation procedure has not been unanimously agreed yet. Even though there are theories able to describe accurately the motion of the particles for long-crested regular wave, there is no reliable formulation to account for the wave-pile interaction for a wide range of wave characteristics accurately. The situation becomes even more complicated for high Reynolds number turbulent flow. Most of the engineering applications occur in turbulent flows and this can be readily seen from the simple case of the vertical pile: as a wave impinges on the pile and the crest passes, the trough reaches the pile and the flow field reverses washing back the previously formed wake, forming a new wake. The complexity of the problem is revealed immediately. All the assumptions made so far are violated, i.e. irrotational flow, small-amplitude waves and small velocity.

In the next paragraphs the wave forces will be described as a composition of inertia and drag force component. There are cases according to the relative size of the structure to the wave length that one component dominates over the other. For large objects at the order of scale of the wave length, the wake effects are not important and inertia force dominates. For smaller objects, the wake plays a significant role and both inertia and drag forces are important. The roughness characteristics of the objects should also be considered. Analytical solutions are not generally available and only physical and sophisticated numerical modelling can provide reliable answers for designers.

3.5.2 From potential flow to Morison equation

To begin with, an ideal flow around a circular cylinder is considered in order to provide a framework for further wave-induced force calculations. For convenience, a section of a vertical pile is considered far from the free surface. The wave force is given by the integral of the pressure distribution around the pile according to potential flow theory. Laplace's equation is employed in three dimensions and it is assumed that the velocity field varies sinusoidally with the wave period at the far field. The pressure distribution around the

cylinder is calculated using Bernoulli's equation. The pressures are readily obtained by substitution of the velocity potential into Bernoulli's equation. For convenience, polar coordinates are used:

$$p(a, \theta) - p(l, 0) = \rho \left[\frac{U^2(t)}{2} - (1 - 4 \sin^2 \theta) + 2\alpha \frac{dU}{dt} \cos \theta - l \frac{dU}{dt} \right] \quad (3.31)$$

where α is the radius of the cylinder and θ is the angle between the velocity vector and the line that connects the point of calculating the pressure with the centre of the cylinder.

It can be seen from the previous equation that pressure is subject to two different contributions: a) the steady flow term, which is proportional to $U^2(t)$ and b) the acceleration or inertia term, due to dU/dt . These terms are analysed separately.

The steady pressure term is given as a function of the angular position around the pile:

$$p(a, \theta) - p(l, 0) = \rho \frac{U^2(t)}{2} (1 - 4 \sin^2 \theta) \quad (3.32)$$

This equation shows that the pressure is symmetrical about the pile and if no wake is considered, the pressure at the front of the pile is equal to the pressure at its back. As a result, the net pressure in the downstream direction is zero and if integrated around the pile, it gives the steady (drag) force per unit elevation, namely dF_D , which is again zero. This analysis dictates that since the pressure distribution is symmetrical, no forces are applied on a pile in ideal steady flows. However, the experimental results for similar cases indicate the existence of forces. This inconsistency lies on the unrealistic assumption of potential flow, which limits the formation of boundary layers and wake.

A more realistic approach is to consider the pressure distribution around a cylinder in a steady flow as a function of the Reynolds number R_e . In this case, R_e is defined as $R_e = UD/\nu$, where U is the velocity normal to the cylinder axis, D is the pile diameter, and $\nu = \mu/\rho$, the kinematic viscosity of the fluid. The kinematic viscosity is given as the ratio of the dynamic viscosity μ to the fluid density ρ .

For the upstream portion of the cylinder, with $\theta \leq \theta_s$, where θ_s is the separation angle, the pressure may be approximated by potential flow theory. However, for $\theta > \theta_s$, the pressure appears nearly constant. In this case, θ is a function of Reynolds number. For $0 \leq \theta \leq \theta_s$, the force on a cylinder can be approximated by the potential flow solution and by assuming a constant pressure wake. Therefore, the drag force per unit elevation reads:

$$dF_D = \rho U^2(t) a \left[\int_0^{\theta_s} (1 - 4 \sin^2 \theta) \cos \theta d\theta + \int_{\theta_s}^{\pi} \frac{p_{wake}}{\rho U^2(t)/2} \cos \theta d\theta \right] \quad (3.33)$$

Since θ_s and p_{wake} are related with the Reynolds number, the whole term within the brackets is a function of R_e . The consequence of the latter is that the term within the brackets can be substituted by another expression that is related to the R_e . The drag force per unit of elevation on the pile can be written as a function of a coefficient called the “drag coefficient”, which is a function of R_e : $C_D(R_e)$.

$$dF_D = C_D(R_e)\rho D \frac{U^2(t)}{2} = C_D\rho \frac{AU^2(t)}{2} \quad (3.34)$$

The drag coefficient C_D and its dependence on the Reynolds number has been determined through physical tests with smooth circular cylinders. C_D is commonly empirically specified and in practice, its value is taken on the order of unity. C_D depends on the roughness of the pile and the Reynolds number.

On the other hand, the unsteady pressure term in the potential flow expression for the pressure is given as an integral of the component of the force in the downstream direction:

$$dF_I = \int_0^{2\pi} \rho \frac{dU(t)}{dt} 2a^2 \cos^2 \theta d\theta - \int_0^{2\pi} \rho \frac{dU(t)}{dt} la \cos \theta d\theta \quad (3.35)$$

The second integral on the right-hand side equals zero ($\int_0^{2\pi} \cos \theta d\theta = 0$), thereby contributing no net force. On the contrary, the first term is non zero and yields:

$$dF_I = 2\rho\pi a^2 \frac{dU}{dt} = C_M\rho V \frac{dU}{dt} \quad (3.36)$$

where V is the volume of the pile per unit length and C_M is defined as the inertia coefficient.

For the case of potential flow about a circular cylinder, the inertia coefficient C_M equals 2.0. As a result, a force is generated due to the fluid acceleration behind a cylinder and it is called inertial force. The equation of the inertial force as given above, is generic and valid for two- and three-dimensional objects of arbitrary shapes. The inertia coefficients changes with the flow direction.

The inertia coefficient is given as a sum of unity and a term called the added mass:

$$C_M = 1 + k_m \quad (3.37)$$

k_m depends on the shape of the object. The interpretation of the inertia coefficient implies that it accounts for the buoyancy force of the object by the unity term and it additionally it includes the added mass through the term k_m . The sense of the added mass lies on the fact that a local pressure gradient accelerates the neighbouring fluid around the cylinder. The force required to accelerate the fluid yields the added mass.

The previous analysis was based on the separate treatment of the drag and inertia force components. However, this independent calculation is not applicable for real cases, since in a wave field both forces occur simultaneously and vary continuously with time. In 1950, Morison et al. proposed a formula for the approximation of the total wave force, which is the sum of the drag and inertia forces. It is known as the “Morison equation”:

$$dF = dF_D + dF_I = \frac{1}{2} C_D \rho A u |u| + C_M \rho V \frac{Du}{Dt} \quad (3.38)$$

It should be noted that the absolute value of the velocity is used to ensure that the drag force is always in the direction of the flow velocity, which changes according to the phase of the passing wave (Dean & Dalrymple, 1991).

3.5.3 Numerical methods for wave loading on large objects of arbitrary shapes

It has been already clear that the phenomenon of wave loading on circular cylinders is quite complex. In case for more complicated cases, such as objects of arbitrary shapes, the employment of numerical models is necessary. Garrison and a number of colleagues (Garrison & Rao, *Interaction of Waves with Submerged Bodies*, 1971) (Garrison & Chow, *Wave Forces on Submerged Bodies*, 1972) (Garrison & Berklite, *Impulsive Hydrodynamics of Submerged Rigid Bodies*, 1973) developed numerical approaches for calculating the wave loading of complex structures. Their method focuses on the boundary condition problem. According to their technique, the surface of the structure is split into a number of elements, each of which has an oscillating source located in its centre. The source term is combined with the wave-induced field and results in satisfying the boundary conditions.

Garrison’s method does not specify the boundary value problem in detail. As in common practice though, no-flow boundary conditions are defined on the seafloor and structure. For illustration purposes and since the problem is treated as linear, the flow field is analysed in two steps. First, the object is regarded as “transparent” to the flow caused by the wave field, meaning that only normal to the surface of the structure velocity components will be considered. The second step is to determine the velocity potential that satisfies Laplace equation, all the boundary conditions and results to a velocity, which is due to the Green’s function and cancels the normal velocity on the structure generated by the incident velocity field (Dean & Dalrymple, 1991).

3.5.4 Spectral approach to wave force prediction

Reviewing Morison's equation, it is apparent that the drag force component is nonlinear to the water particle velocity. Another source of nonlinearity appears for the case of a semi-submerged pile, due to the variation in the immersed length of the structure caused by the oscillation of the free surface. In these cases though, inertia force is dominant and the drag force component can be neglected. The result is a linearization of the equation, since inertia coefficient is a function of water particle acceleration only. Moreover, the linearity is supported from the fluctuation of the free surface as well. Since maximum acceleration of the water particles occurs for wave phase corresponding to zero water surface displacement, the nonlinear effects of phase are limited.

The conclusion of the previous paragraph is that when inertial force dominates, the local and total force can be considered as linear in the wave height. The result is that spectral methods, based on frequency can be directly applied for wave-induced forces calculations (Dean & Dalrymple, 1991).

3.6 Irregular waves

3.6.1 Wind generated waves

All waves presented so far, linear or nonlinear, belonged in the category of regular waves. The common characteristic of regular waves is that they consist of one frequency. In analogy to light waves, single-frequency waves are also called "monochromatic" waves. In real sea though, it is impossible to observe monochromatic waves. The water surface is composed of a large number of waves of different frequencies, phases and amplitudes moving in different directions (Dean & Dalrymple, 1991).

Revising Figure 3.1, it can be seen that waves of periods ranging from 0.1s to 10s are mainly wind-generated waves. From the same figure, it is also apparent that wind waves include significant amount of energy density. Therefore, it is important to be able to forecast these waves efficiently. For short-term time periods the forecast of waves can be done through the forecast of winds. For longer time periods though, wind forecasts are no longer reliable and neither the wave forecast. For these time scales, hindcasting techniques are employed. That means that wave conditions are computed via archived wind fields that have been reconstructed by meteorologists in hindsight. Wave conditions in the past can be simulated to create long-term wave information or to replicate special sea states, such as storm conditions. The problem with hindcasting is that the wind field is very complex and random in all three dimensions and time and therefore direct interpretation for finding the wave field is not possible. In order to utilize the wind data for wave modelling, the horizontal component of the wind vector is taken and it is averaged usually over 10min intervals. The measurement of the wind is usually done at 10m above the mean water level and the corresponding velocity is denoted as U_{10} (Holthuijsen, 2007).

In order to build a wave model that takes into account the wind to generate the waves, some assumptions need to be made. For a simple wave model, the wind is considered as constant in space and time blowing from deep water perpendicularly off a straight and infinitely long coastline. The waves are described by only one characteristic wave height, usually the significant wave height (Eq. 3.4.4), and a characteristic period, like the peak period. Alternatively, the wave field is given through a universal one- or two-dimensional spectrum. Under these assumptions, the characteristics of the waves created depend only

on the wind speed and the free distance to the upwind coastline, namely the fetch F or the time that the wind blows. It is apparent that all these parameters are relevant to the energy transfer from the air to the sea, via stresses on the water surface. Other parameters that can influence the energy transfer are the viscosity of the water, turbulence in the airflow, gustiness and atmospheric stability. Even though these factors are often ignored, they might introduce errors up to 20% in the estimation of the significant wave height.

The four parameters introduced until now (fetch F , duration of wind blowing t , velocity of the wind U_{10} and gravitational acceleration g), can be reduced to three. This can be achieved by expressing t in terms of an equivalent F , i.e. F_{eq} . F_{eq} can be calculated by knowing the distance from the coast, the direction of the wind and the time that the wave needs to reach the coast.

$$F_{eq} = c_g t \cos \theta \quad (3.39)$$

where c_g is the group velocity of the wave and θ is its direction relative to the coast.

The essence of considering an equivalent fetch has to do again with the energy transfer from wind to sea. F_{eq} aims to account for the time that this energy transfer takes place. There are three distinguished cases: a) the actual fetch is shorter than F_{eq} and the fetch is then the limiting factor to the development of the waves, b) the actual fetch is longer than F_{eq} , making the development of the waves duration-limited, which is related to the total time that wind blows and c) both distance and time are long enough and there are no limitations in the development of the sea.

3.6.2 Wave statistics

As it becomes obvious so far, the sea state is so complicated that it can only be treated through statistical analyses of the wave characteristics. For example, for engineering purposes, the maximum wave height for a designing return period has to be estimated in order to identify the maximum loading on a structure during its lifetime. Historically, several ways have been proposed for characterizing a sea state. The most common is the significant wave height, denoted as H_s or $H_{1/3}$. H_s refers to the 1/3 of the highest waves in a sea state and it is very popular among sailors, since it is the wave height mainly observed, so it has an empirical essence for sea conditions characterization. The maximum wave height H_{max} is often used for engineering purposes.

To make these “statistical” definitions clearer, one should consider the timeseries of the surface elevation measured at a point. Subtracting the individual waves from the timeseries and ordering them from higher-amplitude waves to smaller-amplitude waves with numbers from 1 to N , statistical properties can be derived. H_s is then defined as the average of the highest $N/3$ waves. Similarly, H_p , where p represents any value of the wave height, is defined as the average of the first pN waves, with $p \leq 1$.

The probability of a wave height being equal or greater than an arbitrary wave height \hat{H} is:

$$P(H > \hat{H}) = \frac{n}{N} \quad (3.40)$$

where n is the number of waves higher than \hat{H} .

Another commonly used statistical property is the root-mean-square wave height for our group of waves, which is always larger than the average wave height in a real sea. H_{rms} is defined as:

$$H_{rms} = \sqrt{\frac{1}{N} \sum_{i=1}^N H_i^2} \quad (3.41)$$

Statistical theory can be used to obtain other important relationships using distribution functions for the wave height. Making use of the Rayleigh probability density function (Dean & Dalrymple, 1991), (Koutitas, 1988) the probability of exceeding a certain wave height can be obtained:

$$p(H) = \frac{2H}{H_{rms}^2} e^{-\left(\frac{H}{H_{rms}}\right)^2} \quad (3.42)$$

According to Rayleigh distribution more statistical properties for the wave height can be obtained as a function of H_{rms} . The mean wave height \bar{H} and the significant wave height $H_{1/3}$ are given:

$$\bar{H} = H_1 = \frac{\sqrt{\pi}}{2} H_{rms} \quad \text{and} \quad H_{1/3} = H_S = \sqrt{2} H_{rms} \quad (3.43 - 3.44)$$

The maximum wave height H_{max} , which is the wave that had probability of exceeding equal to $1/N$ (Koutitas, 1988), can be calculated by:

$$H_{max} = H_{rms} \sqrt{\ln N} \quad (3.45)$$

From the definition, it is clear that the wider the range of data is (N), the greater H_{max} will be.

It is important to mention that the Rayleigh distribution tends to overpredict the larger wave heights for real seas of large magnitude (Forristall, 1978). A possible explanation is that the energy dissipation caused by wave breaking "trims" the larger heights.

3.6.3 Wave spectrum

As mentioned, a timeseries recorded from a real sea comprises of many components of different frequencies and amplitudes, with different phases. To make the interpretation of the results easier, the amplitude of each component is plotted against the corresponding frequency, resulting to an amplitude spectrum. For practical applications the energy spectrum is more commonly used. The energy spectrum is a plot of the squared value of amplitude a^2 . At the same time, the energy density spectrum, which represents the spreading of $a^2/\Delta f$ over the frequencies, is quite popular, since it gives the total energy in the wave field as the area under the curve (Dean & Dalrymple, 1991).

It is therefore clear, that the knowledge of the wave spectrum can provide useful information for the sea state. The most important contribution in this field was made from the JOint North Sea Wave Project (JONSWAP; Hasselmann et al., 1973). It was observed that the spectrum retains its shape along the fetch, which is a remarkable property regarding the spectral evolution. The first impression might be that the spectral shape sharpens when fetch increases, however normalising the results, a stable evolution of the spectrum is revealed.

All spectra have a main energy “body” and some high-frequency tails. For fetch-limited spectra like JONSWAP, these tails have the same shape as the tails of fully developed spectra. Such spectra were described by Pierson and Moskowitz (1964). The same shape was suggested earlier by Phillips (1958), who assumed a behaviour of the high frequency tails and derived the spectral shape using dimensional analysis. His hypothesis was based on the assumption that the energy of these tails is limited by wave breaking.

The most commonly used spectrum is JONSWAP, which is given by the following expression of the energy:

$$E_{JONSWAP} = ag^2(2\pi)^{-4}f^{-5}exp\left[-\frac{5}{4}\left(\frac{f}{f_{peak}}\right)^{-4}\right]\gamma exp\left[-\frac{1}{2}\left(\frac{f/f_{peak}-1}{\sigma}\right)^2\right] \quad (3.46)$$

where γ is a peak-enhancement factor and σ is a peak-width parameter.

The first part of Equation 3.46, before γ , corresponds to the Pierson-Moskowitz spectrum, while γ gives the amplification in energy near the peak frequency that is the distinguished characteristic of JONSWAP spectra.

In real seas, it is not realistic to assume a unidirectional spectrum. At the same time it is difficult to clearly observe two-dimensional frequency-direction spectrum. Only some of the overall directional characteristics can be observed. Usually, these are the mean direction and the directional width of the spectrum. While the direction is easily understandable, the directional width is practically a cross-section of the two-dimensional spectrum at a given frequency, normalised such that its integral over the direction is unity. For two dimensional spectra, the knowledge of the directional distribution $D(\theta; f)$ is essential (Holthuijsen, 2007).

4. Numerical Modelling

4.1 Introduction

In the analysis of water waves and coastal hydrodynamic processes, numerical modelling is often employed to simulate the main phenomena in ocean and coastal regions. The numerical models and codes for fluids are structured around numerical algorithms that can tackle fluid flow problems.

Numerical modelling has evolved extensively the last decades and nowadays software is distributed in packages that offer great solving power and sophisticated user interfaces. This facilitates the definition of the problem parameters and the assessment of the results. Hence, all codes contain three main elements: (i) a pre-processor, (ii) a solver and (iii) a post-processor.

4.2 Pre-processing

4.2.1 Definition of the problem

The initial step in all numerical modelling applications is the understanding of the physical problem and decisions on the assumptions and the simplifications that will be considered. This process takes place before the execution of the model and it is a part of the pre-processing. The input of the flow problem is usually done via a user interface, which transforms the input data to a form that can be used later by the solver.

One of the main operations that takes place during the pre-processing is the definition of the geometry of the computational domain, which is the virtual area where the fluid flow is developed. It is essential then to split the domain in smaller sub-divisions, where the equations of the fluid motion are solved. These sub-divisions are known as cells, control volumes or elements and the process of their definition is called grid generation.

The next step is to select the physical and chemical phenomena that need to be modelled. It is obvious that this requires profound understanding of the physical problem and of the equations describing the state and the motion of the fluid. At the same time, the definition of the fluid properties, such as density and viscosity must be defined.

Last but not least, the boundary conditions must be specified. The computational domain essentially comprises of the interior part and the boundary cells. The conditions there, for example, solid wall, symmetry, etc need to be specified, so that the model can account for the flow near these regions.

The most demanding and time consuming task in the pre-processing is the generation of the computational mesh. Since the solution of the flow problem is defined at the nodes of each cell, it is obvious that the accuracy and the computational efficiency of the model depends on the number of computational cells. In general, accuracy increases with the number of the cells. At the same time though, the larger the number of cells, the longer the computational time is. The decision depends on available computer power and the scope of the study. In general, the balance comes through the design of non-uniform meshes that are finer in the regions of interest or where high variations of the fluid properties take place. Recently developed numerical models have incorporated self-adaptive meshes. That means that the mesh automatically adjusts its resolution, according to some tolerance criteria defined by the user.

It is also important to mention that most of the major numerical codes are coupled with CAD utilities that facilitate complex grid generation. Most of codes are also able to import geometries created with other software. These capabilities are very important especially for designing structures and devices, as well as the replication of bathymetries. It has been estimated that over 50% of the time invested on numerical modelling in industry is devoted to the designing of the computational mesh (Versteeg & Malalasekera, 2007).

4.2.2 Boundary and initial conditions

According to the classification of the physical problem, described in §4.3.1, different conditions for the flow variables should be considered. Boundary conditions are the values or the mathematical forms that define the ρ , u and T on the borders of the computational domain and on the surface of any other “structures” incorporated in the domain. Initial conditions are the values of the flow variables at time $t = 0$. The definition of the boundary and initial conditions plays a crucial role to the outcome of the simulation and special care should be taken.

For a compressible flow unsteady flow, the initial values of ρ , u and T must be given everywhere in the computational domain. The boundary conditions for both unsteady and steady flows can be specified as follows: a) on solid walls no-slip condition ($u = u_w$), fixed temperature ($T = T_w$) or fixed heat flux ($k \partial T / \partial n = -q_w$) can be defined; b) on fluid boundaries, i.e. inlet and outlet of the domain, ρ , u and T must be defined as a function of the position and via the stress continuity condition respectively. Density can be only specified at the inlet and nowhere else, since the continuity equation for compressible fluids accounts for it. On the other hand, for an incompressible flow, there are no conditions for the density at all and all the other conditions are applied exactly as in compressible flows (Versteeg & Malalasekera, 2007).

There is a set of other boundary conditions that take advantage of the geometrical characteristics of the domain and are applied to save computational time. For example the symmetry and cyclic boundary conditions are often applied for such cases. There are also boundary conditions, named “open boundary conditions” that are used to freely radiate the disturbances in the flow. An example is the reflected waves from a beach passing through the inlet boundary to the “open ocean” without interfering with the inlet boundary condition.

Most of the numerical models have a wide range of options for the boundary conditions to facilitate the accurate representation of the flow. It is recommended to carefully consider the different options in the user’s manual in each model before running the simulations.

4.2.3 Discretisation methods

4.2.3.1 Finite Difference Method

The finite difference method (FDM) is one of the oldest and simplest ways to solve numerically partial differential equations (PDEs), believed to have been introduced by Euler in the 18th century.

The core of the method is based on the fact that the value of a flow variable at a given point is calculated by a certain number of neighbour points. The computational domain has to be split in many cells that form a grid. The equations of the flow are considered in their

differential form and at each point in the domain the solution is approximated by replacing the partial derivatives with approximations by means of the nodal values of the functions. Therefore, the differential equations become algebraic. Only one equation is solved per grid node, which has one variable as unknown. The same variable is also unknown at the neighbouring cells.

The approximation of the first and second derivatives of the variables is obtained by Taylor series expansion or polynomial fitting with respect to the coordinates of the cell. It is also possible to obtain the solution at other locations, different than the grid nodes, by interpolation.

The FDM is applicable only when the domain comprises of a grid. In theory, FDM can be applied at any grid, however it is mainly used for structured grids. This is because on structured grids FDM is very simple to apply and works very efficiently. It is also easy to employ high-order schemes on regular grids. However, using FDM in unstructured grids or complex geometries might raise important issues. This restriction is one of the main drawbacks of the method. Another disadvantage is that the conservation in the equations is not guaranteed, unless care is taken for that (Ferziger & Peric, 2002).

4.2.3.2 Finite Element Method

The finite element method (FEM) is a numerical technique for the solution of PDEs. The main characteristic that distinguishes FEM from the other methods is that it employs variational methods in order to minimize the error of the approximated solution, analogous to the Galerkin method. Historically, the FEM was first used in structural mechanics. The development of FEM for computational fluid dynamics applications is far from trivial and therefore not yet fully-developed; CFD mostly uses FDM and finite volume methods (§4.2.3.3).

The FEM, similar to the FDM, is based on the concept of subdividing a continuum computational domain into many cells, namely the elements, and forming a grid. The difference from the FDM is that the grid can be either structured or unstructured and consist of triangular or quadrilateral elements. Moreover, curved cells can be designed and in combination with the unstructured grid can handle problems with great geometric complexity.

As mentioned, the FEM used variational methods, which practically means that the solution is assumed to have a prescribed form and to belong to a function space. The function space is built by varying functions, such as linear and quadratic. The varying functions connect the nodal points, which can be the vertices, mid-side points, mid-element points etc of the elements. As a result, the geometric representation of the domain plays a crucial role to the outcome of the numerical simulation.

The original PDEs are not solved themselves by the FEM. Instead the solution is approximated locally by an integral form of the PDEs. The integral of the inner product of the residual and the weight functions are constructed. The integral is set to zero and trial functions are used to minimize the residual. The most general integral form is obtained from a weighted residual formulation. The process eliminates all the spatial derivatives from the PDEs and therefore, differential type boundary conditions for transient problems and algebraic type boundary conditions for steady state problems can be considered. That

makes the FEM very efficient, since it can incorporate higher order accuracy and it is flexible on implementing different boundary conditions (Wendt, 2009).

Concluding, the FEM first subdivides the domain in elements where the equations are solved. Then, the discrete equations are constructed from contributions to the element level, which are later recombined. All the previous aspects prove that the FEM is based on a strong and rigorous mathematical foundation.

4.2.3.3 Finite Volume Method

The finite volume method (FVM) is a computational method for solving PDEs by transforming them to algebraic equations around a control volume. Control volumes are the subdivisions of the computational domain where the equations are solved. At the centre of each control volume there is a computational node, where the variables are calculated. Interpolation methods are used in order to derive the values of the variables at the surfaces of the control volume taking into account the neighbour control volumes as well.

The FVM has two major advantages. Firstly, it is able to accommodate any type of grid, making it applicable for domains of high complexity. Secondly, the FVM is conservative by definition, since the control volumes that share a boundary have the same surface integrals, describing the convective and diffusive fluxes.

The greatest disadvantage of FVM is the difficulty in developing high order schemes in three dimensions, compared to FDM. The reason for this is that FVMs require three levels of approximation, namely interpolation, differentiation and integration.

Despite the former drawback, the FVMs are very popular in the engineering community, since they are relatively simple to comprehend and program, thanks to the fact that all the approximated terms have physical meaning (Ferziger & Peric, 2002).

The FVM has succeeded in free surface flow simulations, especially when highly-nonlinear processes are involved, such as wave breaking. The unrivalled advantage of the FVM is that it can simulate multiphase flows and therefore include the effects of the air and the water together. The use of unstructured and self-adjustable meshes is also another reason that caused the adoption of FVM by many CFD developers (Greaves D. , 2009).

4.2.3.4 Spectral Method

Spectral methods are less suited for general purpose CFD simulations than FE and FV methods, but at the same time, they can be very useful for some simulations like wave propagation. The basic difference with the previous methods is that spectral methods provide an approximation of the unknown coefficients, similar to Galerkin methods. The approximation functions and weight functions get some non-zero values in the computational domain (Fletcher, 2006).

The basic concept of spectral methods lies on the fact that Fourier series (or their generalisations) are employed to evaluate the spatial derivatives. Consider a periodic function at a uniform grid of points. It is known that this function can be represented by a discrete Fourier series as follows:

$$f(x_i) = \sum_{q=-N/2}^{N/2-1} \hat{f}(k_q) e^{-ik_q x_i} \quad (4.1)$$

where $x_i = i \Delta x$, $i = 1, 2, \dots, N$ and $k_q = 2\pi q / \Delta x N$.

This formula can be further simplified and read:

$$\hat{f}(k_q) = \frac{1}{N} \sum_{i=1}^N f(x_i) e^{-ik_q x_i} \quad (4.2)$$

When analysing a signal in terms of Fourier series, aliasing plays a crucial role. Aliasing is the effect that causes two different signals to appear identical, due to the way they were sampled. Aliasing is often an important source of error in numerical modelling using nonlinear partial differential equations. In this case, aliasing appears because of the change in the index of the summation from q to $q \pm lN$.

The aim is to be able to differentiate Equation 4.1, in order to produce the Fourier series for the derivative. To achieve that the discrete variable x_i has to be replaced by a continuous variable x . This can be done by interpolating $f(x_i)$ and extending it to the whole domain instead of the grid points only. It is important to note that different interpolants, defined by the different values of q , produce different solutions. The best choice for interpolant is the one that gives the smoothest solution. The derivative of Fourier series reads (Ferziger & Peric, 2002):

$$\frac{df}{dx} = \sum_{q=-N/2}^{N/2-1} ik_q \hat{f}(k_q) e^{ik_q x_i} \quad (4.3)$$

where $ik_q \hat{f}(k_q)$ is the Fourier coefficient of df/dx .

It should be noted that the method described above can be readily generalised to higher derivatives. It is also important to know the performance of the method regarding the errors and the computational efficiency. The error in the computed derivative decreases exponentially with N , supposing that N is sufficiently large. How large N should be depends on the function itself. The errors of spectral methods are therefore much smaller than those of finite difference methods for large values of N . At the same time the computational cost for the calculation of the Fourier coefficients is proportional to N^2 . That makes these methods very costly, however the use of Fast Fourier Transform can decrease the computations to be proportional to $N \log_2 N$.

As it can be seen, spectral methods have many merits compared to finite differences methods. However, they can only be applied easily under certain conditions. The computational mesh has to be uniform and the function must be periodic. The effect of these conditions can be minimised though, if other functions, instead of complex exponentials, are used. In any case, the main drawback of spectral methods is that any change in the geometry or boundary conditions requires considerable alterations in the method, making these models relatively inflexible (Ferziger & Peric, 2002).

4.2.3.5 Boundary Element Method

The Boundary Element Method (BEM) is a numerical technique that lies on the method of the weighted residuals, similarly to the FEM. The difference between the two methods is that the BEM does not need to be developed in a domain. This is because the weighting function is the fundamental solution of the equations and therefore the need of spatial discretization is eliminated. Another way to perceive the concept of the BEM is to consider it as an implementation of boundary integral equations based on Green's formula. In this case, the concept of the FEM is used for the discretization. In a more general outline, the BEM might refer to any numerical methods that use boundary or boundary-like discretization techniques and it is known as boundary integral equation method (BIEM).

The method can be first traced in the 60s and the first applications started to emerge in the middle 70s. The BEM has a unique characteristic compared to the previous methods described. The FD, FEM and FVM are all domain methods. On the contrary, as a boundary method, the BEM requires discretization on the bounding surface only and therefore the discretization is significantly reduced. Considering a 2D case, the spatial discretization is limited to a boundary contour only.

Consequently, the BEM has a considerable advantage compared with the other methods: the computational efficiency. The reduced computational elements require less computer power. At the same time, another advantage over the domain methods arises: the BEM can cope with unbounded domains by automatically accounting for the "infinity". There is no need to specially model the behaviour at infinity at the boundaries of the domain by deploying a mesh there.

Keeping in mind that the designing of the computational mesh takes the most human time in numerical modelling, a technique that does not require an interior computational mesh might be very convenient. Moreover, the implementation of adjustable meshes is much simpler with the BEM, making it a competitive computational tool. However, according to the number of publications, until 2004, the BEM was not the most commonly used discretization method. The FEM was first with more than six times more publications than the BEM, followed by the FDM with twice as many publications as the BEM (Cheng & Cheng, 2005).

4.2.3.6 Smooth Particle Hydrodynamics

The Smoothed Particle Hydrodynamics (SPH) technique was first introduced in 1977 to simulate phenomena in astrophysics. SPH's unique characteristic is that it is a mesh-less method. It was originally in order to tackle problems of very large domains with sufficient accuracy. SPH does not need a grid to calculate the spatial derivatives, which are found by analytical differentiation of interpolation formula. When SPH was first introduced, there were

already accurate finite-difference methods, however they were incapable of handling complex physics in three dimensions (Monaghan, Smoothed Particle Hydrodynamics, 1992).

The basic concept underlying the SPH method is that the fluid is replaced with a set of particles and the equations of fluid dynamics are solved for each particle. Interpolation between the particles reveals the solution for the whole domain. From a mathematical point of view, the particles are the interpolation points, while from a physical point of view the SPH particles represent the material particles.

Although this idea appears to have physical sense, it is not apparent which interactions between the particles will reproduce the equations of fluid and continuum mechanics. In order to derive the equations, Gingold and Monaghan (Monaghan, Smoothed particle hydrodynamics, 2005) used a kernel estimation technique, pioneered by statisticians. The kernel function results to the expression of the equations of fluid dynamics in terms of particle properties. SPH is strongly bonded with statistical concepts. However, issues have arisen due to the differences in the particle number density and the probability density functions. These issues have been tackled over the development process of SPH by adjusting the fundamental algorithm to account for linear and angular conservation of momentum.

After the continuum is decomposed into a set of arbitrarily distributed particles with no connectivity, a spatial distance, known as the "smoothing length", is given to the particles, over which their properties are "smoothed" by a kernel function. The property values for each particle can be calculated by summing the relevant properties of all the particles included in the range of the kernel.

At the heart of SPH is an interpolation method, which allows any function to be expressed in terms of its value at a set of disordered points - the particles. The integral interpolant of any function $A(r)$ is given by:

$$A_I = \int A(r')W(r - r', h) dr' \quad (4.4)$$

Where the function W is the kernel and dr' is a differential volume element. If the kernel is a delta function, the interpolant reproduces A exactly. In practice, the kernels are functions which tend to the delta function as the length scale h , known as the smoothing length, tends to zero. They are normalized to 1 so that the constants are interpolated exactly.

$$\int W(r - r', h) dr' = 1 \quad \text{and} \quad \lim_{h \rightarrow 0} W(r - r', h) = \delta(r - r') \quad (4.5a, b)$$

Since a delta function lacks some required properties for a "well behaved function", such as continuity and differentiability, it is replaced by a kernel function that mimics it.

For numerical application, the integral interpolant is approximated by a summation interpolant:

$$A_s(r) = \sum_b m_b \frac{A_b}{\rho_b} W(r - r_b, h) \quad (4.6)$$

where b denotes the particle label and the summation occurs over all particles. m_b is the mass of the particle, r_b and ρ_b the position and the density of the particle respectively.

In Monaghan's paper (Monaghan, Smoothed Particle Hydrodynamics, 1992), the derivation of the equations of motion can be found, i.e. the momentum, continuity, thermal energy and state equation. Further details of how the properties of one particle are related with the properties of another one are explained in detail.

The following procedure provides a typical solution strategy for solving the governing equations in the SPH method:

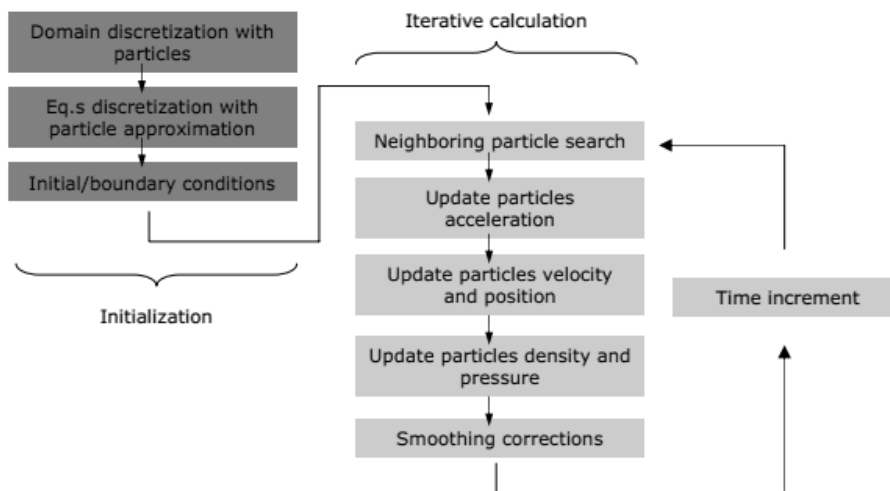


Figure 4.1: The solving process in a SPH model

The SPH method has several advantages compared with the finite difference methods. The first is that pure advection is treated exactly and that is because the SPH is Galilean invariant. Additionally, that with SPH more than one materials can be modelled with their one set of particles relatively easy. The same does not apply to classic CFD methods. The third advantage is that SPH can bridge the gap between continuum and fragmentation in a natural way. Therefore it can give solution to problems of brittle fracture or fragmentation in damaged solids. The other advantage is inherited with the concept of the method. In SPH the resolution can be made to depend on position and time and computations are performed only where matter is. This fact results to important reduction in the computational cost and memory used. Last but not least, thanks to the close similarity between SPH and molecular dynamics, it is possible to include complex physics in the simulations (Monaghan, Smoothed particle hydrodynamics, 2005).

4.3 Solving

The basic equations that describe any fluid flow are the Navier-Stokes equations. However, solving the full Navier-Stokes equations and accounting for all the scales of turbulence modelling requires very complex models and results to high computational cost. Therefore, most of the models have incorporated simplified forms of the Navier-Stokes equations by considering several assumptions. Two of the most common simplifications refer to the removing of the viscosity terms, which results to the Euler equations, and the removing of the vorticity terms, which yields the full potential equations.

4.3.1 Classification of physical behaviours

In chapter 2, the conservation equation have been presented and the equations of the flow have been derived. In paragraph 4.2.2, the different initial and the boundary conditions have been presented. In order to move on to the numerical interpretation of the equations of motion, a set of partial differential equations (PDEs) needs to be developed. At this stage, therefore, a classification of the physical behaviours is essential. There are two categories of physical behaviour: equilibrium and marching problems.

4.3.1.1 Equilibrium problems

Elliptic equations

Equilibrium problems describe steady state situations. Some examples are the steady state temperature distribution in a rod of solid material, the stress distribution of a solid object under a load and many steady fluid problems. These cases are governed by elliptic equations. The basic elliptic equation is the well-known Laplace's equation, used for irrotational flows of incompressible fluids and steady state heat transfer. Laplace's equation in two dimensions reads:

$$\frac{\partial^2 \phi}{\partial x^2} + \frac{\partial^2 \phi}{\partial y^2} = 0 \quad (4.7)$$

Elliptic equations provide unique solution for the whole domain, as long as the conditions of the dependent variable are specified on all the boundaries. These type of problems are called boundary-value problems. A distinguished characteristic of the elliptic equations is that a change in the interior of the domain, influences the solution everywhere else. In practice this implies that a disturbance signal in the computational domain travels in all directions, providing that the numerical schemes used allow one computational cell to be influenced by all the neighbouring cells. The result is that solutions obtained by elliptic equations are always smooth, even in the cases that the boundary conditions are discontinuous. The former is a considerable advantage for the numerical model.

4.3.1.2 Marching problems

Marching or propagating problems include unsteady and transient phenomena, such as transient heat transfer, unsteady flows and water waves. The governing equations have either parabolic or hyperbolic form. It is important to mention though, that there are steady-like marching problems. Some steady flows can be described as marching phenomena, assuming that the flow direction acts as a time-like co-ordinate along which marching is possible.

Parabolic equations

Parabolic equations are time-dependent and their distinguished characteristic is the significant amount of diffusion that they involve. Simple examples to consider are unsteady viscous flows and unsteady heat conduction. The basic parabolic equation is the diffusion equation, given as:

$$\frac{\partial \phi}{\partial t} = \alpha \frac{\partial^2 \phi}{\partial x^2} \quad (4.8)$$

Parabolic phenomena require the definition of all the boundary and initial conditions in the entire domain for all times greater than $t_0 = 0$. As a result, parabolic problems are called initial-boundary-value problems.

The characteristic of parabolic problems is that a change in the interior is able to influence the solution in later times. Therefore, any disturbance propagates in time and diffuses in space. It is apparent that the effect of the diffusion ensures the smoothness of the solution in the interior of the domain, preventing any possible discontinuities in the initial conditions to corrupt the results at times $t > 0$.

Parabolic problems reach steady states as time increases, which has an elliptic form. This behaviour can be readily identified if in the parabolic equation $\partial \phi / \partial t$ is set to zero, representing the steady state condition.

Hyperbolic equations

Hyperbolic equations are mainly used for oscillation problems. Hyperbolic phenomena are characterized of negligible energy dissipation and are distinguished to elliptic and parabolic phenomena, because they allow a signal to propagate at a finite speed. Hyperbolic equations appear in time-dependent problems, such as waves. Therefore, the propagation speed is usually called the wave speed and hyperbolic equations are also known as wave equations. The form of the equation is:

$$\frac{\partial^2 \phi}{\partial t^2} = c^2 \frac{\partial^2 \phi}{\partial x^2} \quad (4.9)$$

The equation above describes the transverse displacement of a string under tension during small-amplitude vibrations (replacing ϕ with y) and acoustic oscillations as well. c is the constant wave speed.

Hyperbolic equations also describe initial–boundary-value problems and three boundary conditions need to be specified: two initial conditions on the displacement of y and one on all boundaries for times greater than zero.

Defining the initial amplitude as a , the solution of the problem becomes:

$$y(x, t) = a \cos\left(\frac{\pi ct}{L}\right) \sin\left(\frac{\pi x}{L}\right) \quad (4.10)$$

It is apparent for this solution that the amplitude of the oscillation remains constant, implying that there is no damping in the system. This fact has an important application: as any shape of oscillation can be considered in the initial conditions, thanks to the lack of damping in the system, Fourier series can be used for the analysis of this initial shape. The shape can be therefore represented as a sum of sine (linear) waves. Since the governing equation is also linear, the Fourier components and the sum persists in time without change of the amplitude.

In hyperbolic problems, the disturbance at a point in the domain can only influence a limited region, depending on the wave speed. This is in contrast to parabolic and elliptic equations that assume infinite propagation speeds.

Hyperbolic equations are also employed for the description shockwaves, where the flow becomes compressible and the disturbance travels above the speed of sound. The flow in this case can be treated as inviscid.

Table 4.1: Classification of physical behaviours

	Steady flow	Unsteady flow
Viscous flow	Elliptic	Parabolic
Inviscid flow	Elliptic	Hyperbolic
Thin shear layers	Parabolic	Parabolic

Table 4.1 provides a generic classification of the physical behaviours. In practice though, many fluid flows behave in a complex way. In general one can say that the steady Navier-Stokes equations and energy equations are elliptic. On the other hand, the unsteady equations are parabolic. Cases like thin shear layers, such as boundary layers, jets, mixing layers, wakes and fully developed duct flows, are described by parabolic equation. That is because the velocity derivatives in x and z direction are significantly smaller than in the cross-stream direction y .

4.3.2 Potential flow

Potential flow assumes that turbulence is negligible where the effects of viscosity are sufficiently small and the flow is frictionless and irrotational. Thus potential flow is often used for analysing external flows over solid surfaces at high Reynolds numbers providing the flow remains laminar.

Applying the continuity equation for incompressible fluids (Eq. 2.5), the velocity potential satisfies the Laplace equation:

$$\nabla^2 \phi = 0 \quad (4.11)$$

When the turbulence is neglected and the boundary layer is thin, the NSE's are reduced to Laplace equations based on potential flow theory. Potential theory can be applied for both incompressible and compressible flows. Regarding compressible flows, which is rarely the case of water waves, potential theory is applicable for sub, trans- and super-sonic flows at arbitrary angles of attack.

It should be stated clearly that since potential flow assumes that the flow is irrotational it is incapable of describing breaking or over-turning waves. Hence, it should not be used for wave breaking or interaction of waves with small bodies. At the same time, it is not applicable for flows that include boundary layers.

4.3.3 Hydrostatic pressure models

Most of the numerical models used for ocean circulation and regional studies are rooted in the Navier-Stokes equations. However, for these scales the full Navier-Stokes equations are computationally difficult to handle. A simplified version is employed instead: the "hydrostatic primitive equations" (HPEs). In HPEs, the vertical momentum equation is reduced to an approximation of hydrostatic balance.

The pressure is computed according to the hydrostatic approximation, while the vertical component of the velocity is calculated through the vertical momentum equation, which becomes in this case a diagnostic relation for the hydrostatic pressure. On the contrary, in full Navier-Stokes equations, all the velocity components are obtained directly from the momentum equations (Marshall, Hill, Perelman, & Adcroft, 1997).

The pressure difference between two points in the domain is $p_b = p_a + \int_z^\eta \rho g dz$. The full set of hydrostatic equations as mentioned comprises of the continuity equation (Eq. 2.5) and the Navier-Stokes equations (Eq. 2.21a and 2.21b). The difference is in Equation 2.21c. The 3D hydrostatic model equations can be found in (Roelvink & Reniers, 2012).

4.3.4 Shallow water equations

When water waves enter very shallow water, particles move basically horizontally and the vertical accelerations are negligible. The propagation of the wave in this case can be described by the shallow-water equations (Holthuijsen, 2007).

Shallow water equations are derived from the depth averaging of the Navier-Stokes equations assuming that the horizontal length scale is much greater than the vertical. Using the conservation of mass, it can be shown that the vertical velocity is small; while using the momentum equation the vertical pressure gradients are hydrostatic. Therefore, the velocity profile is uniform in depth and the vertical components very small.

In the case of ignoring the Coriolis force, the frictional and viscous forces, the mathematical description of SWE is:

$$\frac{\partial \eta}{\partial t} + \frac{\partial(\eta u)}{\partial x} + \frac{\partial(\eta v)}{\partial y} = 0 \quad (4.12a)$$

$$\frac{\partial(\eta u)}{\partial t} + \frac{\partial}{\partial x} \left(\eta u^2 + \frac{1}{2} g \eta^2 \right) + \frac{\partial(\eta u v)}{\partial y} = 0 \quad (4.12b)$$

$$\frac{\partial(\eta v)}{\partial t} + \frac{\partial(\eta u v)}{\partial x} + \frac{\partial}{\partial y} \left(\eta v^2 + \frac{1}{2} g \eta^2 \right) = 0 \quad (4.12c)$$

where η is the total fluid column height; the 2D vector (u, v) is the fluid's horizontal velocity in the x and y direction, averaged across the vertical column; g is the acceleration due to gravity.

The first equation is derived from mass conservation and the second & third equations from momentum conservation.

4.3.5 Boussinesq equation

Before waves enter shallow waters, the motion of the particle cannot be considered as horizontal and therefore shallow-water equations are not applicable. At the same time, the transitional state of waves in intermediate waters cannot be described by linear theory. The region between deep and shallow waters is described by the Boussinesq model.

The vertical velocity distribution is not calculated by the nonlinear balance equations. Instead the horizontal component of the velocity is assumed to be constant in the water column and the vertical component of the velocity varies almost linearly over depth. The original Boussinesq equations were derived for a horizontal seabed by substituting the velocity potential function into the nonlinear dynamic and kinematic surface boundary conditions.

The following one-dimensional Boussinesq equations refer to a non-horizontal bottom:

$$\frac{\partial \eta}{\partial t} + \frac{\partial}{\partial x} [(d + \eta) \bar{u}_x] = 0 \quad (4.13a)$$

$$\frac{\partial \bar{u}_x}{\partial t} + \bar{u}_x \frac{\partial \bar{u}_x}{\partial x} + g \frac{\partial \eta}{\partial x} = \frac{1}{2} d \frac{\partial^3 (d \bar{u}_x)}{\partial t \partial x^2} - \frac{1}{6} d^2 \frac{\partial^3 \bar{u}_x}{\partial t \partial x^2} \quad (4.13b)$$

where \bar{u}_x is the vertically averaged horizontal velocity

Essentially these equations are the shallow-water equations with corrections for the vertical acceleration, seen on the right hand side. The third order derivatives are the result of the Laplace equation forcing the vertical velocity of the velocity potential function to be expressed in terms of the horizontal velocity distribution. These equations can be readily expanded into two horizontal dimensions.

Many researchers have introduced different implementations in the Boussinesq equations creating Boussinesq-type models being able to be applied for propagation in deep water and the process of wave-breaking. A recent overview on Boussinesq-type models can be found in M. Brocchini's paper (Brocchini, 2013).

4.3.6 Mild-slope equation

As it becomes apparent of its name mild-slope equation was originally developed to describe the propagation of the waves over low gradient seabeds. Mild-slope equation is commonly used in coastal engineering, since it can account for the effects of diffraction and refraction of the waves due to coastlines or structures.

Eckart in 1952 first introduced the mild-slope equation which was later improved in 1972 by Berkhoff. Mild-slope equations are a type of depth-averaged equation, applied in both deep and shallow waters for monochromatic waves (Lin, 2008). They are derived from potential flow theory and describe the combined effects of diffraction and reflection of water waves, modelling the propagation and transformation when water depth and interactions are varied. The approximate model observes wave-field changes near harbours and coasts, in particular the interaction with cliffs, seawalls and breakwaters.

The equations can be found in various forms which include the effects of wave breaking, nonlinearity of waves, wave-current interactions and seabed friction. They calculate the wave amplitude or wave height, but if there is a constant water depth, the mild-slope equation reduces to the Helmholtz equation for wave diffraction.

As the mild-slope equation was first introduced by (Berkhoff, 1972), it assumed that the wave is linear and the slope is mild. These assumptions yield the following relationship:

$$\nabla (cc_g \nabla \hat{\eta}) + k^2 cc_g \hat{\eta} = 0 \quad (4.14)$$

where c refers to the wave celerity, c_g to the group velocity and k is the wave number.

To simplify the equation, the transformation by Radder (1979) was introduced:

$$\hat{\phi} = \hat{\eta} / \sqrt{cc_g} \quad (4.15)$$

Within the accuracy up to the first order in the bottom slope, this will become a Helmholtz equation:

$$\nabla^2 \hat{\phi} + k^2 \hat{\phi} = 0 \quad (4.16)$$

where the time-dependent quantity, ϕ , corresponding to $\hat{\phi}$ is expressed as $\phi = \hat{\phi} e^{-i\omega t}$ (Isobe, 1994).

The original MSE has limitations, because it is only applicable to linear waves, on mild bottom geometry and the equation does not contain energy dissipation. There have been numerical advances to employ the inclusion of energy dissipation and weakly non-linear waves with steeper bottom slopes. These can be called modified MSE's (MMSE) and are further explained on page 252 (Lin, 2008).

Mild-slope equation has been developed with different formulations in order to account for the existence and propagation of a wave field. Time-dependent wave fields, steady-state wave fields and simplified steady-state wave fields can be described by hyperbolic (Dingemans, 1997), elliptic (Berkhoff, 1972) and parabolic (Lin, 2008) formulation of the mild-slope equation respectively.

4.3.7 Modelling of viscous turbulent flows

The most challenging part in the modelling of fluid flows is the accurate representation of turbulence. Most practical engineering applications include turbulent flows and therefore the numerical models need to be developed in such a way that can encounter for that. Important engineering parameters, such as frictional drag, flow separation, transition from laminar to turbulent flow, thickness of boundary layers, extend of secondary flows and spreading of jets and wakes, are determined by turbulence.

Depending on the application, turbulence might have different states and different scales. This range is quite rich and complex when examining various industrial applications. Turbulence has been extensively studied theoretically, experimentally and numerically for many decades and it is unanimously agreed that, due to the complexity of the phenomenon, there is not a generally valid universal mathematical model of turbulence (WS Atkins Consultants & NSC, 2002). At the same time, the extensive research on the turbulence modelling has resulted to the development of many different approaches of the mathematical description of turbulence that can be grouped in three general categories: : a) Turbulence models for Reynolds-Averaged Navier-Stokes (RANS) equation, b) Large eddy simulation (LES) and c) Direct numerical simulation (DNS) (Versteeg & Malalasekera, 2007).

4.3.7.1 RANS equation for incompressible flow

The Reynolds-Averaged Navier-Stokes (RANS) is the most popular method of solving the Navier-Stokes equations used in computational fluid dynamic applications in industry and research, because of each efficiency and relatively low computational cost. A lot of

experience has been built in using RANS models, thanks to the great spreading of these models. In the next paragraphs, the essence of “averaging” will be presented.

To begin with, a control volume of fluid in two dimensions is considered that has turbulent shear flow parallel to x axis with mean velocity gradients in the y direction. Strong mixing takes place in the control volume, due to the existence of the vertical eddy. The presence of random currents transports fluid across the boundaries of the control volume. These currents are related to the passage of eddies near the boundaries of the control volume. Mass is not created or destroyed because of these recirculating motion, but momentum and energy is transferred into and out of the control volume. The net output is momentum exchange, which is caused by the convective transport of the eddies. This momentum exchange causes acceleration to slower moving layers of fluid and deceleration to faster moving fluid layers. The changed in momentum imply the existence of additional turbulent stresses that as described in chapter 2 are known as Reynolds stresses.

A typical measurement of the velocity at a point in a turbulent flow will reveal a behaviour like the one depicted in Figure 4.2. It can be seen that the velocity is random, but it can be decomposed in a steady mean value U and in a fluctuating value $u'(t)$.

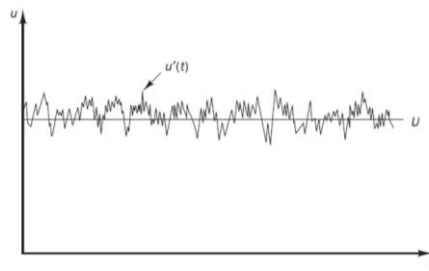


Figure 4.2: Typical measurement of the velocity in turbulent flows

This interpretation of the velocity can be used in the Navier-Stokes equations that, as it has mentioned already, can describe any turbulent flow. The same interpretation is considered for all the components of the velocity and for the pressure are well:

$$u = U + u' \quad v = V + v' \quad w = W + w' \quad p = P + p' \quad (4.17)$$

RANS model is based on the time averaging of the continuity and the Navier-Stokes equations. The time averaging yields the continuity equation of the mean flow and the time-averaged x -, y -, z - momentum equations. The time averaged Navier-Stokes in a Cartesian co-ordinate system read as shown in Eq. 4.17. It can be seen that the terms contain products of the fluctuating velocities and they are associated with the convective momentum transfer due to turbulent eddies. There are additional turbulent stresses on the mean velocity components U , V and W caused by the later mentioned terms.

$$\frac{\partial U}{\partial t} + \text{div}(UU) = -\frac{1}{\rho} \frac{\partial P}{\partial x} + \nu \text{div}(\text{grad}(U)) + \frac{1}{\rho} \left[\frac{\partial(-\rho \overline{u'^2})}{\partial x} + \frac{\partial(-\rho \overline{u'v'})}{\partial y} + \frac{\partial(-\rho \overline{u'w'})}{\partial z} \right] \quad (4.18a)$$

$$\frac{\partial V}{\partial t} + \text{div}(VU) = -\frac{1}{\rho} \frac{\partial P}{\partial y} + \nu \text{div}(\text{grad}(V)) + \frac{1}{\rho} \left[\frac{\partial(-\rho \overline{u'v'})}{\partial x} + \frac{\partial(-\rho \overline{v'^2})}{\partial y} + \frac{\partial(-\rho \overline{v'w'})}{\partial z} \right] \quad (4.18b)$$

$$\frac{\partial W}{\partial t} + \text{div}(WU) = -\frac{1}{\rho} \frac{\partial P}{\partial x} + \nu \text{div}(\text{grad}(W)) + \frac{1}{\rho} \left[\frac{\partial(-\rho \overline{u'w'})}{\partial x} + \frac{\partial(-\rho \overline{u'w'})}{\partial y} + \frac{\partial(-\rho \overline{w'^2})}{\partial z} \right] \quad (4.18c)$$

This set of equations is called RANS and it is accompanied with the Reynolds stresses. These stresses can be written in longhand for easier apprehension. There are three normal stresses:

$$\tau_{xx} = -\rho \overline{u'^2} \quad \tau_{yy} = -\rho \overline{v'^2} \quad \tau_{zz} = -\rho \overline{w'^2} \quad (4.19a, b, c)$$

and six shear stresses

$$\tau_{xy} = \tau_{yx} = -\rho \overline{u'v'} \quad \tau_{xz} = \tau_{zx} = -\rho \overline{u'w'} \quad \tau_{yz} = \tau_{zy} = -\rho \overline{v'w'} \quad (4.19d, e, f)$$

The derivation of the RANS from the time-dependent Navier-Stokes equations has important consequences. The physical meaning of the time averaging eliminates the effect of the unsteadiness of the small structures of the flow that are expressed by the mean effects of the flow via the Reynolds stresses.

The problem that rises now is the interpretation of the Reynolds stresses in terms of calculated time-averaged variables. That is necessary in order to close the system of the RANS equations and make it solvable. The closure becomes possible through the development of mathematical models, namely turbulence models that include correlations for the unknown quantities. There is a great range of turbulent models for RANS equations, which can be grouped in four main categories: a) Algebraic, else known as zero-equation models, b) One-equation models, c) Two-equation models and d) Stress transport models. Each category consists of many models and each model might have different ways of implementations and many parameterizations. The choice of the turbulence model depends on the application itself and it cannot be considered as trivial issue (WS Atkins Consultants & NSC, 2002). Three of the most commonly used turbulence models will be discussed in detail are: a) $\kappa - \varepsilon$ model b) $\kappa - \omega$ model and c) Reynolds stress model.

The $\kappa - \varepsilon$ model

The $\kappa - \varepsilon$ and the $\kappa - \omega$ models belong to the generic category of two-equation model, which solve two separate transport equations and they are the most commonly used in industrial applications since it is the simplest level of closure which does not require geometry or flow regime dependent input. The underlying assumption of both these models is that the turbulent viscosity μ_t is isotropic: in other words that the ratio between Reynolds stress and mean rate of deformation is the same in all directions. This assumption fails in many complex flows where it leads to inaccurate predictions.

The most popular version of two equation models is the $\kappa - \varepsilon$, which allows for the effects of transport of turbulence properties by convection and diffusion and for production and destruction of turbulence. Two transport equations (PDEs), one for the turbulent kinetic energy κ and a further one for the rate of dissipation of turbulent kinetic energy ε , are solved. ε corresponds to the rate at which turbulent energy is dissipated by the action of viscosity on the smallest eddies (WS Atkins Consultants & NSC, 2002).

The standard $\kappa - \varepsilon$ model (Launder and Spalding, 1974) comprises of two model equations, one for κ and one for ε , which are based on the best understanding obtained so far of the processes associated with these variables. κ and ε are used to define the velocity scale ϑ and the length scale l representative of the large-scale turbulence (Versteeg & Malalasekera, 2007):

$$\vartheta = k^{1/2} \quad \text{and} \quad l = \frac{k^{3/2}}{\varepsilon} \quad (4.20 \text{ \& } 4.21)$$

Applying dimensional analysis the eddy viscosity can be obtained as follows:

$$\mu_t = C_\mu \rho \vartheta l = \rho C_\mu \frac{k^2}{\varepsilon} \quad (4.22)$$

where C_μ is a dimensionless constant.

The transport equations used in the standard $\kappa - \varepsilon$ read:

$$\frac{\partial(\rho k)}{\partial t} + \text{div}(\rho k U) = \text{div} \left[\frac{\mu_t}{\sigma_\kappa} \text{grad} k \right] + 2\mu_t S_{ij} \cdot S_{ij} - \rho \varepsilon \quad (4.23)$$

$$\frac{\partial(\rho \varepsilon)}{\partial t} + \text{div}(\rho \varepsilon U) = \text{div} \left[\frac{\mu_t}{\sigma_\varepsilon} \text{grad} \varepsilon \right] + C_{1\varepsilon} \frac{\varepsilon}{k} 2\mu_t S_{ij} \cdot S_{ij} - C_{2\varepsilon} \rho \frac{\varepsilon^2}{k} \quad (4.24)$$

where S_{ij} are the rates of deformation of a fluid element and σ_κ and σ_ε are the Prandtl numbers connecting the diffusivities of κ and ε to the eddy viscosity μ_t .

The equations above in words mean:

Rate of change of κ and ε	+	Transport of κ or ε by convection	=	Transport of κ or ε by diffusion	+	Rate of production of κ or ε	-	Rate of destruction of κ or ε
--	---	--	---	---	---	---	---	--

It is noticeable that the transport equations include five adjustable constants: C_μ , σ_κ , σ_ε , $C_{1\varepsilon}$ and $C_{2\varepsilon}$. The values for these constants have been obtained by comprehensive data fitting to the standard $\kappa - \varepsilon$ model for a wide range of turbulent flows. These values are:

Table 4.2: Values of $\kappa - \varepsilon$ model coefficients

$C_\mu = 0.09$	$\sigma_\kappa = 1.00$	$\sigma_\varepsilon = 1.30$	$C_{1\varepsilon} = 1.44$	$C_{2\varepsilon} = 1.92$
----------------	------------------------	-----------------------------	---------------------------	---------------------------

Reynolds stresses can be computed using the Boussinesq relationship:

$$-\overline{\rho u_i' u_j'} = \mu_t \left(\frac{\partial U_i}{\partial x_j} + \frac{\partial U_j}{\partial x_i} \right) - \frac{2}{3} \rho k \delta_{ij} = 2\mu_t S_{ij} - \frac{2}{3} \rho k \delta_{ij} \quad (4.25)$$

where δ_{ij} is the Kronecker delta.

The diffusion term causes the equations of κ and ε to be elliptic. As mentioned before in §4.3.1.1, elliptic equations require a set of boundary conditions. For the $\kappa - \varepsilon$ model the boundary conditions are found in Table 4.3.

The issue with the standard $\kappa - \varepsilon$ model is that the detailed boundary conditions need to operate the model cannot be easily obtained. Measurements of κ and ε are not available for every case examined and therefore, industrial CFD users need to refer to literature for the appropriate values of κ and ε and explore the sensitivity of the results to these inlet distributions (Versteeg & Malalasekera, 2007).

Table 4.3: Boundary conditions for the $\kappa - \varepsilon$ model

Inlet:	Distributions of κ and ε must be given
Outlet, symmetry axis:	$\partial\kappa/\partial n = 0$ and $\partial\varepsilon/\partial n = 0$
Free stream:	κ and ε must be given or $\partial\kappa/\partial n = 0$ and $\partial\varepsilon/\partial n = 0$
Solid walls:	Approach depends on Reynolds number

One of the most commonly used versions of the $\kappa - \varepsilon$ model is the so called RNG $\kappa - \varepsilon$ model that has attracted a lot of interest. RNG stands for renormalization group, which is proposed by Yakhot and Orszag of Princeton University. This model has its roots in the statistical mechanics approach that can provide robust basis for the extension of eddy viscosity models. These statistical approaches can be associated with the statistics of small-scale turbulence in order to develop the model. Yakhot and Orszag approach is able to treat the small scale turbulence as a random forcing function in the Navier-Stokes equations. The result of the renormalization is the systematic substitution of the small scales of motion in the governing equations by means of their effects on large scale motions and a modified viscosity. The mathematics included to the derivation of the RNG model are abstruse and only the version of RNG $\kappa - \varepsilon$ for high Reynolds number is presented in (Versteeg & Malalasekera, 2007).

The $\kappa - \omega$ model

As it was mentioned in the previous paragraph, in the $\kappa - \varepsilon$ models the kinematic eddy viscosity ν_t is calculated through the velocity scale $\vartheta = \sqrt{\kappa}$ and the length scale $l = \kappa^{3/2}/\varepsilon$. However, the length scale can be described by other terms as well, apart from the dissipation of turbulence kinetic energy ε . That yields the formulation of other two-equation turbulence models, like the $\kappa - \omega$ model proposed by Wilcox in 1988. Wilcox employed the turbulence frequency $\omega = \varepsilon/\kappa$ (dimensions s^{-1}) as the second variable. Under this consideration, the length scale and the eddy viscosity are given as:

$$l = \frac{\sqrt{k}}{\omega} \quad \text{and} \quad \mu_t = \frac{\rho k}{\omega} \quad (4.26 \ \& \ 4.27)$$

As usual, the Reynolds stresses are computed with the Boussinesq expression. At high Reynolds numbers, the transport equations for κ and ω read as follows:

$$\frac{\partial(\rho k)}{\partial t} + \text{div}(\rho k U) = \text{div} \left[\left(\mu + \frac{\mu_t}{\sigma_k} \right) \text{grad}(k) \right] + P_k - \beta^* \rho k \omega \quad (4.28)$$

where

$$P_k = \left(2\mu_t S_{ij} \cdot S_{ij} - \frac{2}{3} \rho k \frac{\partial U_i}{\partial x_j} \delta_{ij} \right) \quad (4.29)$$

is the rate of production of turbulent kinetic energy and

$$\frac{\partial(\rho\omega)}{\partial t} + \text{div}(\rho\omega U) = \text{div} \left[\left(\mu + \frac{\mu_t}{\sigma_\omega} \right) \text{grad}(\omega) \right] + \gamma_1 \left(2\rho S_{ij} \cdot S_{ij} - \frac{2}{3} \rho \omega \frac{\partial U_i}{\partial x_j} \delta_{ij} \right) - \beta_1 \rho \omega^2 \quad (4.30)$$

In words:

Rate of change of κ and ω	+	Transport of κ or ω by convection	=	Transport of κ or ω by diffusion	+	Rate of production of κ or ω	-	Rate of destruction of κ or ω
---	---	---	---	--	---	--	---	---

Table 4.4: Values of κ - ω coefficients

$C_k = 2.0$	$\sigma_\omega = 2.0$	$\gamma_1 = 0.553$	$\beta_1 = 0.075$	$\beta^* = 0.09$
-------------	-----------------------	--------------------	-------------------	------------------

The advantage of κ - ω is that it does not require wall-damping functions in low Reynolds numbers for the integration to the wall. That is the reason that it was adopted in many industrial applications. At the wall the value of the turbulent kinetic energy κ is set to zero, while the frequency ω tends to infinity. Alternatively, a very large value can be given to ω at the wall or, as it was proposed by Wilcox, a hyperbolic variation can be used $\omega_p = 6\nu/(\beta_1 y_p^2)$ at the near-wall grid point. In practice though, it has been shown that the results are not very sensitive to the precise value of ω .

The boundary conditions need to be specified as follows: at the inlet, the values of κ and ω must be defined and at the outlet, zero gradient conditions are specified. The most difficult case is the description of the boundary condition of ω in a free stream, where both the turbulent kinetic energy and turbulent frequency tend to zero. The problem in this case is that the eddy viscosity μ_t is indeterminate or infinite as $\omega \rightarrow 0$. A convenient solution is to specify a very small value of ω , instead of setting it to zero. However, even though that solves the problem for some cases, it might have a strong impact on the results in other applications, since the results depend on the assumed value of ω . Such applications are aerodynamics and aerospace applications, where free stream boundary conditions are used very often (Versteeg & Malalasekera, 2007).

The Reynolds Stress Model

The two-equation turbulence models presented before have proven to be useful for many industrial applications. The main assumptions are that the turbulent stresses are a linear function of the rate of strain by a scalar turbulent viscosity and that the principal strain directions are aligned to the principal stress directions. These assumptions are adequate for many cases, as long as the constants of the models are calibrated correctly. However, they might be unrealistic for complex strain fields resulting from complex geometries, swirls and body forces, such as buoyancy.

In these cases, the employment of a more rigorous relationship between the stresses and the strains is necessary. For this reason, models that do not depend on the turbulent viscosity have been developed, i.e. Reynolds stress transport models (RSM). According to RSM, the turbulent stresses are directly determined by solving a transport equation for each stress component. That means that six additional coupled equations are required together with an equation for ϵ to provide a length scale.

RSM is a very advanced tool able to handle complex strain and deal with non-equilibrium flows. At the same time though, it is computationally very expensive and more difficult to use, since it requires the definition of the boundary conditions for all the new parameters. Moreover, convergence problems have been reported. These drawbacks have caused the adoption of RSM to lag behind in industrial engineering applications (WS Atkins Consultants & NSC, 2002).

Launder et al. (1975) suggested a solution strategy for the RSM. In the analysis that follows the same principles will be followed. The Reynolds stresses are denoted as $R_{ij} = -\frac{\tau_{ij}}{\rho} = \overline{u'_i u'_j}$. However, for the sake of clarity these stresses are the kinematic Reynolds stresses. The form of the transport equation reads:

$$\frac{DR_{ij}}{Dt} = \frac{\partial R_{ij}}{\partial t} + C_{ij} = P_{ij} + D_{ij} - \epsilon_{ij} + \Pi_{ij} + \Omega_{ij} \quad (4.31)$$

In words it is describes as:

Rate of change of $R_{ij} = \overline{u'_i u'_j}$	+	Transport of R_{ij} by convection	=			
Rate of production of R_{ij}	+	Transport of R_{ij} by diffusion	-	Rate of dissipation of R_{ij}	+	Transport of R_{ij} due to turbulent pressure-strain interactions
					+	Transport of R_{ij} due to rotation

If analyses, the transport equation describes nine partial differential equations, six of which are independent. The independent Reynolds stresses are: $\overline{u_1'^2}$, $\overline{u_2'^2}$, $\overline{u_3'^2}$, $\overline{u_1' u_2'}$, $\overline{u_1' u_3'}$, $\overline{u_2' u_3'}$ and $\overline{u_2' u_1'} = \overline{u_1' u_2'}$, $\overline{u_3' u_1'} = \overline{u_1' u_3'}$, $\overline{u_3' u_2'} = \overline{u_2' u_3'}$.

The convective C_{ij} , production P_{ij} and rotational Ω_{ij} term in the transport equation can be obtained in their exact form.

$$C_{ij} = \frac{\partial(\rho U_k \overline{u'_i u'_j})}{\partial x_k} = \text{div}(\rho \overline{u'_i u'_j} U) \quad (4.32)$$

$$P_{ij} = - \left(R_{im} \frac{\partial U_j}{\partial x_m} + R_{jm} \frac{\partial U_i}{\partial x_m} \right) \quad (4.33)$$

$$\Omega_{ij} = -2\omega_k (\overline{u'_j u'_m} e_{ikm} + \overline{u'_i u'_m} e_{jkm}) \quad (4.34)$$

where ω_k and e_{ikm} represent the rotational vector and the alternating symbol respectively.

e_{ikm} can take only three scalar values: $e_{ikm} = +1$ if i, j and k are different and in cyclic order, $e_{ikm} = -1$ if i, j and k are different and in anti-cyclic order; and $e_{ikm} = 0$ if any of the indices are the same.

The equation of transport requires further models that describe the diffusion D_{ij} , the dissipation ε_{ij} and the pressure-strain correlation terms Π_{ij} . In the next paragraphs these models will be derived.

Diffusion term D_{ij} : this term is usually modelled assuming that the rate of transport of Reynolds stresses by diffusion is proportional to gradients of Reynolds stresses. The concept of the gradient diffusion is very common in turbulence modelling. The simplest form, which is often employed in commercial CFD packages, reads as follows:

$$D_{ij} = \frac{\partial}{\partial x_m} \left(\frac{V_t}{\sigma_\kappa} \frac{\partial R_{ij}}{\partial x_m} \right) = \text{div} \left(\frac{V_t}{\sigma_\kappa} \text{grad}(R_{ij}) \right) \quad (4.35)$$

with $V_t = C_\mu \frac{\kappa^2}{\varepsilon}$, $C_\mu = 0.09$ and $\sigma_\kappa = 1.0$

Dissipation term ε_{ij} : the assumption is that small dissipative eddies are characterised by isotropy. ε_{ij} is given in such a way that it affects only the normal Reynolds stresses ($i = j$) and each component of them evenly. The equation for ε_{ij} reads:

$$\varepsilon_{ij} = \frac{2}{3} \varepsilon \delta_{ij} \quad (4.36)$$

where ε is the dissipation of turbulent kinetic energy and δ_{ij} is the Kronecker delta.

Pressure-strain correlation terms Π_{ij} : These terms have the most significant effect in the transport equation of the RSM, but at the same time their modelling is very challenging. There two distinct physical processes that are associated with the pressure-strain interactions: 1) The reduction of anisotropy between the eddies caused by their mutual interaction, namely the slow process and 2) the rapid process, which refers to the production of eddies such that the anisotropic production of turbulent eddies is opposed. The rapid process is a result of the interactions between turbulent fluctuations and the mean flow strain. The total effect of both these processes is that energy is redistributed among the normal Reynolds stresses, causing the flow to be more isotropic, and reduce the shear Reynolds stresses.

The slow and the rapid processes are modelled in order to retrieve the Π_{ij} . The slow process assumes that the rate of return to isotropy is proportional to the degree of anisotropy (a_{ij}) of the Reynolds stresses ($a_{ij} = R_{ij} - \frac{2}{3}P\delta_{ij}$) divided by a characteristic time scale of the turbulence k/ε . The rapid process is modelled in such a way that it is proportional to the production of anisotropy. Taking into account the previous assumptions, the pressure-strain term is derived in its simplest form:

$$\Pi_{ij} = -C_1 \frac{\varepsilon}{k} \left(R_{ij} - \frac{2}{3} k \delta_{ij} \right) - C_2 \left(P_{ij} - \frac{2}{3} P \delta_{ij} \right) \quad (4.37)$$

with $C_1 = 1.8$ and $C_2 = 1.8$

Term k represents the turbulent kinetic energy, which can be found by simple addition of the three normal stresses:

$$k = \frac{1}{2} (R_{11} + R_{22} + R_{33}) = \frac{1}{2} (\overline{u_1'^2} + \overline{u_2'^2} + \overline{u_3'^2}) \quad (4.38)$$

The dissipation rate ε and the six equations for Reynolds stress transport are solved together. A model for ε is necessary for that, which can be the exact form, however for most of the commercial applications a simplification based on the standard $\kappa - \varepsilon$ model is sufficient. Therefore, ε is given as:

$$\frac{D\varepsilon}{Dt} = \text{div} \left(\frac{V_t}{\sigma_\varepsilon} \text{grad} \varepsilon \right) + C_{1\varepsilon} \frac{\varepsilon}{k} 2V_t S_{ij} S_{ij} - C_{2\varepsilon} \frac{\varepsilon^2}{k} \quad (4.39)$$

with $C_{1\varepsilon} = 1.44$ and $C_{2\varepsilon} = 1.92$

In words:

Rate of change ε	+	Transport of ε by convection	=	Transport of ε by diffusion	+	Rate of production of ε	-	Rate of destruction of ε
---------------------------------	---	---	---	--	---	--	---	---

Table 4.5: Boundary conditions for elliptic flows solved with RSM

Inlet:	Distributions of R_{ij} and ε must be given
Outlet, symmetry axis:	$\partial R_{ij}/\partial n = 0$ and $\partial \varepsilon/\partial n = 0$
Free stream:	$R_{ij} = 0$ and $\varepsilon = 0$ must be given or $\partial \kappa/\partial n = 0$ and $\partial \varepsilon/\partial n = 0$
Solid walls:	Use wall functions relating R_{ij} to either κ or u_τ^2

Concluding about RSMs, it is clear that these models might be very complex, but in the end, they are the simplest way to describe all the mean flow properties and the Reynolds stresses without having to adjust all the coefficients for each different case. However, due to their high computational cost, RSMs are not widely used in industry and therefore they are not as well validated as the $\kappa - \varepsilon$ model. At the same time, as noted in the introduction, convergence issues related to the coupling of the mean velocity and the turbulent stress fields through source terms might cause problems to the application of the models (Versteeg & Malalasekera, 2007).

4.3.7.2 Large Eddy Simulation (LES)

As outlined in the previous paragraph, a general-purpose RANS turbulence model has not been developed yet, so, a specific model with appropriate calibration has to be used for each application. The reason for that is mainly the different behaviour of large and small eddies. Considering a turbulent flow with high Reynolds numbers, the behaviour of small eddies appears to be nearly isotropic and to have a universal character. In contrast to the small eddies, larger eddies seem to behave according to the geometry of the domain, the boundary conditions and the body forces. Large eddies interact with the main flow by extracting energy from it. In general, they are characterised by anisotropy. The problem with RANS models is that they describe the behaviour of all eddies in a single way, while the flow mainly depends on the largest eddies. Therefore, a different approach that accounts specifically for the larger eddies is needed. The turbulent model named Large Eddy Simulation (LES) considers a time-dependent simulation for the larger eddies, while it employs a compact model based on the universal behaviour of the smaller eddies.

In this paragraph the operating principles of LES will be described. The difference with RANS models is that LES does not time-average. Instead, LES uses a spatial filter to separate larger and smaller eddies. This filter is based on a function with a specified cut-off width and when applied on the time-dependent flow equations, it distinguishes the eddies that have a length scale greater than the cut-off width. Now that the smaller eddies are separated from the larger, the flow information associated with the smaller, filtered-out, eddies is destroyed. At this stage, a sub-grid-scale (SGS) model needs to be employed that

describes the effects of the resolved eddies, the smaller unresolved eddies and the interaction between the large eddies on the resolved flow.

When the finite volume method is used, the space-filtered equations are solved in control volumes together with the SGS model of the unresolved stresses. This results to the description of the mean flow characteristics and yields all turbulent eddies which are larger than the cut-off width.

The LES model is derived for incompressible flows on Cartesian coordinates. Based on equations 2.4 and 2.21a,b,c, which refer to the continuity equation and the Navier-Stokes equations respectively. Since the flow is incompressible, $div(\mathbf{u}) = 0$ and therefore, hence the viscous momentum source terms S_u, S_v and S_w are zero. The filtering function of the LES method is applied to the computational domain for further simplification of the equations. A filtering function of the form $G(x, x') = G(x - x')$, indicates that variable G is independent of position x . The advantage of a linear filter, like the previous one, is that it allows a swap of the order of filtering and differentiation with respect to time, as well as the order of filtering and differentiation with respect to space. Filtering of the continuity equation and the Navier-Stokes equations, yields the flow equations used in LES:

$$\frac{\partial \rho}{\partial t} + div(\rho \bar{u}) = 0 \quad (4.40)$$

$$\frac{\partial(\rho \bar{u})}{\partial t} + div(\rho \overline{u u}) = -\frac{\partial \bar{p}}{\partial x} + \mu div(grad(\bar{u})) \quad (4.41a)$$

$$\frac{\partial(\rho \bar{v})}{\partial t} + div(\rho \overline{v u}) = -\frac{\partial \bar{p}}{\partial y} + \mu div(grad(\bar{v})) \quad (4.41b)$$

$$\frac{\partial(\rho \bar{w})}{\partial t} + div(\rho \overline{w u}) = -\frac{\partial \bar{p}}{\partial z} + \mu div(grad(\bar{w})) \quad (4.41c)$$

where the overbar indicates a filtered variable.

Moving further, the calculation of the convective terms $div(\rho \overline{\varphi u})$ on the left hand side of the equations is necessary. This can be achieved by writing $div(\rho \overline{\varphi u}) = div(\rho \bar{\varphi} \bar{u}) + (div(\rho \overline{\varphi u}) - div(\rho \bar{\varphi} \bar{u}))$, keeping in mind that the only available terms are the filtered velocity field \bar{u} , \bar{v} , \bar{w} and pressure field \bar{p} . In the previous expression, the first hand side can be calculated from the filtered $\bar{\varphi}$ – and \bar{u} – fields, while the second term is found by the model.

After this consideration, Equations 4.41 are transformed as follows, yielding the LES momentum equations:

$$\frac{\partial(\rho\bar{u})}{\partial t} + \text{div}(\rho\bar{u}\bar{u}) = -\frac{\partial\bar{p}}{\partial x} + \mu \text{div}(\text{grad}(\bar{u})) - (\text{div}(\rho\bar{u}\bar{u}) - \text{div}(\rho\bar{u}\bar{u})) \quad (4.42a)$$

$$\frac{\partial(\rho\bar{v})}{\partial t} + \text{div}(\rho\bar{v}\bar{u}) = -\frac{\partial\bar{p}}{\partial y} + \mu \text{div}(\text{grad}(\bar{v})) - (\text{div}(\rho\bar{v}\bar{u}) - \text{div}(\rho\bar{v}\bar{u})) \quad (4.42b)$$

$$\frac{\partial(\rho\bar{w})}{\partial t} + \text{div}(\rho\bar{w}\bar{u}) = -\frac{\partial\bar{p}}{\partial z} + \mu \text{div}(\text{grad}(\bar{w})) - (\text{div}(\rho\bar{w}\bar{u}) - \text{div}(\rho\bar{w}\bar{u})) \quad (4.42c)$$

This set of LES momentum equations has some obvious analogies with the RANS momentum equations (4.18). The last term in each equation is a result of the filtering operation, similar to RANS momentum equations, where the corresponding terms are a result of time averaging. These terms cause a divergence to the set of τ_{ij} stresses. The τ_{ij} stresses are mainly dependent on the convective momentum transport due to the interactions between the unresolved and SGS eddies. Therefore, the divergence of the τ_{ij} , is known as sub-grid-scale stresses. A major difference between LES and RANS is that the first model contains further contributions in the SGS stresses, while RANS does not account for them. LES utilises a decomposition of a flow variable to estimate these contributions, however analysing this in further detail is not in the scope of this document (Versteeg & Malalasekera, 2007).

4.3.7.3 Direct Numerical Simulation (DNS)

The four equations that describe the fluid flow, namely the continuity equation and the three Navier-Stokes equations, are a closed set of equations with four unknowns, i.e. u , v , w and p . In contrast with RANS and LES, DNS uses sufficiently fine spatial and time resolution to develop a transient solution for the whole range of turbulent eddies and the fastest fluctuations in the flow.

Such a detailed solution provides very useful information for the flow regime and it has some important benefits. At first, all the turbulence parameters can be calculated precisely at any point in the domain. These parameters cannot be measured instantaneously in a physical model and the turbulence structures created cannot be visualised and probed. The biggest advantage of this is that this information can be used to validate and calibrate other turbulence models. Some databases with DNS results are already available for that reason. Moreover, new and advanced experimental techniques can be evaluated by comparison with DNS simulations. Last but not least, DNS can be used for fundamental turbulence research on flows that cannot occur in reality. Some examples have been listed by Moin and Mahesh (1998), such as shear-free boundary layers developing on walls at rest with respect to the free stream, effect of initial conditions on the development of self-similar turbulent wakes etc.

On the other hand, there are some serious drawbacks that caused DNS to lag behind. The wide range of length and time scales due to different eddies in a turbulent flow makes the application of DNS very difficult. It has been shown that the ration of the smallest to the

largest length scales is proportional to $Re^{\frac{3}{4}}$. As an example, a turbulence flow with a moderate $Re = 10^4$ can be considered. To resolve the whole range of turbulence length scales, a DNS would require 10^3 points in each coordinate direction. Therefore, a 3D simulation requires 10^9 points, which is equivalent to $Re^{\frac{9}{4}}$, to describe the processes at all scales. At the same time, sufficiently small time steps are required to acquire meaningful time-averaged flow results and turbulence statistics. In practice, this implies that the computational cost of DNS is significantly higher than RANS and LES. The result is that DNS is rarely employed for industrial and even research applications (Versteeg & Malalasekera, 2007). Thus, it is beyond the scope of this report to go further in the analysis of DNS methods. However, the accelerating developments in super-computers is expected to promote the utilization of DNS.

4.4 Post-processing

Post-processing is the operation that takes place in a numerical simulation. The results from the solver comprise of a huge amount of data, usually in a numeric form, which are very difficult to comprehend. An interpretation of the results is needed, so that they become more informative and illustrative. This is achieved through post-processing that improves the visualization of the results by turning them to a graphical form. Since, many codes consist of 3D models, an appropriate display of the results is necessary. Post-processing is belongs to the wider category of Computer-aided engineering (CAE), which refers to the employment of computer software for facilitating engineering analysis.

Most of the numerical models have post-processing tools readily available as a part of their distribution package. The increasing computer power also helped the spreading and the development of more advanced visualization tools. These tools include domain geometry and mesh display; vector plots; line and shaded contour plots; 2D and 3D surface plots; particle tracking; viewing manipulation, such as translation, rotation, scaling; colour PostScript output; animation for dynamic result display etc. (Versteeg & Malalasekera, 2007).

In most of the cases, the programs used for the post-processing has a graphical user interface, which makes them easier to use, even by non-specialists. However, one should keep in mind that the post-processing is not a strictly technical task, but it involves a considerable amount of aesthetic work of art, in order to make the results nicely presented (Anderson, 1995).

4.5 Errors and uncertainties

4.5.1 Introduction

Before closing the chapter of numerical modelling, a point needs to be made clear. No matter how analytical the governing equations are and how sophisticated and efficient the numerical code is, the numerical models are representations of the physical phenomenon and therefore they are to a certain degree only approximations of the nature. Keeping that in mind, the numerical models should always be used carefully and with full awareness of their capabilities and weaknesses. That can be achieved via good knowledge of the underlying physics, presented earlier, and some other potential errors and uncertainties, human or computer created that will be presented in this paragraph.

Errors refer to recognisable deficiencies and they are distinguished from uncertainties, which are defined as potential deficiencies caused by lack of knowledge. In theory, errors can be removed if special care is taken. On the other hand, uncertainties are related to fundamental lack of understanding of a physical process and therefore cannot be removed from the numerical model.

There is not a universal classification of errors, but according to ERCOFTAC BPG there are seven different groups of errors and uncertainties: a) Model error and uncertainty, b) Discretisation or numerical error, c) Iteration or convergence error, d) Round-off errors, d) User errors and e) Code errors (WS Atkins Consultants & NSC, 2002).

4.5.2 Model error and uncertainty

Usually, the governing equations of the flow in a model include some assumptions and therefore they do not represent the exact solution of the physical problem. Sometimes, this representation of the reality is not adequate and significant differences between the real flow and the simulation arise. In short the errors and uncertainties described here are an inevitable consequence of solving the “wrong” equations.

As an example, the viscous flows can be mentioned, where the potential errors are a result of the utilization of turbulence model to approximate the turbulence.

4.5.3 Discretisation or numerical error

As it was described in §4.2.3, the equations of in numerical models are discretised, on a mesh or on particles, and therefore they are not solved for the whole domain. Due to the fact that the solution at a certain point is an interpolation of the exact solution of the adjacent points, errors arise. Theoretically, this problem can be confronted by increasing the number of the cells. However, in practice grid refinement is not enough and both the distribution of the grid cells and the interpolations schemes play an important role.

Good designing of the mesh and employment of high order numerical schemes can improve the results. The mesh refinement however, should be performed in such a level that does not make the simulation computationally uneconomical.

4.5.4 Iteration or convergence error

These errors arise due to the differences between a fully-converged solution and non-converged solution. As discussed in §4.5.3, the accuracy of the model is subject to the discretization level. In most of the cases, depending on the type of flow, the results tend to converge to a specific solution, as the fineness of the mesh increases. The same happens also when the time step decreases or when the tolerance in some criteria is reduces, for example a decrease of the Courant–Friedrichs-Lewy (CFL) number. However, there are some turbulent flows that convergence cannot be reached and the solution fluctuate between some limits no matter how many times the mesh is refined.

The equations in most of the numerical models are solved iteratively, starting from an initial approximation of the flow solution, gradually finding a solution for the whole domain by trying to satisfy the boundary conditions according to some tolerance criteria. The general

recommendation is to perform sensitivity tests for the grid resolution and the tolerance criteria. Even if the computational cost for a fully-converged solution is too high, one should be able to assess the errors inherited in a non-converged simulation.

4.5.5 Round-off errors

Round-off errors arise from the limited number of computer digits available for storage of a value. As a result, a value is not the exact mathematical value, but a rounded approximation of it. Numerical models approximate the value in accuracy of six or more decimal places. At a first glance, it does not seem to cause a significant error. However, through the thousand, million or even billion of iterations that take place in the solving problem, the errors tend to accumulate. The former might result to unrealistic solutions or instabilities in the model.

4.5.6 User errors

These types of errors are a result of human mistakes or carelessness. Mistypes or inserting the wrong parameters will not cause the model to stop from calculating according to the input values. However, the results will not correspond to what it was initially expected. Usually, the more experienced the user is the less possibilities to do such mistakes or the higher the possibilities to realize them and fix them in time.

Computers do not forgive carelessness, something summarised in programmers' popular saying as "garbage in, garbage out".

4.5.7 Code errors

Most of the numerical models have a complex structure and consist of many different algorithms of hundreds or thousands lines of code. Programming errors, compiler errors, inconsistency with the hardware used might cause the models to stop running or to generate unrealistic results. These bugs are most of the times very difficult to spot and to fix beforehand. The users' contribution to the enhancement of the models is invaluable. Small bugs are discovered through different applications of the model and by reporting them to the developers, the model is improved overall.

4.5.8 Recommendations and guidelines

There is a long list of guidelines for efficient and accurate numerical modelling. Here, recommendations drawn from the guidelines given by (WS Atkins Consultants & NSC, 2002) are presented.

The convergence errors can be handled if thorough overview and control over the residuals is enabled. In order to achieve that the residuals should be dimensionless and their spatial distribution should be monitored. Residuals for be checked on global balances, such as conservation of mass, momentum, turbulent kinetic energy, mass flow balance at certain plains in the flow domain. Moreover, apart from the residuals themselves, the rate of their change should be checked with increasing iterations. Convergence should be assessed purely in terms of the levels of residual error. The solution should be monitored in certain

areas or points in the computational domain according to the target values of the parameters examined. Apart from convergence, the monitoring of residual can yield areas in the computational domain with poor mesh design or unrealistic velocities caused by wrong boundary conditions.

The round-off errors can be minimized by increasing the accuracy of the representation of real numbers. A general advice for the developers is to program in 64-bit platforms, which corresponds to double precision on common UNIX workstations.

Regarding the discretization, there are errors associated with the spatial and the temporal discretization. To reduce the errors related to the first one, it is recommended to employ high order numerical schemes. Even though first order schemes, like the upwind scheme, tend to be more robust, there are only useful to commence a simulation and they are not efficient for convergence problems. In any case, an estimation of the error in the calculation is always useful to evaluate the quality of the results. The error can be estimated with mesh refinement/coarsening studies. The temporal errors are associated with the time step and the numerical time schemes used in the simulation. In general, second or higher order schemes should be used and, similarly to the spatial convergence tests, time convergence tests should be performed to check the influence of the time step in the accuracy of the simulation. For time dependent flows, the time and space discretization errors are strongly bonded and the overall accuracy of the simulation is determined by the lower order component of the discretization. The time step should always be in accordance to the resolution of the grid in order to fulfil the numerical stability criteria, such as the CFL condition.

As has become apparent, the correct mesh design is the most important element of a successful simulation. Usually, the mesh is designed with CAD software and then it is transferred to the numerical model. Common mistakes here might be, wrong dimension units or co-ordinate system. The file might also be misread by the numerical program or be corrupted during the transfer process. One should always check visually the mesh before running a model. Other things to take into account are the local refinement that might be necessary, due to some local grid details that need to be properly considered, and the deformation of the geometry, due to hydrodynamic, mechanical and thermal loads.

The user errors can be summarised in potential concerns in the “solution strategy”. To begin with, the user has to be able to understand the underlying physics and choose the appropriate methods in order to model a certain phenomenon. Research of the literature is needed to assess if there is need for validation of the model results. If there are enough similar studies for comparison, validation might not be necessary. However, one should not be seduced by the colourful results of the simulations and instead compare them with literature or experimental data. Two other things that are common sources of errors are caused by the use of independent software for meshing and post-processing. The user should always keep in mind that inconsistencies between different software are possible, such as units, names of the parameters etc. An important strategic aspect is to choose a model according to the computational resources available. At the outset, the objectives and the requirements of the simulation should be clear in order to design an efficient simulation.

5. Commonly Used Software

5.1 Navier-Stokes solvers (CFD)

5.1.1 Introduction

The introduction is unique for this sub-chapter only. However, it gives some general information to the reader that can be useful for the other software categories as well.

The term CFD stands for Computational Fluid Dynamics and it is a specific field of fluid mechanics that utilizes numerical approaches to examine fluid flows, heat transfer and chemical reactions. Therefore the term CFD could be used to describe any numerical model that is used for fluid flow modelling, however, in practice the term mainly refers to computer codes that solve the fully non-linear Navier-Stokes (NS) (Eq. 2.21) in all three dimensions. As a result, CFD refers to very powerful computer-based simulations that can handle very complex phenomena and its applications spans from aerodynamics and turbomachinery to marine and biochemical engineering. CFD is a cutting-edge robust technique for industrial and research applications, however, its high computation cost often demands the use of high performance computers.

Historically, CFD was first used in 1960s in the aerospace industry. However, the immense computational cost of running CFD codes meant that the methodology was mainly used in research environments until the 1990s, when powerful computers started becoming affordable, and the technique became more commonplace for design and for more general use by engineers and researchers. Since then, many different CFD codes have been developed using a wide range of pre-processing, solving and post-processing tools and methods.

The minimum cost of suitable hardware for running a CFD simulated is estimated between £5,000 and £10,000, although this is very case dependent, and the license fee can vary between £10,000 and £50,000 depending on the specifications of the software (solvers, post-processing tools, parallelization, etc) (Versteeg & Malalasekera, 2007). At the same time, one can find a broad list of open-source, freely distributed codes. However, the potential user should have some programming skills in order to be able to use the software and be able to validate the results with other broadly used, well validated models or experimental results.

A list of the available free and commercial CFD codes can be found at the CFD-wiki webpage (CFD Online, 2013). The software is divided into solvers, mesh generators and post-processing software (visualization). Each code uses different approaches for solving the NS equations, different numerical schemes and different tools for pre- and post-processing. Important aspects to consider when selecting which software to use are a) how well-validated the model is, b) how well-documented it is and c) the size of the “community” that uses the software. In other words, the confidence and the supporting services that each model offers. For that reason, it is recommended to perform a thorough review in the literature and applications for different CFD models, before deciding which model is the most appropriate for the case that it will be used for.

Two of the most commonly used CFD programs are presented in more detail in the following sections. From the list of free codes, OpenFOAM is selected and from the commercial software, ANSYS CFX. These two codes are also well validated for many marine and ocean engineering applications.

5.1.2 OpenFOAM

OpenFOAM (Open source Field Operation and Manipulation) is an extensive software package that has been widely used in industrial and academic applications. It is a freely distributed and open source CFD Toolbox, which has a broad range of features that enable it to deal with complex fluid flows, chemical reactions, heat transfer, solid dynamics and electromagnetics.

OpenFOAM includes tools for pre- and post-processing that come either as utilities or as third party software. Over 80 solver applications and over 170 utility applications are included in the latest version 2.2.x. OpenFOAM was initially developed in the late 1980s at Imperial College, London in FORTRAN. Later it was rewritten in C++, due to its high modularity and object oriented features. In 2012, the ESI group announced the acquisition of OpenFOAM Ltd and since then ESI-OpenCFD is responsible for the development and maintenance of OpenFOAM. New releases of the software are regularly announced, which include bug fixes reported by users and corrected by the OpenFOAM Team. OpenFOAM is run on a Linux operating system.

The users of OpenFOAM can benefit from the freedom that it offers to customise and extend the solvers to suit the specific physical problem that they want to simulate. The customized libraries can then be compiled independently and simply linked with the other libraries and utilities. However, the users need to have good knowledge of the underlying numerical methods and physics, and good programming skills.

The most important advantages of OpenFOAM are: a) the zero license cost, b) the user-friendly syntax for partial differential equations, c) the parallelization of its applications to a theoretically unlimited number of processors and d) the wide range of applications, models and numerical schemes offered with the basic installation.

On the other hand, there are some drawbacks that can be summarised as the absence of an integrated user interface and the lack of maintained documentation.

Structure of the model

Above all, OpenFOAM is a C++ library that creates executables, named applications. The applications of OpenFOAM can be divided in two categories: solvers, that solve a specific problem in continuum mechanics; and utilities, that deal with data manipulation and pre-processing tasks.

One of the strengths of OpenFOAM is that new solvers and utilities can be created by its users with some pre-requisite knowledge of the underlying method, physics and programming techniques involved.

The simplistic sketch in Fig. 5.1 gives an overview of OpenFOAM structure.

Pre-processing

Mesh generation is one of the most important parts of pre-processing. OpenFOAM supports unstructured meshes containing cells of any shape, which practically means that cells can have any number of faces and faces can have any number of edges. That feature gives

great flexibility and gives OpenFOAM the ability to accommodate complex shapes and different refinement techniques. At the same time OpenFOAM can accept meshes created using third-party and commercial mesh generators. There are converters that they deal with the task of exporting meshes to file formats that OpenFOAM can read.

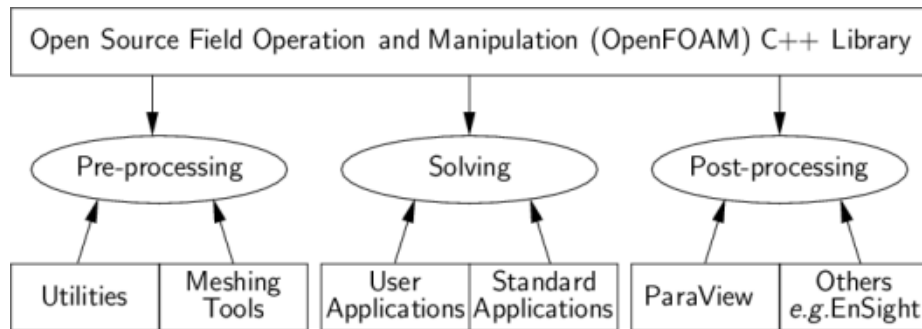


Figure 5.1: Structure of OpenFOAM

Solving

The source code supplies users with the libraries that include the physical models, but, as mentioned before, users can add and compile their own libraries as well. A list of the main solvers existing in the latest version and particularly useful for marine and ocean engineering applications are given here:

- Incompressible flows: there is a long list of incompressible solvers, from which the most favourable for marine engineering problems are:
 - icoFoam Transient solver for incompressible, laminar flow of Newtonian fluids
 - shallowWaterFoam Transient solver for inviscid shallow-water equations with rotation
 - rhoPorousMRFSimpleFoam Steady-state solver for turbulent flow of compressible fluids with RANS turbulence modelling, implicit or explicit porosity treatment

- Multiphase flows: can be used for free-surface flows and complicated problems, such as run-up on structures, wave breaking etc.
 - interFoam Solver for two incompressible, isothermal immiscible fluids using a VOF (volume of fluid) phase-fraction based interface capturing approach

- `interDyMFoam` Solver for two incompressible, isothermal immiscible fluids using a VOF (volume of fluid) phase-fraction based interface capturing approach, with optional mesh motion and mesh topology changes including adaptive re-meshing.
- `porousInterFoam` Solver for two incompressible, isothermal immiscible fluids using a VOF (volume of fluid) phase-fraction based interface capturing approach, with explicit handling of porous zones.

In both incompressible and multiphase flows the porous solvers are listed because they can be very useful for breakwater applications, such as energy dissipation over rumble mount armour.

There are also many other solvers, not strictly linked with marine applications, but that might be useful when examining complicated problems, such as loads on structures, response of power take off mechanisms etc. These solvers may also be used for combustion problems, buoyancy-driven flows, conjugated heat transfer, compressible flows, particle methods, solid dynamics and electromagnetics.

For situations involving turbulent flow, a wide range of turbulence models are available. The methods vary from Reynolds-average simulation (RAS), also known as Reynolds-averaged Navier-Stokes (RANS), models to Direct Numerical Simulation (DNS) (See chapter 4). Some of them are briefly mentioned below:

RANS equations are obtained by replacing each variable in the NS equations with its time average and turbulent fluctuation. The RANS equations are solved for time average variables and a turbulence closure model is required to solve for so-called Reynolds Stress terms that are comprised of fluctuating components.: there are different turbulence models available in OpenFOAM, such as $\kappa - \varepsilon$, $\kappa - \omega$, etc.

Large eddy simulation (LES): Large turbulent structures in the flow are resolved by the governing equations, while the effect of the sub-grid scales (SGS) is modelled.

Detached eddy simulation (DES): It is a hybrid technique according to which near-wall regions are treated with RANS approach, while the bulk flow with LES method.

Direct numerical simulation (DNS): It solves the full Navier-Stokes equations at very fine time and grid scales without any turbulence modelling and so simulates all scales of turbulence directly. This approach is only possible for very small space and time scales.

Post-processing

ParaView is the post processing tool supplied and compiled with OpenFOAM and gives great flexibility in manipulating the results of the simulations. It uses the Visualisation Toolkit (VTK) as its data processing and rendering engine and it can therefore read any data in VTK format. `foamToVTK` utility is used to convert data from its native format to VTK format. This means that any other VTK-based software can be utilised to post-process OpenFOAM's results.

Another very interesting feature is the “run-time post-processing”. This means that specific results can be extracted from a simulation while running. It is achieved with the use of “function objects”. Velocities, pressures, surface elevation and iso-surfaces are written in separate files while the simulation runs, which are accessible before the simulation finishes (OpenFOAM Foundation, 2011-2013), (OpenFOAM, 2012).

Applications

OpenFOAM is considered to be a well validated CFD program. Regarding the marine and ocean engineering applications, there are two recently released libraries: IHFOAM (Higuera, Lara, & Losada, 2012) and waves2Foam (Jacobsen, Fuhrman, & Fredsøe, 2012). Both are based on RANS models, using the VoF method and include special features for wave generation and absorption. Despite the fact that these libraries are new, there are already many examples of their use in various applications available in the literature, such as wave-structure interaction (Ransley, Hann, Greaves, Raby, & Simmonds, 2013) and focused wave groups (Vyzikas, et al., 2013).

5.1.3 ANSYS CFX

ANSYS CFX is a commercial CFD software designed to simulate fluid flows. It has been applied to a wide range of engineering applications, such as water flowing past ship hulls, gas turbine engines, aircraft aerodynamics, pumps, fans, HVAC systems, mixing vessels and many others. ANSYS CFX has its roots in Flow3D and TASCflow, which were developed by United Kingdom Atomic Energy Authority (UKAEA) and Advanced Scientific Computing (ASC) in Canada respectively. Flow3D was released in late 1980s and it has been renamed CFX-4 in the middle 1990s. Initially, CFX-4 was orientated to multiphase chemistry models, while TASCflow was basically used for turbo-machinery applications delivering solutions of hydrodynamic flow properties (velocities and pressures). Both of the ancestors of ANSYS CFX offered multi-block structured hexahedral meshing codes (Wikipedia: ANSYS CFX).

The latest version contains a wide variety of physical models that are able to reproduce virtually any type of phenomena related to fluid flows. The solver is highly parallelised and developed to provide reliable solutions quickly and robustly (ANSYS, www.ansys.com, 2013).

Pre-processing

As meshing is the most crucial and time consuming part of pre-processing, different pieces of ANSYS software can help the user create very complex geometries. The valid mesh elements in CFX are tetrahedral, pyramidal, prismatic (wedge) and hexahedral (ANSYS, ANSYS CFX -Solver Theory Guide, 2009). ANSYS DesignModeler is used to prepare the CAD geometry for the CFD model and ANSYS Mesh component allows the user to mesh the geometry automatically or manually.

Furthermore, mesh import API (Application Programming Interface) enables customization of 3D meshes generated from third-party mesh files. At the same time, a number of API

functions allow more advanced users to program in C and FORTRAN and create their own custom mesh import executables.

Solver

ANSYS CFX solver can replicate a wide range of physical models including steady-state or transient incompressible or compressible flows varying from subsonic to hypersonic, laminar or turbulent flows, Newtonian or non-Newtonian flows and ideal or real gases.

The main focus of ANSYS CFX software is to deliver fast and reliable convergence, which is scalable with mesh size. This is achieved by using coupled algebraic multi-grid techniques. Boundary layers can be captured efficiently with high-aspect ratio mesh cells without influencing the accuracy. The accuracy is also enhanced by using a second-order advection numerical scheme by default. For dynamic meshes, there is an adaptive central bounded numeric scheme that locally adjusts the discretization to be close to the second order, ensuring the stability in the simulation. These features make the program able to replicate flows in which inter-equation coupling is significant, such as rotating flows with strong Coriolis terms, combusting flows and high-speed flows with strong pressure gradients.

As most of the industrial applications include turbulent flows, ANSYS CFX has incorporated many classic and customized turbulence models to account for turbulent effects. A long list of two-equation models is available, as well as Reynolds-stress models. The shear stress transport (SST) model is mainly promoted by the developers as equally economical to $\kappa - \varepsilon$ model, but more reliable for separated flows and including better treatment of near-wall conditions. The ANSYS CFX SST model is combined with numerous other turbulence modelling innovations, such as automatic wall treatment for maximum accuracy in wall shear and heat transfer predictions and a number of other extensions. Moreover, the efficiency of the simulation can be improved by predicting the location where the laminar flow becomes turbulent and model the transition. This is achieved with the Menter-Langtry $\gamma - \theta$ laminar-turbulent transition model, which is a powerful tool able to describe the transition mechanisms.

In addition, scale-resolving turbulence models, such as LES (large eddy simulation) and DES (detached eddy simulation) are available in ANSYS CFX. Furthermore, a novel scale-adaptive simulation (SAS) has been developed, which provides a steady solution in stable flow regions and resolves turbulence in transient instabilities. The SAS model is the highlight of ANSYS CFX turbulence models and has been validated for many cases.

Common solvers for marine and ocean engineering

More specifically, for marine and ocean engineering there are solvers that are designed for multiphase flows, fluid-structure interaction and immersed solids. Multiphase flows: free surface flows can be simulated successfully in ANSYS CFX. Examples are open channel flow, flow around ship hulls, tank filling and sloshing. Users are also able to distinct the air (Finnegan W. , 2013) velocity field from the water one, in order to allow for separation to be simulated with strong mixing or entrainment.

There are two transport models: a) Lagrangian for simulating disperse phases discretely distributed in a continuous phase and b) Eulerian for capturing the exchange of mass, momentum and energy. That makes ANSYS CFX capable of replicating phenomena such as primary and secondary spray break-up, wall erosion due to particle impact and phase changes due to evaporation, cavitation, condensation or boiling. Lastly, the multiple size group (MUSIG) allows bubbles of different sizes to breakup or to collate.

Fluid-structure interaction (FSI) can be modelled by using ANSYS CFX FSI, which is linked to ANSYS Workbench environment, so no extra third-party software needs to be purchased. FSI algorithm can deform a background fluid mesh to account even large boundary movements. The displacement can be defined by the user or can be calculated from ANSYS structural mechanics software or from the rigid body solver. The boundary displacements are diffused into the internal mesh, while consideration is taken to allow near-wall elements to deform less. These deformations can take place in a single mesh topology, but if extreme motion needs to be reproduced, there is an automatic remeshing tool which connects to ANSYS ICEM CFD taking advantage of all its features. At the same time, any other scriptable meshing software can be used.

FSI includes the immersed solid method. This technique allows unlimited motion of solid objects through regions of fluid without any deformation or remeshing. The concept of the method relies on the identification of the overlap area as the solid moves in the fluid and then the fluid solution is adjusted to account for the presence of the solid.

Post-processing

ANSYS CFX has post-processing tools able to translate the results from the CFD simulations to graphs, animations and reports that are easily transferable. The data can also be exported to ANSYS CFD-Post, third-party graphics and CAE packages for further interpretation. Using ANSYS Workbench CFD data can be mapped to ANSYS simulation surfaces as added thermal and pressure loads.

Add-On modules

There are extra modules that can be purchased separately and extend the capabilities of ANSYS CFX. Most of the add-on modules facilitate mesh generation and manipulation. The add-on modules are: a) Geometry Defeaturing and Editing, b) Six-Sigma Analysis and Design Exploration, c) Advanced Meshing, d) Rapid 3-D Blade Design Tool, e) Turbo-Specific Meshing Tool and f) Rapid 2-D Through-Flow Analysis.

Advantages

One of the most important features of ANSYS CFX is its modern, intuitive and flexible graphical user interface (GUI). It offers many abilities of customization and automation for more advanced users. In any case, a friendly GUI is convenient for new users or for average-skilled programmers.

Moreover, the developers of ANSYS CFX focused on the integration of their model with other software, in order to facilitate the pre- and post- processing processes. ANSYS CFX

operates as a workbench platform with bi-directional linkage to the all major CAD systems and meshing tools, while having an embedded easy drag-and-drop transfer of data between its applications. ANSYS workbench platform offers quick preparation of the grid geometry, mesh, physics and post-processing, generating new CFD results very easily. This is a very useful feature when examining multiphysics phenomena. For example, it has a two-way connection to ANSYS structural mechanics products, which enables the study of fluid-structure interaction in the same easy-to-use environment.

Applications

Most of the applications have been already mentioned in the main text. There is extensive literature covering the simulation of ship motion and propeller rotation and optimization. Important work has also been done with turbines and other mechanical parts. ANSYS CFX has also been employed for marine renewable energy simulations, like tidal current turbines (Goundar & Ahmed, 2013) and wave energy converters (Finnegan W. , 2013).

5.1.4 SPHysics & DualSPHysics

SPHysics is a Smoothed Particle Hydrodynamics numerical model developed for simulating free-surface flows. SPHysics and later DualSPHysics are the products of an international collaboration among the Johns Hopkins University (US), the University of Vigo (Spain) and the University of Manchester (UK).

The first version of the software was called SPHysics and it was released in August 2007 as a free open-source software. The model was first coded in FORTRAN 90 with a modular form and many available compiling options. More recently, DualSPHysics was coded in C++ and CUDA language in order to be able to handle simulations on CPU (Central Processing Unit) and GPU (Graphics Processing Unit) respectively (Crespo, et al., 2013). The fact that the code is open and the recently developed user interface encourage researchers to contribute relatively easily to SPHysics project.

Several test cases confirmed the capability of the program to deal with free surface flows in two and three dimensions. The test cases comprised of the classic dam break simulation; waves generated by a paddle in a beach; a tsunami generated by a sliding wedge; floating objects in waves; floating bodies with 2D periodicity and focused wave group approaching a trapezoid (Gesteira, Rogers, Dalrymple, Crespo, & Narayanaswamy, 2010).

The current release of DualSPHysics is version 3, which can be compiled both in Microsoft Windows and Linux operating systems. DualSPHysics works only with 64bit systems. It is a well-documented open-source code and can be downloaded from the website (DualSPHysics, DualSPHysics Homepage, 2013) together with the relevant documentation and tutorials.

There are several codes using the SPH method. A list of the available codes includes freely available open-source codes and commercial packages (ERCOFTAC, 2013). This website is designed by the SPH European Research Interest Community (SPHERIC) and many interesting aspects regarding the method and its applications can be found there.

Mathematical model

SPHysics, as an SPH model, has in its core the integral interpolants (§ 4.2.3.6). In discrete notation, any function $A(r)$ for a particle is approximated by the following equation:

$$A(\vec{r}) = \sum_b m_b \frac{A_b}{\rho_b} W_{ab} \quad (5.1)$$

where the summation covers the particles over the region of the kernel function. m_b and ρ_b refers to the mass and density of a particle b . W_{ab} is the weight function or commonly named kernel.

The performance of an SPH model is highly dependent on the choice of the kernel function. In SPHysics the user has the option of four different kernel functions: a) Gaussian, b) Quadratic, c) Cubic spline and d) Quintic. A detailed description is found at the SPHysics User Guide (Gesteira, Rogers, Dalrymple, Crespo, & Narayanaswamy, 2010).

The momentum equation in a continuum field is given by:

$$\frac{D\vec{v}}{Dt} = -\frac{1}{\rho} \nabla P + \vec{g} + \vec{\theta} \quad (5.2)$$

where \vec{v} is the velocity vector; ρ is the fluid density; P is the pressure; \vec{g} is the gravitational acceleration; and $\vec{\theta}$ refers to the diffusion terms.

There are three different approaches for modelling the diffusive terms: a) artificial viscosity, b) laminar viscosity and c) full viscosity, which refers to a combination of laminar viscosity and Sub-Particle Scale (SPS) turbulence. All the formulations are described by Gesteira, et al., January 2010.

The continuity equation is employed for calculating the fluid density:

$$\frac{d\rho_\alpha}{dt} = \sum_b m_b \vec{v}_{ab} \nabla_a W_{ab} \quad (5.3)$$

where the subscripts a and b refer to particles a and b respectively.

Regarding the equation of state, the fluid is assumed to be weakly compressible. This treatment for determining the fluid pressure through the equation of state is faster than using the Poisson equation for pressure. The relationship between the pressure P and the density ρ is assumed to follow the expression of the equation of state:

$$P = B \left[\left(\frac{\rho}{\rho_0} \right)^\gamma - 1 \right] \quad (5.4)$$

where $\gamma = 7$, $\rho_0 = 1000 \text{ kg m}^{-3}$ and B is the reference density, which is related to the speed of sound at the reference density state.

The particles are moved using the XSPH variant described in Monaghan's work in 1989, according to which a given particle moves with velocity close to the average velocity of the neighbouring particles.

In the user manual, the formulations of the thermal energy, the density reinitialization, the kernel renormalization and the Reimann solver are stated under the corresponding headings (Gesteira, Rogers, Dalrymple, Crespo, & Narayanaswamy, 2010).

Numerical Model

The description of the numerical model will be divided in pre-processing, solving and post-processing.

In the latest version, DualSPHysics has implemented a pre-processing interface (DPI) based on Java in order to facilitate the input of the most common parameters needed for launching a simulation. For more complex cases DSI can be used to define the geometrical properties and the resulting XML file can be manually edited. More specifically, two very useful pre-processing tools included in the DualSPHysics package are: a) GenCase and b) DualSPHysics Pre-processing Interface (DPI). The first comes as part of the software and it is used to turn XML based simulation definitions into a particle data set ready for solving. DPI is available separately from the main software package and it provides detailed descriptions of each parameter via in-application tool tips, as well as a case builder with real-time visual feedback.

The SPH solver includes many features and options. To begin with, there are two time integration schemes (Verlet and Symplectic) and the time step is variable. The core of a SPH code is the kernel functions. Cubic Spline and Quintic Wendland kernel are employed in DualSPHysics. The density filters comprise of a Shepard filter and a Delta-SPH formulation (Crespo, et al., 2013). The fluid is treated as weakly incompressible, using Tait's equation of state. Moreover, the solver is capable of dealing with floating objects and boundary conditions can be defined as dynamic or as periodic open boundaries. At the same time, the developers' team is planning to incorporate many new features in the future, such as Multi-GPU implementation, Multiphase solvers for gas-solid-water simulations, coupling with SWASH model etc.

It is worthwhile to discuss briefly the unique solving technique that DualSPHysics uses to increase the computational efficiency. As mentioned in the introduction, the software uses both CPU and GPU computing to accelerate the simulations. Both the CPU and GPU versions share the main code and only a few differences distinguish the two versions. The CPU version uses the OpenMP API parallelization method. The GPU solving scheme is presented in the flow chart shown in Figure 5.2.

The post-processing of DualSPHysics results provides all the useful information regarding the magnitudes of interest, such as vorticity at different planes, forces exerted on different objects, maximum wave heights or just plotting the different physical quantities of the particles. Isosurfaces are used in the latest version to provide better visualization of the free-surface. The open-source software ParaView (see §5.1.2) can be used for further interpretation of the numerical results. The results of the simulation are written in ASCII or in Binary (BINX2) format. The binary format is recommended for memory saving purposes. Moreover, VTK format is also available for better visualization of the results, because it supports many data types, such as scalar, vector, tensor, texture, and different algorithms such as polygon reduction, mesh smoothing, cutting, contouring and Delaunay triangulation.

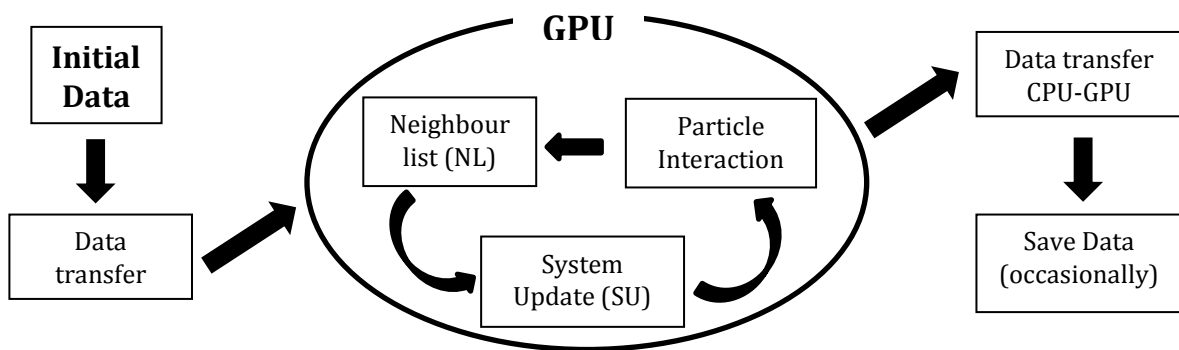


Figure 5.2: GPU solving scheme

Limitations

One of the major limitations of the SPH method, similar to CFD Navier-Stokes solvers, is the high computational cost of the simulations. Even though the problem is partially tackled with parallel processing, the computational times are unrealistic for large domains and real life engineering problems. However, SPHysics has implemented some innovative techniques in order to make use of the full processing power. GPUs are used as an alternative to CPUs for numerical modelling with impressive performance. For this reason SPHysics is also coded in CUDA (Compute Unified Device Architecture) framework using some extensions to the C/C++ language.

Another limitation of the code is incorporated in the mathematical model. In the SPH formulation the fluid is treated as weakly compressible. The compressibility is adjusted to slow the speed of sound and control the time stepping in the model using a Courant criterion. At the same time the second limitation that rises with compressibility is that the sound speed should be about ten times faster than the maximum fluid velocity, in order to keep the density variations to within less than 1% (Gesteira, Rogers, Dalrymple, Crespo, & Narayanaswamy, 2010).

More generally, there are several other drawbacks with SPH that result from the basic concept of the method. During an SPH simulation the particles become disordered. The exact form of the disorder depends on the dynamics and therefore it is not possible to estimate errors in the traditional ways used for finite differences or finite elements. However,

the particles are disordered in an orderly way, due to the inconsistency of probability function estimates with the dynamics.

The errors associated with SPH include errors in the integral interpolant, errors in the summation interpolant and errors when the particles are disordered (Monaghan, Smoothed particle hydrodynamics, 2005).

Since SPH is a relatively new technique and experience is being built for the pitfalls and limitations of the method through its use. It is suggested that a potential user should refer to the following applications for reference.

Applications

Smoothed Particle Hydrodynamics (SPH) is a relatively new method for examining the propagation of highly nonlinear and breaking waves. Therefore a number of cases had to be used in order to identify the capability of the method for modelling water-related phenomena. SPHERIC (ERCOFTAC, 2013) has used some validation tests as benchmark test cases for that reason. These cases include 2D driven cavity, 3D dam break, sloshing wave impact, 2D flow over a rippled bed etc. In this section, instead of providing examples only for DualSPHysics, applications from different SPH solvers will be presented regarding marine and ocean engineering. If one wants to find applications only for DualSPHysics, there is a list of publications at the website (DualSPHysics, DualSPHysics References , 2013).

At Johns Hopkins University a computational tool using the SPH method has been under development since 2000, that later became the basis of SPHysics and DualSPHysics. This model was used to replicate waves breaking on beaches, green water overtopping on decks and wave-structure interaction (Dalrymple & Rogers, 2006).

In another study, large water wave generation due to landslides, also known as impulse wave generation, is simulated using SPH. The numerical results have been compared with experimental particle image velocimetry (PIV) results. This study is very useful to indicate how tsunamis are born and propagated (ERCOFTAC, 2013) (Heller & Spinneken, 2013).

There are some other applications of SPH method, not necessarily with DualSPHysics, but considered useful here as examples of the applicability of the method.

SPH has been applied to calculate the extreme wave and green water loading on ships and offshore structures. The highly non-linear fluid and structural behaviour is tackled using a coupled FE-SPH approach (Campbell, Vignjevic , & Patel, 2008). The employment of SPH for wave-structure interaction has found application to partially immersed breakwater. An SPH-LES model was used for tracking the free surface without numerical diffusion and analysing turbulence and eddy vortices near the breakwater (Gotoh, Shao, & Memita, 2004).

SPH has been applied for marine renewable energy research as well. The fluid-structure interaction of wind turbines and waves has been examined and the numerical model seems to be promising (Manenti & Ruol, 2008).

It should be noted that despite the fact that SPH is a relatively new method, it has shown very good potential for ocean and marine engineering and that newer and improved

methods, like Nearest Neighbouring Particle Searching (NNPS), which are based on SPH, have shown very good performance for complex problems of water wave dynamics (Zheng, Soe, Zhang, & Hsu, December 2010).

5.2 Hydrostatic models

5.2.1 POM

POM (Princeton Ocean Model) is a community general circulation numerical ocean model which was developed at Princeton University by G.Mellor and A.Blumberg in 1977. The numerical model focuses on ocean circulation in areas like semi-enclosed seas and open and global oceans. It calculates a wide range of wave properties including current, temperature and salinity.

POM is an open source model that can be downloaded from the website (POM, 2013).

Mathematical model

The equation below follows the sigma coordinates system, depicted in Figure 5.3, in order to deal with complex topographies (Mellor, 2004). The reader should refer to Philips (1957) and Blumberg and Mellor (1980, 1987) for further information.

$$x^* = x, y^* = y, \sigma = \frac{z - \eta}{H + \eta}, t^* = t \quad (5.5)$$

where x, y, z are the conventional Cartesian coordinates; $H(x, y)$ is the bottom topography and $\eta(x, y, t)$ is the surface elevation. $D = H + \eta$; $\sigma = 0$ at $z \equiv \eta$ and $\sigma = -1$ at $z \equiv H$.

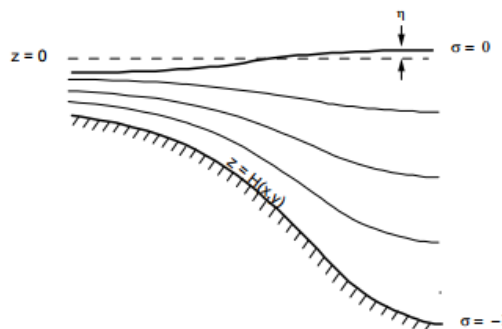


Figure 5.3: The sigma (σ) coordinate system

After conversion to sigma coordinates and deletion of asterisks, the basic equations may be written in horizontal Cartesian coordinates, as described by Mellor.

$$\frac{\partial DU}{\partial x} + \frac{\partial DV}{\partial y} + \frac{\partial \omega}{\partial \sigma} + \frac{\partial \eta}{\partial t} = 0 \quad (5.6)$$

Numerical model

The model includes the Mellor-Yamada turbulence scheme, which contains an embedded second moment turbulence closure-model to provide vertical mixing coefficients. The vertical coordinate is scaled on the water column depth in the sigma coordinate system. Curvilinear orthogonal coordinates are used for the horizontal grid together with the "Arakawa C" differencing scheme. The vertical differencing is implicit whereas the horizontal one is explicit. A split time step and a free surface are applied in the model. As a result, the external mode is 2D, it uses a short time step and it is based on the external wave speed, whereas the internal mode is 3D, it uses a long time step and the internal wave speed. Therefore, it is possible to use the complete thermodynamics.

The method to solve this equation uses the external mode calculation, which is contained in program pom2k. The external mode calculation updates the two main parameters: surface elevation (EL) and vertically averaged velocities (UA, VA). Meanwhile the internal mode calculation results in updates for the other parameters: U, V, T, S and the turbulence quantities.

The program is written in Fortran 90 as described below:

The first step is the model initialization by setting the parameters and initial values. Then an imbedded loop in the internal mode time stepping is introduced by the index IINT. This allows the subroutines ADVCT and BAROPG to run. ADVCT calculates the horizontal advection (including curvature terms) and the diffusion parts. On the other hand, BAROPG computes the baroclinic and vertical involving density. At the same time, a second loop is embedded with the external mode time step index IEXT.

There are two different ways that can be used to solve the equation:

The first method adjusts the integrals of U, V to match UT, VT. This is achieved with the use of subroutines VERTVL and BCOND(5), which correspond to the sigma coordinate transformed vertical velocity and the lateral boundary conditions at the coastlines. Subroutines ADVQ(Q2) and ADVQ(Q2L) correspond to the advective terms for the turbulence quantities. PROFQ solves for the vertical part and BCOND(6) is used for the boundaries; Subroutines ADVT(T), ADVT(S), PROF(T), PROF(S) and BCOND(4) are used to calculate temperature and salinity. Subroutines ADVU, ADVV, PROFU, PROFV and BCOND(3) deal with horizontal advection and bottom boundary conditions. The external loop finishes and it returns to the internal mode time stepping via index IINT.

The second computes the surface elevation; In this case, subroutine BCOND(1) for the boundaries and ADVAVE for the advective and horizontal diffusion terms are employed. Vertically averaged velocity (UA, VA) are computed and then UT and VT, which time averaged UA and VA respectively over the interval DT=DTI (internal mode time step). Subroutine BCOND(2) runs before the end of the loop.

Limitations

The Courant-Friedrichs-Levy (CFL) computational stability condition is integrated in the external mode and it limits the time step when solving the transport equation. This is considered to be the most stringent restriction. There are other restrictions as well, but this one usually controls the time step by 90%. However, it is possible to circumvent this constraint during the simulation. A proposed technique is to map the bottom topography on the grid and then calculate the CFL limiting time step for each grid point.

Furthermore, the time step should not be too small, because more time steps would be computed and the computational cost will increase. On the other hand, if the CFL limit becomes greater, the time step also increases.

Another limitation is the difficulty to compute the internal pressure gradient, especially over a steep topography in the sigma coordinate systems.

Applications

PROFS-Princeton Regional Ocean Forecasting System (GOM) was used to develop and conduct high-resolution, accurate model simulations in coastal oceans and semi-enclosed seas (Gulf of Mexico, Caribbean Sea, the Santa Barbara Channel and the Santa Monica Bay) under realistic ocean environments utilizing nested grid-techniques, data-assimilations and high-resolution atmospheric models (Oey, 2008).

POM has also been applied for investigating atmosphere-ocean coupled processes that might occur over the Yellow and East China Sea shelves in winter (Iwasaki, Isobe, & Kako, 2014).

5.2.2 COHERENS

COHERENS (COupled Hydrodynamical Ecological model for REgioNal Shelf Seas) is three-dimensional multi-purpose numerical model used for simulating coastal and shelf seas, estuaries, lakes and reservoirs. This numerical tool was developed in order to understand better the relevant physical and ecological processes and to predict and monitor waste disposals. It can be used for process studies, predictive or operational purposes. It was developed between 1990 and 1998 by a European group called the "MAST project" (Luyten, Jones, Proctor, Tabor, Tett, & Wild-Allen, 1999). The partners were the Management Unit of Mathematical Models of the North Sea and Schelelt Estuary, Brussels, Belgium and the Napier, Edinburgh University (MUMM).

COHERENS is freely available and can be downloaded from the official website after registration (Luyten, 2000). The model is available as a free source code for the scientific community. It is easy to implement across a range of computing platforms.

Numerical Model

COHERENS is attractive to modellers with expertise and need for sophisticated modelling products. Its clear modular structure and its flexibility, thanks to the options to select

different processes, schemes and types of forcing for a particular application, are important advantages. It is relatively simple to model some processes like predictive and operational setups without deep knowledge of the program structure in detail.

The first version of the model is denoted as COHERENS VI. Since then, the code has been translated in FORTRAN 90. It can run in sequential and parallel mode. For the latter, the MPI method is used. The output can be exported in netCFD format. For the creation of the model mesh, both curvilinear and general σ -coordinates are available.

COHERENS consists of four main components: a) a module for solving advection-diffusion equations for the physical part; b) a simple microbiological module about the dynamics of organic matter (microplankton, detritus) or dissolved inorganic gases (nitrogen, oxygen); c) an Eulerian sediment module about organic particles or deposition and resuspension of inorganic; and d) a component transport model for contaminant distributions (both Eulerian and Lagrangian).

Moreover, the equations are discretized on an Arakawa C-grid using either Cartesian or spherical coordinates. For the vertical diffusion, a variety of schemes is available varying from one equation schemes to RANS models, while for the horizontal diffusion, a constant coefficient or Smagorinsky formulation can be selected.

By default, the model run in barotropic mode, but temperature and salinity can optionally be included.

Limitations

In the current version (COHERENS V2.0) the modules for biology, sediments and particle tracers and a wave-current interaction module have not been implemented.

Applications

At the beginning, the main focus of COHERENS was to simulate conditions in the North Sea. In a test case COHERENS was used to simulate seasonal cycle of temperature and the microbiological and resuspension processes in the central part of the North Sea (Luyten, 2000).

There are also other applications cited at the website (<http://www2.mumm.ac.be/coherens/>), such as the calculation of mean currents around the Belgian coastal zone and the water renewal time scales for Hervey bay situated at the central eastern coast (Australia).

5.2.3 Delft3D

Delft3D is a software suite developed by Deltares, formerly known as Delft Hydraulics, for 3D computations in coastal, river and estuarine areas. It covers numerical modelling of flows, sediment transport, waves, water quality, morphological developments and ecology. Delft3D is composed of several modules which can be executed independently or can be coupled together and interact with one another, by exchanging information automatically via the communication file.

Delft3D-FLOW is one of these modules, which is a program used for 2D (depth-averaged) or 3D hydrodynamic and transport simulations. It can calculate non-steady flow and transport phenomena caused by tidal and meteorological forcing on a rectilinear or curvilinear boundary fitted grid. The sigma co-ordinate system can be used in 3D simulations for the vertical grid.

In greater detail some of the areas of Delft3D application are: tide and wind-driven flows, such as storm surges; stratified and density driven flows; river flow simulations; simulations in deep lakes and reservoirs; simulation of tsunamis; hydraulic jumps; bores and flood waves; fresh-water river discharges in bays; salt intrusion; thermal stratification in lakes, seas and reservoirs; cooling water intakes and waste water outlets; transport of dissolved material and pollutants; online sediment transport and morphology; wave-driven currents and non-hydrostatic flows.

Delft3D is an open source freely available software that can be downloaded from its homepage (Deltares, Delft3D Open Source Community, 2013).

Mathematical model

Delft3D-FLOW solves the Navier-Stokes equation for an incompressible fluid, based on the shallow water with the Boussinesq approximation (Deltares, User Manual, Delft3D-FLOW version 3.15, 2011). The system of equations, which consist of the horizontal momentum equations, the continuity equation, the transport equation and a turbulence closure model (Lesser, Roelvink, van Kester, & Stelling, 2004).

Taking into account the shallow water assumption, the vertical accelerations can be neglected and the vertical momentum equation reduces to the hydrostatic pressure equation. Delft3D can operate in σ and Cartesian coordinates. The equations that follow are derived in the Cartesian coordinate system (x, y, z, t) :

$$\frac{\partial P}{\partial z} = -\rho gh \quad (5.7)$$

The continuity depth-averaged equation is given:

$$\frac{\partial \zeta}{\partial x} + \frac{\partial [h\bar{U}]}{\partial y} + \frac{\partial [h\bar{V}]}{\partial z} = S \quad (5.8)$$

where ζ is the water surface elevation and h the water depth. S represents the contributions per unit area due to discharge or withdrawal of water, evaporation and precipitation. U and V refer to the Generalized Lagrangian mean (GLM) reference frame velocities.

The momentum equations in x and y directions read:

$$\frac{\partial U}{\partial t} + U \frac{\partial U}{\partial x} + V \frac{\partial U}{\partial y} + \frac{w}{h} \frac{\partial U}{\partial \sigma} - fV + \frac{1}{\rho_0} P_x - F_x - M_x - \frac{1}{h^2} \frac{\partial}{\partial \sigma} \left(v_V \frac{\partial U}{\partial \sigma} \right) = 0 \quad (5.9a)$$

$$\frac{\partial V}{\partial t} + U \frac{\partial V}{\partial x} + V \frac{\partial V}{\partial y} + \frac{w}{h} \frac{\partial V}{\partial \sigma} - fU + \frac{1}{\rho_0} P_y - F_y - M_y - \frac{1}{h^2} \frac{\partial}{\partial \sigma} \left(v_V \frac{\partial V}{\partial \sigma} \right) = 0 \quad (5.9b)$$

where v_V is the vertical turbulent eddy viscosity and the horizontal pressure terms P_x and P_y at a certain depth z are determined by the Boussinesq approximations. f is the Coriolis parameter. ρ_0 is the reference density. The contributions due to external sources or sinks of momentum are represented by M_x and M_y . F_x and F_y represent the horizontal friction terms, which are also known as the Reynold's stresses. They are determined by the Rodi formulas using the eddy viscosity (Lesser G. R., 2009).

Further information regarding the mathematical background and the analytical governing equations of Delft3D can be found in the user manual under the heading "Conceptual description" (Deltares, User Manual, Delft3D- FLOW version 3.15, 2011).

Numerical modelling

The numerical model of the FLOW module is based on finite differences. The geographical area is discretized on a curvilinear grid, where the 3D shallow water equations are solved. In general, the grid is assumed to be a well-structured orthogonal grid and the coordinates can be Cartesian or spherical. The water flow is described by the water level (ζ) and the velocity components (u, v, w). A staggered grid arrangement of variables is used in Delft3D and corresponds to the Arakawa C-grid.

The time integration of the 3D SWE is described in detail in the user manual (Deltares, User Manual, Delft3D- FLOW version 3.15, 2011). There are some interesting parts that need to be summarized here. The time integration could be performed explicitly satisfying the Courant number for the wave propagation: $CFL_{wave} = 2\Delta t \sqrt{gH} \sqrt{\frac{1}{\Delta x^2} + \frac{1}{\Delta y^2}} < 1$, where H is the water depth the Δx and Δy refer to the smallest grid spaces. However, that yields very small time steps and it is not recommended for long runs. As a result, implicit time integration is necessary. The time integration method used is based on the Alternating Direction Implicit (ADI) method, which splits each time step into two stages. On the other hand, the spatial discretization of the horizontal advection terms is achieved by three different schemes: the WAQUA-scheme, the Cyclic method or the Flooding scheme (Deltares, User Manual, Delft3D- FLOW version 3.15, 2011).

Delft3D is an integrated simulation package that is composed of a set of modules. Each one focuses on certain aspects of research and engineering problems and can be run independently or coupled with one another. When different modules are coupled, information has to be exchanged between them. This is achieved through a communication file, where each module reads the information written by the other modules and writes information that other modules require in order to run. Furthermore, there are specific

modules for visualization of the results. Delft3D is equipped with a menu shell that allows access to the various modules.

Delft3D-FLOW consists of several utilities designed for pre-processing, post-processing and solving. The most important for pre-processing are Delft3D-RGFGRID, Delft3D-QUICKIN and Delft3D-NESTHD, which are used for generation of curvilinear grids, for preparation and manipulation of grid oriented data (bathymetries, initial water levels, salinity or concentration of constituents) and for offline generation of the boundary conditions for a nested model respectively. The utilities Delft3D-TRIANA and Delft3D-TIDE are employed for performing offline tidal analysis of time series and tidal analysis on time-series of measured water levels or velocities. For post-processing, there are two tools: Delft3D-GPP and Delft3D-QUICKPLOT. They are both used for visualization and animation of the simulation results.

As mentioned before, apart from Delft3D-FLOW, there are several other modules included in Delft3D that can be coupled with the Delft3D-FLOW module. Delft3D-FLOW is used to calculate the hydrodynamic properties, i.e. velocities, water elevations, density, salinity, vertical eddy viscosity and vertical eddy diffusivity. These results can be used as input to other modules for further calculations, such as short wave propagation, far-field water quality, mid-field water quality and particle tracking, ecological modelling and cohesive/non-cohesive sediment transport. These properties are calculated by Delft3D-WAVE, Delft3D-WAQ, Delft3D-PART, Delft3D-ECO and Delft3D-SED respectively. The following schematic shows a simplistic representation of the connection between the various modules (Deltares, User Manual, Delft3D- FLOW version 3.15, 2011).

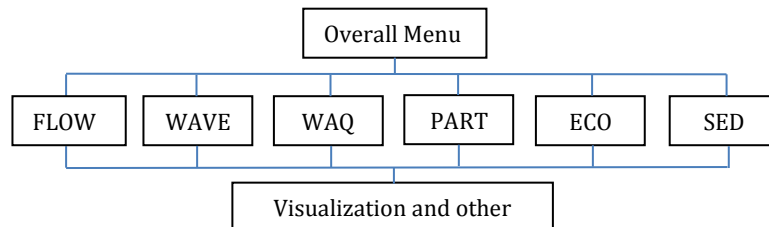


Figure 5.4: Modules of Delft3D

Assumptions

A list of the principal assumptions and approximations underlying Delft3D-FLOW can be found in the user's manual in the chapter of "conceptual description" (Deltares, 2011). The most important are summarized here:

When using the σ coordinate system, the depth is assumed to be much smaller than the horizontal length scale. If this assumption is valid, the vertical momentum equation reduces to the hydrostatic pressure relation. If the vertical acceleration is important, this assumption is not valid and a "non-hydrostatic" model can be optionally employed.

The effect of variable density is considered only in the pressure term.

In a Cartesian grid the curvature of Earth is not taken into account and the Coriolis parameter is assumed to be uniform by default.

The model is valid only for mid-field and far-field dispersion simulation of discharged water. This is because the immediate effect of buoyancy on the vertical flow is not taken into account.

In theory, Delft3D-FLOW is able to resolve the turbulence scales using the LES. In practice, usually the grids are too coarse to account for the turbulent fluctuations. For that reason the RANS equations with a turbulence closure model are employed.

In the σ coordinate system the long wave equation is solved. This means that the pressure is assumed hydrostatic and the short waves are not simulated. As a result, the equations are averaged in analogy to turbulence, and radiation stresses are introduced, which are related to the wave quantities via a closure model.

Limitations

As a numerical model, Delft3D-FLOW follows all the restrictions embedded in a model. That means that the solution produced is only an approximation of the exact solution and the accuracy is subject to the numerical schemes used, to the discretization of the bottom topography and the assumptions made on the physical processes.

The time integration influences the wave propagation. The limitation here is that free surface waves can be propagated correctly only when a small time step is selected. In this case, the computational cost increases significantly.

The computational domain of the model is only a small part of the physical domain and therefore open boundaries have to be implemented. These boundaries should ideally leave the waves to propagate freely through them. In practice, reflections take place on them which can be observed by spurious oscillations superimposed on the physical results. Another problem that might appear with the open boundaries is artificial re-circulation flow caused by non-linear phase variation of the tidal forcing along them. A similar effect is observed when the Coriolis force is not accounted for in the boundary conditions.

Other important limitations refer mainly to the time stepping. Analytical description and ways to increase accuracy can be found in the user guide (Deltares, User Manual, Delft3D-FLOW version 3.15, 2011).

Applications

Delft3D has been applied in many applications in the field of coastal engineering. More specifically, applications can be found on the website (Deltares, Delft3D Open Source Community, 2013) regarding the hydrodynamics, i.e. wind-driven longshore currents, tidal currents along open coast, wave driven currents (rip currents). Other applications refer to the response of submerged breakwaters, such as scouring effects.

Delft3D has been extensively used for sediment transport, such as suspended load and bar dynamics. An application of Delft3D assessing the impact of a storm on the breaching

process is investigated for the channel of Maumusson in France that was hit by the Xynthia storm in 2010 (Bergsma, 2012).

Recent studies for Marine Renewable Energy have employed Delft3D. Some of studies refer to wave energy resource assessment (Magar, Joshi, Williams, & Conley, 2013) and to Tidal Stream Energy resource characterization. Many case studies can be found in the literature, such as for Philippines (Abundo, Nerves, Paringit, & Villanoy, 2012) and the North-West of Spain (Carballo, Iglesias, & Castro, 2008).

5.2.4 TELEMAC-MASCARET

TELEMAC-MASCARET was initially developed by the Laboratoire National d'Hydraulique et d'Environnement (LNHE), which is a department of Electricite de France.

It is an integrated suite of solvers for use in the field of free-surface flows: current, waves, transport of tracers and sedimentology. It is also used for dimensioning and impact studies. The program is coded in FORTRAN.

It uses high-capacity algorithms based on the finite element method, where space is discretized in the form of an unstructured grid of triangular elements. This structure allows further refinement at specific areas of interest.

It could run on numerous systems including Linux, Unix and Windows. The hydrodynamics section of the program comprises of five key functions which can be used for free surface numerical models:

1. ARTEMIS: Wave agitation in harbours
2. MASCARET: One-dimensional flows
3. TELEMAC-2D: Two-dimensional flows – Saint Venant equations
4. TELEMAC-3D: Three-dimensional flows – Navier-Stokes equations
5. TOMAWAC: Wave propagation in the coastal area

TELEMAC-MASCARET is a freely available open source software that can be downloaded from the website (TELEMAC-MASCARET, 2013).

Telemac-3D

TELEMAC-3D is designed to solve the three-dimensional equations as free surface flow equations. The code can be run in hydrostatic pressure mode, but also in hydrodynamic mode. The transport-diffusion equations are solved for temperature, salinity and concentration. TELEMAC-3D solves the transport equations of several tracers which can be grouped into two categories, namely “active” tracers (temperature and salinity) and “passive” tracers, which do not affect the flow.

The main results of the simulation are the three components of the velocity and the concentrations of transported quantities. Its prominent applications can be found in seas and rivers (TELEMAC-3D Software, March 2013).

Mathematical model

TELEMAC-3D solves the Navier-Stokes equations of an incompressible fluid with the free surface changing in time. It also uses the Boussinesq approximation for the momentum. It describes the velocity field (u, v, w) and the water depth h (and, from the bottom depth, the free surface S is calculated) at each time step.

The three dimensional equations being solved are:

$$\frac{\partial U}{\partial x} + \frac{\partial V}{\partial y} + \frac{\partial W}{\partial z} = 0 \quad (5.10)$$

$$\frac{\partial U}{\partial t} + U \frac{\partial U}{\partial x} + V \frac{\partial U}{\partial y} + W \frac{\partial U}{\partial z} = -g \frac{\partial Z_S}{\partial x} + \nu \Delta(U) + F_x \quad (5.11a)$$

$$\frac{\partial V}{\partial t} + U \frac{\partial V}{\partial x} + V \frac{\partial V}{\partial y} + W \frac{\partial V}{\partial z} = -g \frac{\partial Z_S}{\partial y} + \nu \Delta(V) + F_y \quad (5.11b)$$

$$P = P_{atm} + \rho_0 g (Z_S - z) + \rho_0 g \int_z^{Z_S} \frac{\Delta \rho}{\rho_0} dz \quad (5.12)$$

$$\frac{\partial T}{\partial t} + U \frac{\partial T}{\partial x} + V \frac{\partial T}{\partial y} + W \frac{\partial T}{\partial z} = \nu \Delta(T) + Q \quad (5.13)$$

where h is the water depth; S the free surface elevation; U, V, W the three dimensional components of velocity; T the passive or active (acting on density) tracer; ν the velocity and tracer diffusion coefficients; Z is the bottom depth; ρ_0 the reference density, $\Delta \rho$ the variation of density; t the time; x, y the horizontal space components; z the vertical space component; F_x, F_y the source terms; Q the tracer source of sink; h, U, V, W and T are the computational variables.

Numerical model

All the simulation modules are written in FORTRAN 90. When using a simulation module from the TELEMAC system, the user may have to program specific subroutines which are not in the code's standard release. These subroutines are written so that they can be modified with the help of the "Guide for programming" in the TELEMAC System, provided that the user has a basic knowledge of FORTRAN language.

The procedure to be carried out is to recover the standard version of the user subroutine, as supplied in the distribution, and copy it into the current directory. Then the subroutine should be amended according to the needs of the simulation and at last the set of subroutines need to concatenate into a single FORTRAN file. This file has to be compiled during the TELEMAC-3D launching process.

During that programming stage, the user can gain access to the various variables of the software through the FORTRAN 90 structures. All the data structures are gathered within FORTRAN files, which are known as modules. Nearly all the arrays which are used by TELEMAC-3D are declared in the form of a structure.

Assumptions

The fluid is assumed to be incompressible. The hydrostatic pressure hypothesis is applied and is linked to condition of small vertical movements, but a non-hydrostatic Navier-Stokes module is available as well.

In the model, there is a Boussinesq approximation for the momentum (the density variations are not taken into account in the gravity term).

Limitations

TELEMAC-3D has fast and implicit schemes, but at the expense of a problem with negative depths. To cope with this negative parameter, a specific smoothing algorithm has been designed, but this can sometimes lead to the drawback of water slowly creeping above dykes, when the discretization is performed with only a few points.

Mesh refinement requires a restriction on the time step to be taken for the calculations.

Applications

The main example given in the website (TELEMAC-MASCARET, 2013) is the Saint-Chamas hydraulic power plant in the Berre lagoon (France) with studies of quantification of different flows (incoming, outgoing and total), the exchanges between the Mediterranean Sea and the lagoon and the influence of power plant losses on the canal flows and the salinity of the lagoon (Ricci, Piacentini, Weaver, Ata, & Goutal, 2013). The software allows monitoring water temperature or salinity, sedimentary issues or vertically heterogeneous flows.

5.2.5 MIKE 21

MIKE 21 was developed by DHI (Danish Hydraulic Institute) Water Environment Health and it is used to simulate physical, chemical and biological processes in coastal and marine waters (DHI webpage, 2011). MIKE 21 is designed for 2D free surface modelling of flow and waves; sediment transport and environmental processes for estuarine and coastal applications. Since 1985, when DHI Software developed their first modelling tools, a wide range of models have been released, i.e. MIKE URBAN, WEST, MIKE 21, MIKE 3,

LITPACK, MIKE Animator, MIKE C-MAP, ECO Lab, MIKE 11, MIKE flood, FEFLOW, MIKE SHE, MIKE BASIN and MIKE 21C, that are employed for modelling ranging from the marine environment to water resources (DHI, 2011).

MIKE 21 SW is a state-of-the-art third generation spectral wind-wave model that simulates the growth, decay and transformation of wind-generated waves and swells in offshore and coastal areas. It includes two different formulations: A fully spectral formulation and a directional decoupled formulation. The first formulation is based on the wave action conservation equation and the second one is based on a parameterization of the wave action conservation equation.

The physical phenomena that are described by the fully spectral model are: a) the wind induced wave growth; b) the non-linear wave-wave interaction; c) the wave-current interaction; d) the dissipation due to white-capping, bottom friction and depth-induced wave breaking; e) the refraction and shoaling caused by the depth variations; f) the effect of time-varying water depth and g) the effect of ice coverage on the wave field (MIKE 21, MIKE 21 Wave Modelling Spectral Waves, 2011).

MIKE 21 is a commercial software and the license can be purchased from DHI. MIKE 21 can run on Microsoft Windows machines (32 or 64 bit).

Mathematical model

In MIKE 21 SW, the wave action density spectrum $N(\sigma, \theta)$ is used to represent the wind waves. The independent phase parameters in the wave action spectrum are the intrinsic angular frequency, given by $\sigma = 2\pi f$, and the direction of the wave propagation θ . The linear dispersion relationship relates σ with the absolute angular frequency ω :

$$\sigma = \sqrt{gk \tanh(kd)} = \omega - \bar{k} \cdot \bar{U} \quad (5.14)$$

where d is the water depth and \bar{U} is the current velocity vector and \bar{k} is the wave number vector with magnitude k and direction θ .

Then the action density $N(\sigma, \theta)$ is related to the energy density $E(\sigma, \theta)$ by $N = E/\sigma$. The governing equation of the fully spectral formulation is the wave action balance equation written in Cartesian or spherical coordinates. In horizontal co-ordinates, the conservation equation for wave action reads:

$$\frac{\partial N}{\partial t} + \nabla \cdot (\bar{v}N) = \frac{S}{\sigma} \quad (5.15)$$

where $N(\bar{x}, \sigma, \theta, t)$ is the action density; t is the time; $\bar{x} = (x, y)$ is the Cartesian coordinates \bar{v} is the propagation velocity of a wave group in the four-dimensional phase space; S is the source term for energy balance equation.

The source term S is the summation of the momentum transfer of wind energy to wave generation (S_{in}), the energy transfer due to nonlinear wave-wave interaction (S_{nl}), the dissipation of wave energy due to white-capping (deep water breaking) (S_{ds}), the dissipation due to bottom friction (S_{bot}) and the dissipation due to depth-induced breaking (S_{surf}). The wind wave generation is based on Janssen's quasi-linear theory, according to which the momentum transfer from the wind to the sea depends both on the wind stress and the sea state itself. The DIA approach is used for the four-wave interaction. More details on the source terms can be found in the description of MIKE 21 SW (MIKE 21, MIKE 21 Wave Modelling Spectral Waves, 2011).

Numerical model

The governing equation is solved using the cell-centred finite volume method. The spatial discretization is based on an unstructured mesh approach, which currently supports triangle and quadrilateral polygons, while the integration in time is achieved through a fractional step approach with the application of a multi-sequence explicit method.

MIKE 21 SW is mainly used for simultaneous wave analysis on regional and local scale. A coarse mesh and large time steps are employed for the regional scale, while a high resolution boundary and depth-adaptive mesh is used for the shallow water areas. Note that MIKE 21 comprises of a hydrodynamic module (MIKE 21 FLOW MODEL) that supports nested simulations. For further details, one can refer to the user guide (DHI Software, 2007).

One of the most important pre-processing tasks is the mesh design. Setting up the mesh is vital for obtaining reliable results. The process comprises of the definition of the bathymetry, flow, wind and wave fields and the land boundaries. The geographical resolution should be such that it does not affect the stability of the simulation. Other input parameters, which need to be selected are: the coordinate type; the equations, discretization and solution methods; the forcing parameters (water level, current, wind, ice); the source function parameters; the initial conditions; and the boundary conditions.

It should be mentioned for the initialization method that the simulation can have a "cold start" or a "hot start", meaning that can start with zero-spectrum from scratch or based on a previous simulation respectively (MIKE 21, MIKE 21 Wave Modelling Spectral Waves, 2011). Regarding the boundaries, open and closed boundaries are accommodated in MIKE 21 and for the first type the user must specify either the surface elevation or the flux (DHI Software, 2007).

MIKE 21 outputs the integral wave parameters split into wind sea and swell. A constant or a dynamic threshold frequency can be used in order to distinguish the wind sea and the swell. The results include: the significant wave height, the peak wave period, the averaged wave period, the zero-crossing wave period, the wave energy period, the peak wave direction, the mean wave direction, the directional standard deviation, the wave height with direction and the radiation stress tensor.

For the post-processing of the results, MIKE 21 uses "Data Viewer", which is provided in the common MIKE Zero shell. This tool is suitable for analysis and visualization of unstructured data (meshes, spectra, bathymetries etc.). For further analysis, more tools are provided that

are capable for editing and plotting, such as “Time Series Plot” and “Polar Plot” (MIKE 21, MIKE 21 Wave Modelling Spectral Waves, 2011).

MIKE 21 can run in parallel using both shared memory (OpenMP) and distributed memory architecture (MPI) method. The performance of the model, after the 2009’s release, seems to reach the optimum theoretical performance.

Limitations

In the user guide (DHI Software, 2007) after each section there are “Remarks and Hints” that help the user to improve the simulation. These refer to bed resistance, boundary conditions, disk space, eddy viscosity, flooding and drying, output files, simulation type, soft start, source and sinks, wave radiation stresses and wind conditions.

According to experienced users special care needs to be taken for the drying grid cells on the open boundaries and different approaches have been developed to overcome some inherent weaknesses of the model.

Another rather common issue refers to the artificial backwater effects from the boundaries. However, that can be easily minimized by allowing enough distance from the boundaries to the region of interest in the computational domain.

Applications

MIKE 21 has been applied to a large number of offshore and coastal applications. The model has been validated for the fundamental processes of wave propagation, depth-induced and current-induced shoaling and refraction, wind-wave generation and dissipation, with measurements from wave buoys and analytical solutions.

One example is the validation against data collected at the Ekofisk offshore platform (70m water depth) in the North Sea. The comparison of the significant wave height, peak and mean wave period show good agreement. Another more realistic test case is for the Danish West Coast and the Baltic Sea (17.5m water depth). The model showed good performance for this case as well (DHI, 2011). In the same document, there is reference to the application of MIKE 21 for prediction of the wave climate at the complex Horns Rev (reef) in the south east part of the North Sea where an offshore wind farm of 80 turbines has been established at depths varying from 6.5 to 13.5m.

Regarding more applications for Marine Renewable Energy, MIKE 21 has been employed for resource assessment. One example is for tidal energy in Ireland: MIKE 21 was used to estimate the tidal currents around Ireland. In this study a grid of 405m spacing was designed, which enabled more accurate bathymetries and seabed conditions (O’Rourke, Boyle, & Reynolds, 2010). In another study, MIKE 21’s flexible mesh version was employed for high resolution metocean modelling at UK’s marine energy test sites. The study focused on the Orkney Islands and the influence of the local topographic features to tidal and wave dynamics (Lawrence, Kofoed-Hansen, & Chevalier, 2009). MIKE 21 was applied again for the Orkney Islands, this time in order to determine the change of the wave climate around an array of hypothetical wave devices with different degrees of absorption. Spectral and

Boussinesq waves were used for this purpose, while the devices were modelled as porous structures with various porosity levels (Venugopal & Smith, 2007).

5.3 Potential flow

5.3.1 ANSYS AQWA

ANSYS AQWA provides an integrated toolset based on a potential flow solver (Clauss, 2009) for the examination of the effects of waves, wind and currents on floating and fixed offshore and marine structures, including spars, floating production storage and offloading (FPSO) systems, semi-submersibles, tension leg platforms (TLPs), ships, renewable energy systems and breakwater design.

There are three ANSYS AQWA value-based packages available to meet typical analysis requirements: ANSYS AQWA Diffraction, ANSYS AQWA Suite and ANSYS AQWA suite with Coupled Cable Dynamics. A detailed description of their specifications can be found in the ANSYS brochure (ANSYS Inc, 2010).

ANSYS AQWA is a commercial software package.

Numerical model

AQWA Hydrodynamic Diffraction is mainly used for calculating the primary hydrodynamic parameters in complex motions and responses analysis. It is a three-dimensional linear radiation and diffraction solver and can be used to examine multiple body hydrodynamic interaction. The water depth is not a restriction, because the computation of second-order wave forces is calculated with full quadratic transfer function matrices.

At the same time the model is able to calculate the pressure and inertial loading on the structures. The results can be transferred to ANSYS Mechanical FEM for further computation. There is an advanced mapping method when transferring the results to ANSYS Mechanical that automatically fixes the mesh differences between the hydrodynamic and the finite element model.

AQWA includes also a Hydrodynamic response part of the software, which assesses the global performance of floating structures in the time domain. The motion of one structure affects the motions of another. Mooring lines, fenders and articulations can be included as physical connections that result in restraining conditions on the vessels. A typical application is shielding effects of one vessel on another and forward speed effects can also be included in the interaction.

For large floating bodies, a description of the hull form is required. A standard panel discretization of the hull is utilized in the radiation/diffraction stage of the simulation. Static and dynamic solvers are available for the time domain solutions. This can be achieved in one of several ways: a) For ship-form shaped vessels, there is an automated mesh generator that works from the ship's lines plan (or offsets); b) For more general vessel forms, the user can take advantage of ANSYS DesignModeler in order to generate the geometry directly or to import geometry from other CAD systems into the ANSYS AQWA hydrodynamic diffraction analysis system that includes its own meshing capabilities. The

following table summarizes the capabilities of the different product packages (ANSYS Inc, 2010).

Table 5.1: Capabilities of different ANSYS AQWA packages

	ANSYS AQWA Diffraction	ANSYS AQWA Suite	ANSYS AQWA Suite with Cable Dynamics
Model generation	✓	✓	✓
Hydrostatics	✓	✓	✓
Radiation/Diffraction	✓	✓	✓
Load mapping to FEA	✓	✓	✓
Static position analysis (with moorings)		✓	✓
Dynamic motions analysis in frequency domain		✓	✓
Dynamic motions analysis in time domain		✓	✓
Quasi-static mooring model		✓	✓
Dynamic mooring models (includes drag & inertial effects)			✓

Limitations

Although ANSYS AQWA has advanced mesh designing capabilities, in the current version it is not possible to employ symmetry in the AQWA Editor. Therefore the full model must be meshed, a fact that results in increased computational cost.

Another drawback is the high computational cost in some cases. It is well-known that frequency domain simulations are very fast and can determine whether the cable dynamics need to be considered. On the other hand, time domain runs provide greater accuracy with higher computational cost. For example, in order to compute the slam coefficient the time-step used in a time history analysis must be sufficiently small to account for the added mass at each stage of immersion/emergence. Practically, this introduces a severe restriction of the size of the time-step and makes this type analysis appropriate only when slam forces on individual elements during critical stages of the simulation period are examined.

Applications

A large number of AQWA applications have already been mentioned in the description of the program. AQWA has recently been applied for modelling of ocean wave energy converters (Bosma, 2013) in order to provide a methodology for industrial developers.

Another application for MRE is the calculation of the dynamic response of a two-body floating WEC anchored to the sea bed with moorings and a PTO (Finnegan & Goggins, 2012).

Moreover, a technical report by Green Ocean Energy Ltd (Smith, 2009) describes how AQWA can be used to calculate the kinematic response and power output of a WEC and the structural analysis that follows to determine the stress distribution and deformation of the device components.

5.3.2 WAMIT

WAMIT (Wave Analysis at Massachusetts Institute of Technology) was first released in 1987 by the MIT (Massachusetts Institute of Technology). “Version 1” became quickly popular in industry and research thanks to its ability to analyse complex structures accurately and efficiently. Since then, upgrades are announced in two-year intervals.

The latest update, “Version 7” is a radiation/diffraction panel program developed for the linear analysis of the interaction of surface waves with various types of floating and submerged structures. (WAMIT INC, 2012). WAMIT Version 7 updates from the 6.4 Version and has additional extensions that mainly reduce the computational time. Features include: a) parallel processing and b) Random Access Memory replacing scratch file storage.

Version 7 is compiled using Intel Visual FORTRAN Version 12.1. This version is available for use with either Windows or Linux systems and is able to run in 64bit operating systems taking advantage of all the available RAM memory.

WAMIT is a commercial licensed software.

Mathematical model

WAMIT is utilized to compute the unsteady hydrodynamic pressure, loads and motions of a body in a fluid flow. At the same time the pressure and the velocity of the fluid domain is calculated as well. The body is designed in the 3D domain and it interacts with progressive waves in water of finite depth.

The flow is assumed to be potential and therefore flow separation and lifting effects do not occur. The free-surface and body-boundary conditions are linearized and harmonic time dependence is adopted.

According to potential flow theory, the gradient of the velocity potential Φ satisfies the Laplace equation. The harmonic time dependence allows the definition of a complex velocity potential φ , related to Φ by:

$$\Phi = Re(\varphi e^{i\omega t}) \quad (5.16)$$

where Re denotes the real part, ω is the frequency of the incident wave and t is time.

The free-surface conditions are linearized: $\varphi_z - K\varphi = 0$ on $z = 0$, where $K = \frac{w^2}{g}$ is the infinite-depth wavenumber.

The velocity potential of the incident wave is defined by:

$$\varphi_o = \frac{igA \cosh[k(z+h)]}{w \cosh kH} e^{-ikx \cos \beta - ikys \sin \beta} \quad (5.17)$$

where k is the real root of the dispersion relation and β is the angle between the direction of propagation of the incident wave and the positive x -axis.

More information can be found in the WAMIT user manual under the heading theory (WAMIT INC, 2012).

Numerical model

WAMIT is based on the linear and second-order potential theory which analyses floating or submerged bodies in the ocean. This method uses the Boundary Integral Equation Method (BIEM), also known as the panel method. After Version 6, several extensions have been added that allow a more advanced higher-order panel method, which is based on a continuous B-spline representation for the velocity potential. The order of the B-splines is specified in the input parameters. Recent versions also include several alternative schemes for defining the geometry of the body surface. Planes of symmetry can be also added in the geometry to help reduce the computational cost.

The water depth can be infinite or finite. Single body response to waves or multiple interacting bodies can be analysed. The bodies can be set to float on the free surface. Alternatively, the bodies can be submerged, or mounted on the sea bottom. The dynamic analysis of bodies which are freely floating, restrained, or fixed in position can be performed. Additionally, there are options to define the bodies as rigid, and moving with six degrees of freedom (6 DoF) motion.

WAMIT consists of two subprograms: a) POTEN, which is a solver for the velocity potential accounting for radiation and diffraction and b) FORCE, which is employed for the hydrodynamic response of the structure and computes hydrodynamic coefficients, motions and first and second order forces. The following quantities can be evaluated by WAMIT: hydrostatic coefficients; added-mass and damping coefficients; wave exciting forces and moments; motion amplitudes and phases for a freely-floating body; forces restraining a body which is freely-floating in some modes; hydrodynamic pressure and fluid velocity on the body surface and in the fluid domain; free surface elevation; all components of the drift force and moments by integration over a control surface; mean yaw moment by integration in the far field; all components of the drift force and moment by local pressure integration over the body surface and drift force and moment in bidirectional waves.

Assumptions

In WAMIT, the flow is assumed to be ideal and time-harmonic. The free-surface condition is linearized, except from Version 6.4S. Therefore the analysis is considered to be linear or first-order. However, the mean second-order forces can be rigorously computed from the linear solution. The velocity potentials induced by radiation and diffraction are computed using Green's theorem, with the free-surface source-potential as the Green function.

Limitations

The linear system which must be solved for the velocity potentials is not as well conditioned in the low-order method. The second-order pressure due to the square of the fluid velocity is unbounded at sharp corners. The user must specify the control surface as an additional input to avoid problems.

The mean drift forces are calculated using control volumes. The main two drawbacks of that method is that the user needs to specify the control surface beforehand and that the run time is increased for the FORCE module because the elevation of the momentum flux needs to be calculated at a sufficiently large number of points (WAMIT INC, 2012).

Applications

There is a long list of applications of WAMIT for marine structures. Some benchmark examples are presented in the table below (WAMIT, 2008). For the latest version, 37 test cases have been run. 12 of them regard low-order and 25 of them high-order applications.

Table 5.2: Applications of WAMIT

1	Array of eight buoys	Analyse the interactions between the different wave buoys. Higher-order method used and geometry created in GEOMXACT.DLL
2	Drillship Navis explorer	Higher-order method used represented by MultiSurf.
3	ISSC Tension-Leg Platform	4048 panels used. Low-order method used.
4	Spar buoy	With helical strakes, represented by dipole panels of zero thickness
5	Semi-sub	Generated by the subroutine in GEOMXACT.DLL. Test run 15 used along with higher-order method.
6	FPSO (Floating, Production, Storage and Offloading vessel)	Test Run 22 using higher-order. Represented by rectangular patches
7	Air-cushion vehicle	Defines surface elements of the body as pressure surfaces. Test 25 used
8	Tension-Leg Platform (TLP)	Second-order wave loads used, which includes nonlinear forcing of the free surface.

An interesting comparison is presented by Clauss (Clauss, 2009). ANSYS AQWA and WAMIT were employed to test the motion behaviour of a new offshore LNG transfer system at harsh operational conditions. The system is based on the flexible cryogenic pipes of 16", which allow fast loading/offloading procedures. Results from the frequency and the time domain regarding the dynamic behaviour of the multi-body system were in good agreement.

Last but not least, there are recent publications that refer to the modelling of MRE devices. The numerical complexity of such simulations is quite high. In order to confront that, an innovative approach is adopted where the hydrodynamics are simulated in the frequency domain by WAMIT and the dynamic motion of the WECs is solved in the time-domain (McComb, Lawson, & Yu, 2013).

5.3.3 QALE-FEM

The QALE-FEM (Quasi Arbitrary Lagrangian-Eulerian – Finite Element Method) was first developed in 2005 by Ma and Yan (Ma & Yan, 2006) and it was based on a fully nonlinear potential theory (FNPT) using a quasi Lagrangian – Eulerian finite element method for simulating water waves. It was created to simulate complex interactions between large steep waves and structure or to deal with three-dimensional overturning waves over complex seabeds (S. Yan, 2010).

There are three main techniques for discretizing the equations that describe a fluid flow. The Eulerian method, which is the most classic one, is based on a fixed computational mesh and the fluid moves relative to it. If the mesh is fine enough the Eulerian method can handle large distortions of interfaces between two different materials, like water and air, however the computational cost is high. It is even more difficult to apply it when there are bodies in the domain, such as cylinders. Lagrangian formulations allow sharp interfaces between different materials, since the fluid particles are represented from different nodes. However, if large distortions occur and certain nodes become too close or too far from others, a computational breakdown might occur. The ALE (Arbitrary Lagrangian Eulerian) formulation makes use of the merits of both of the two techniques. The QALE method is developed in order to minimize the computational cost of regenerating the mesh at each time step. The complex mesh is generated only once at the beginning and it is moved at all the other time steps to follow the movement of the fluid and the structures.

The computational cost was also the main incentive for adopting Finite Element Method (FEM) instead of boundary element method (BEM). However, a drawback of FEM is that an unstructured mesh requires remeshing at each time step, which is a problem overcome by the employment of the QALE technique.

At the moment, there is no specific software that can be downloaded, but the research code QALE-FEM is included as a method likely to be used a lot in the future for free surface flow problems.

Mathematical model

There are two types of method used to generate nonlinear waves. The first one is to utilize a piston or paddle wave-maker which is mounted at one end of the tank. At the other end of the tank there is a damping zone with a Sommerfeld condition to suppress reflections. The

second one is to specify the initial condition for the position of and the velocity potential on the free surface. In this case, the wave-maker is treated as a fixed boundary. Arbitrary forms of seabed geometry may appear. A Cartesian coordinate system is adopted with the origin Oxy on the mean free surface, coinciding with the central longitudinal vertical plane of the tank and the z -axis being positive upwards.

The velocity potential (ϕ) satisfies Laplace's equation in the fluid domain:

$$\nabla^2 \phi = 0 \quad (5.18)$$

On the free surface $z = \zeta(x, y, t)$, the velocity potential satisfies the kinematic and dynamic conditions in the following Lagrangian form:

$$\frac{Dx}{Dt} = \frac{\partial \phi}{\partial x}; \quad \frac{Dy}{Dt} = \frac{\partial \phi}{\partial y}; \quad \frac{Dz}{Dt} = \frac{\partial \phi}{\partial z} \quad (5.19)$$

$$\frac{D\phi}{Dt} = -gz + \frac{1}{2} |\nabla \phi|^2 \quad (5.20)$$

where (D/Dt) is the substantive (or total time) derivative following fluid particles and g is the gravitational acceleration.

On all rigid boundaries, the velocity potential satisfies:

$$\frac{\partial \phi}{\partial n} = \vec{n} \cdot \vec{U}(t) \quad (5.21)$$

Numerical Model

As mentioned before, when FEM deals with a complex unstructured mesh, the mesh has to be re-meshed every time step, which has high computational demands. QALE-FEM differs from this method, where the complex mesh is generated only once at the beginning and is moved at all other time steps to follow the free surface motion. This is achieved by using a spring analogy method for the nodal displacement which is stated below (Ma & Yan, 2006).

$$\Delta \vec{r}_i = \frac{\sum_{j=1}^{N_i} k_{ij} \Delta \vec{r}_j}{\sum_{j=1}^{N_i} k_{ij}} \quad (5.22)$$

where $\Delta \vec{r}_i$ is the displacement of node I ; k_{ij} is the spring stiffness and N_i is the number of nodes that are connected to node I .

The spring stiffness is given as below:

$$k_{ij} = \frac{1}{l_{ij}^2} e^{\gamma \left[1 + \frac{(z_i + z_j)}{2d}\right]} \quad (5.23)$$

where l_{ij} is the distance between nodes I and J ; z_i and z_j are the vertical coordinates of nodes I and J ; d is the water depth; and γ is a coefficient that should be assigned a larger value if the springs are required to be stiffer at the free surface. Numerical tests indicate that $\gamma = 1.7$ is suitable.

QALE-FEM improves the computational efficiency and it is stated that “It may require less than 15% of the CPU time required by the conventional FEM to achieve the same level of accuracy” (S. Yan, 2010). In the same paper, the case of 3D overturning waves is described in detail, along with the treatment of the fluid velocity on the free surface. Validation cases with other numerical and experimental results are presented.

Assumptions

For this model, potential flow assumes that turbulence is negligible where the effects of viscosity are ignored and the flow is frictionless and irrotational. Potential flow is often used for analysing external flows over solid surfaces at high Reynolds number providing the flow remains laminar. Its unstructured mesh is moving at every time step using a specially developed spring analogy method for free surface problems and the velocity is calculated by a three-point technique suitable for any mesh structures. The numerical technique used for moving mesh enables the simulation of 3D overturning waves, which would not normally be described by potential theory.

Limitations

Cutting a solid body out of a background Cartesian mesh can generate sharp corners and a variety of different cut cell types. Extending this method to three-dimensions is not a trivial task and small cells arising near solid boundaries due to the Cartesian mesh intersecting a solid body can restrict the stability of the Cartesian solvers.

Applications

The QALE-FEM was utilized to simulate the Draupner wave that occurred near Draupner platform in the North Sea. The Draupner wave is considered to be “freak” for the corresponding sea state and the measurement of such a wave is rare. There are some studies about rogue waves, but their formation has not been satisfactorily explained. The paper concludes that Draupner wave might have resulted from two crossing waves-group

whose mean wave directions were separated by about 90° or more (Adcock, Taylor, Yan, Ma, & Janssen, 2011).

5.3.4 OrcaFlex

OrcaFlex is a marine dynamics software package developed by Orcina for static and dynamic analysis of many different offshore systems, including all types of marine risers (rigid and flexible), global analysis, moorings, installation and towed systems (Orcina Ltd, 2013).

More specifically, OrcaFlex is a 3D non-linear finite element solver for lines (ie., long, slender) structures. The element is a linear beam element (aka a lumped mass element), which is very robust and has been proven to be as accurate as higher-order beam elements. This robustness allows further development of the program to include additional force terms and constraints on the system to meet new engineering requirements. Regarding the analysis of catenary systems, such as flexible risers and umbilical cables, the software provides fast and accurate analysis under wave and current loading.

Both time domain analysis and spectral analysis are available in OrcaFlex, giving important flexibility to the extracted features of the simulation. A full list of the technical specification can be found in the relevant document (Orcina Limited, 2013).

It is important to mention that OrcaFlex is designed to facilitate extensive use of graphics at all the levels of the simulation, i.e. pre- and post-processing and solving. At the same time the program can operate in batch mode and it has special post-processing fully integrated fatigue analysis features.

OrcaFlex is a commercial software provided by Orcina. It is designed to run in parallel and it can operate in Microsoft Windows systems of 32 or 64 bit. OrcaFlex serves relevant applications in the following industrial sectors: Offshore Oil & Gas, Defence, Oceanography and more recently Renewable energy.

Mathematical model

OrcaFlex is an integrated software. In order to facilitate the presentation of the mathematical theories behind it, this section will be split in wave theories, vessel theory and line theory (Orcina Ltd., 2013). OrcaFlex includes other modelling objects, e.g. 6D buoys, 3D buoys, winches, links and shapes. Details of their functionality can be found in the user manual.

Waves

The wave can be defined as a regular wave, a random wave or through a time history file. Regular waves include linear Airy waves, as well as non-linear waves, such as Dean Stream function, Stokes' 5th order and Cnoidal waves. The wave is defined by its height, period and direction. Random waves include five standard frequency spectra: JONSWAP, ISSC (also known as Bretschneider or modified Pierson-Moskowitz), Ochi-Hubble, Torsethaugen and Gaussian Swell. The user defines a number of linear wave components and the frequency bandwidth and the program synthesises the wave time history by the linear superposition of the different wave components. The component frequencies are

chosen by an equal energy approach, while the phases are calculated by a pseudo-random method. Note that the equal energy approach can result in poor modelling near the tails of the spectrum, where the spectral energy is low. To tackle this problem the user can specify a maximum component frequency range.

OrcaFlex can also accommodate directional spectra. The directional spreading spectrum is described by:

$$S_d(\theta) = K(n) \cos^n(\theta - \theta_p) \quad (5.24)$$

For $-\pi/2 \leq \theta - \theta_p \leq \pi/2$, where $K(n)$ is a normalising constant, n is the spreading exponent, θ is the wave direction and θ_p is the principal wave direction. The total spectrum is given by $S(f, \theta) = S_f(f) \cdot S_d(\theta)$, where S_f is the frequency spectrum.

Another interesting feature regarding the non-linear waves is the “kinematic stretching”. With this process linear Airy waves are extended to provide fluid velocity and acceleration at points above the mean water level. This is because in linear wave theory kinematics are not calculated above the mean water level.

Regarding wave breaking, OrcaFlex is able to report a warning if the wave height exceeds the breaking wave height. For breaking in shallow waters $H_B = 0.14L$, where L is the wave length. For all water depths Miche’s formula is used: $H_B = 0.88k^{-1} \tanh(0.89kd)$, where $k = 2\pi/L$ is the local wave number as calculated by Airy wave theory.

OrcaFlex also has the option to implement currents together with any wave theory. It allows a uniform Eulerian current, but issues arise for non-linear waves and currents. For a linear wave, the current can simply be superimposed on the wave field. For the non-linear waves, the current used to analyse the wave is taken to be the component of current in the wave direction at the mean water level (C_w). To calculate the fluid velocity V at any given point in time, one must take into account the fluid velocity V_w containing uniform current C_w together with the current C at the point in question, as specified by the current profile. The formula is: $V = V_w - C_w + C$.

Vessel

The vessel theory includes all the aspects related to: vessel rotations; RAOs (Response Amplitude Operators) and phases; RAO quality checks; wave drift and sum frequency loads; sea state disturbance; stiffness, added mass and damping; impulse response and convolution; manoeuvring load; current and wind loads. Specific details can be found in the user manual.

Lines

OrcaFlex uses a finite element model for the lines. The calculation is conducted in five stages. First the tension forces are calculated. After that the bending moments and the

shear forces are found. The torsion moments follow and at the end the total load is calculated including the non-structural load contributions (weight, drag, added mass etc.).

In the user manual, all the other theories related to the simulations performed by OrcaFlex are explained under the general heading "Theory".

Numerical model

In the user manual there is a very elaborate description of the general operation of the model for some simple cases. The graphical user interface is easy to use and employs 3D graphics for better overview of the physical problem.

Objects and lines are easily introduced into the model by clicking the relative buttons. The static analysis can start by clicking on the "Statics" button. The "Results" button exports the results in numerical or graphical form. The dynamic analysis starts by clicking on the "Run Dynamic Simulation" button. As the simulation runs, an animated replay is shown in a separate window. The results can be exported as Excel compatible spreadsheets for further processing. Further numerical results are available in tabular form by selecting Summary Results, Full Results, Statistics and Linked Statistics.

OrcaFlex includes both frequency and time domain vortex induced vibration (VIV) models. VIVA and Shear7 are 3rd party frequency domain programs called from OrcaFlex. Both allow a riser model to be built in OrcaFlex and then VIV calculations to be run using the existing interface. The frequency domain calculations are based on energy balance. The results can be accessed from within OrcaFlex itself or exported for external examination. The results include the amplitudes of vibration and the mean effective drag coefficients. On the other hand, there are four built-in time domain VIV models. Two of them are wake oscillator models and the other two are vortex tracking models. The vortex force for the static analysis is the standard Morison drag force (whose drag coefficients can optionally include VIV effects, which is later smoothly changed by the ramping function taking into account the vortex force given by the VIV model.

Limitations

There are several simplifications that introduce relevant limitations to OrcaFlex. Most of them are included in the official documentation as warnings (Orcina Ltd., 2013). Some of them will be briefly mentioned here, but it is recommended that users study the documentation in order to assess the impact of the modelling assumptions for their particular application. One practical issue with OrcaFlex lies on the parallel processing method. The program performs parallel calculation of the model's line objects. So computational performance for a single model is improved only when more than one line is simulated. However, most analyses will need multiple variant files (load cases, parametric studies, etc) and these are all launched independently on separate threads.

When the movement of a vessel is calculated instead of being imposed, the theory of wave drift damping assumes that the vessel velocity is small compared to the wave speed. If that is not the case, the formulae used can result to unreasonable effects.

The OrcaFlex line static calculation is seamlessly applied in 2 'steps'. Step 1 omits certain load and interaction effects, resulting in a line configuration, which is a first approximation to the full static equilibrium line position. This approximation is then used by the Step 2 calculation as a starting configuration, which the omitted load and interaction effects are applied on. So, at the end of Step 2 the line has a true equilibrium configuration. Whilst the user can select to not perform the Step 2 calculations, this is not the default selection of the program and is almost never done in practice.

Care should be taken for pipe stress calculation when the material is not homogenous. For the simple cases of pipes made of uniform material, such as steel and titanium, the pipe is treated like a homogenous cylinder. For composite pipe cross sections the stress diameters must set separately. The bending stress and shear stress are calculated by OrcaFlex accounting for the non-homogenous and non-isotropic pipes.

Last but not least, there are some options where the user cannot use the implicit integrator to solve for the floater behaviour. In particular, any use of the 3DoF Calculated option, or the 6DoF Calculated option, where there are additional superimposed motions defined. The program will warn the user if these combinations are inadvertently selected, allowing them to run with the alternative Explicit scheme instead. But mostly, for study of compliant offshore renewable systems, only the Calculated 6DoF is needed and the implicit integrator can be used.

Applications

OrcaFlex is used for many applications involving long, slender, compliant structures – a list of these are on the Orcina website. However, OrcaFlex can also be used for less common applications. The emphasis in this section will be on moored marine renewable energy related applications.

One interesting environmental study has employed OrcaFlex to assess the scouring effect on bottom sediments and consequent disruption of benthic habitats. Matlab was used for further analysis of OrcaFlex's results of the time series of the touching points of the mooring lines and the bed. The results show that the area of benthic habitat adversely affected by the leading mooring line on a typical wave energy converter (WEC) monotonically increases with the increase in wave height (Krivtsov & Linfoot, 2012).

Another study has utilized OrcaFlex to analyse the loading and fatigue effects of multiple wave parameters on dynamic power cables of a floating wave energy converter. Two common umbilical configurations were examined: catenary and lazy wave. The mechanical load conditions and failure modes were also compared with experimental results (Thies, Johanning, & Smith, 2011).

Moreover, the tuning of a wave energy converter to the local wave climate should take into consideration the response of the mooring system, because it can alter the ability of the device to extract power from the waves. WECs are relatively small compared to other offshore systems and the effects of waves and currents on them can be significant. The damping and top-end loading can be importantly influenced by the axial line stretching and high-frequency "top-end" dynamics. The reliability and survivability of WEC's moorings was experimentally and numerically studied using OrcaFlex (Johanning, Smith, & Wolfram, 2007).

OrcaFlex v9.1d was employed for the design process of the Multi-catenary Spread Mooring System of OCEANTEC WEC, which is a relatively new wave energy converter. A time-domain analysis of different environmental loading cases was performed obtaining data from experimental testing (Ruiz-Minguela, Rodriguez, Ricci, Maron, Prieto, & Taboada, 2008).

The software is also used for tidal energy applications. OrcaFlex was employed to characterize the complex hydro-elastic behaviour of ropes, used as a mooring system of ocean currents energy harnessing devices (López, Somolinos, Núñez, & Santamaría, 2011).

5.4 Shallow Water Equations

5.4.1 S.HY.F.E.M.

SHYFEM (Shallow water Hydrodynamic Finite Element Model) was developed at ISMAR-CNR (Institute of Marine Sciences – National Research Council). It is a 3D shallow water hydrodynamic model, coupled with a wind wave model, which uses a semi-explicit algorithm for integration in time, combining the advantages of both the explicit and the implicit schemes. This package is able to solve the hydrodynamic equations in lagoons, coastal seas, estuaries and lakes.

The bottom friction is formulated by the Strickler method, allowing the friction coefficient to vary with the depth. Sub-grid processes are simulated by using the General Ocean Turbulence Model (GOTM) turbulence closure model (The SHYFEM Group, 2009). At the open boundaries the Dirichlet condition determines the water level. The model also includes Eulerian and Lagrangian transport modules, which allow the simulation of the advection and diffusion of tracers.

SHYFEM is provided freely as open source software and it can be downloaded from the website (SHYFEM, 2013).

Mathematical model

SHYFEM resolves the shallow water equations vertically integrated in their formulation with water levels and transports (The SHYFEM Group, 2009):

$$\frac{\partial U}{\partial t} + gH \frac{\partial \zeta}{\partial x} + RU + X = 0 \quad (5.25a)$$

$$\frac{\partial V}{\partial t} + gH \frac{\partial \zeta}{\partial y} + RV + Y = 0 \quad (5.25b)$$

$$\frac{\partial \zeta}{\partial t} + \frac{\partial U}{\partial x} + \frac{\partial V}{\partial y} = 0 \quad (5.26)$$

where ζ is the water level; u , v the velocities in the x and y direction; U , V the vertical integrated velocities (total or barotropic transports):

$$U = \int_{-h}^{\zeta} u dz \quad V = \int_{-h}^{\zeta} v dz \quad (5.27a, b)$$

Moreover, the total water depth $H = h + \zeta$, where h is the undisturbed water depth; $R \equiv$ Friction coefficient = $g \frac{\sqrt{u^2+v^2}}{C^2H}$; $C \equiv$ Chezy coefficient = $k_s H^{1/6}$; $K_s \equiv$ Strickler coefficient.

In general, SHYFEM works with a fixed time step, which is acceptable in the case when the conditions are stable. However, the consideration of advective and viscous terms can introduce instabilities and the Courant number restriction to the time step can be enforced to ensure numerical stability.

Finite Element Model

Staggered finite elements are used for the special discretization. The water levels and the velocities are described using form functions of different order. The standard linear form functions are used for the water levels and the constant form functions for the velocities.

The finite element equation is described below (The SHYFEM Group, 2009):

$$\int \Phi_N(\zeta^{n+1} - \zeta^n) d\Omega + \left(\frac{\Delta t}{2}\right) \int \Phi_N \left(\frac{\partial(U^{n+1} - U^n)}{\partial x} \right) + \Phi_N \left(\frac{\partial(V^{n+1} - V^n)}{\partial y} \right) d\Omega = 0 \quad (5.28)$$

Using an advanced unstructured mesh generator, SHYFEM is especially suitable for application to a complicated geometry and bathymetry.

Numerical model

The model needs a parameter input file that is read on standard input and some external files that are specified in this parameter input file.

The input parameter file controls the performance of the model, defines the general behaviour of the simulation and determines output files. All the essential information for the main routine to run the model are included there. When a parameter is not listed, it takes the default values. However, some parameters should be defined in the input parameter file. Compulsory time parameters define the duration of the simulation and the integration time step.

Post-processing of results is performed by several routines. In the model framework no program is supplied to do time series plots. However, there are utility routines that can

extract data from the output files. These data can be imported into a spreadsheet or any other plotting program that facilitates their presentation.

Limitations

Version 4.93 (2005) resolves the depth integrated SWE and therefore is recommended for applications of very shallow basin or well mixed estuaries. The 2D version is not suited for application to baroclinic driven flows or large scale flows, where the Coriolis acceleration is important.

Some other limitations that are inherited from the SWE assumptions are: a) that it is possible to use these equations only in the case where the horizontal wave length is much greater than the vertical length scale and b) that since the SWE have only one vertical level, they cannot account for any factor varying in the water depth. However, even if the vertical velocity term is absent from the equations, it is not necessarily set to zero.

Applications

This model has been applied by to six Mediterranean lagoons (SHYFEM, 2013): the Venice lagoon and the Marano-Grado lagoon in the Northern Adriatic Sea; the Taranto basin in the Ionian Sea; the Cabras lagoon in Sardinia; the Mar Menor in Spain and the Nador lagoon in Morocco. A comparison has been carried out between them. The study has been mainly focused on hydrodynamics, exchange rates and residence time description. Wind and tidal stirring, which are the main forcings, normally prevent the lagoons from developing stratification, which justifies the application of the 2D version of the model.

At another study, SHYFEM was applied as a coastal model along the Montenegro and Albania Littoral. In this application a study of Bokakotorska hydrodynamics was carried out for the year 2008, analyzing different freshwater input scenarios (SHYFEM, 2013).

SHYFEM simulated a period of one year (2005) to reproduce the temperature distribution and water movement for Lake Geneva (SHYFEM, 2013).

5.5 Boussinesq

5.5.1 FUNWAVE

FUNWAVE 1.0 is a phase-resolving, time-stepping Boussinesq model for ocean surface wave propagation in the nearshore. It is based on the SWE equations for non-dispersive linear wave propagation, which are extended to include the lowest order effects of nonlinearity and frequency dispersion. The Boussinesq equations as derived by Peregrine (1967) use depth-averaged velocity and they are invalid for intermediate and deep water. Madsen *et al.* (1991) and Nwogu (1993) extended the Boussinesq equations in order to obtain the best possible dispersion relation and the optimal linear shoaling. Despite the improved dispersion relation, Boussinesq equations are limited to simulating only weak interactions. However, by introducing energy dissipation due to wave breaking and eddy viscosity SWE Boussinesq-type equations are able to simulate wave propagation in coastal regions and handle surf zone hydrodynamics (Kirby. J. T, 1998).

FUNWAVE-TVD (Total Variation Diminishing) was developed at the centre for Applied Coastal Research in the University of Delaware. This version has some new features compared to the older versions 1.0 and 1.1. It includes several theoretical and numerical enhancements, such as a) a more complete set of fully nonlinear Boussinesq equations, b) a MUSCLE-TVD finite volume scheme together with adaptive Runge Kutta time stepping, c) Shock-capturing wave breaking scheme, d) wetting-drying moving boundary condition with HLL construction method for the scheme and d) code parallelization using MPI method. The need to develop FUNWAVE-TVD was to model tsunami waves in regional and coastal scale, coastal inundation and wave propagation at basin scale (Fengyan, Kirby, Tehranirad, Harris, & Grilli, 2012).

FUNWAVE is an open-source model available to the public.

Mathematical model

The fully nonlinear Boussinesq equations derived by Wei et al. (1995) are given below (Kirby, J. T, 1998):

$$\eta_t + \nabla \cdot \left\{ (h + \eta) \left[u_\alpha + \left(z_\alpha + \frac{1}{2}(h - \eta) \right) \nabla (\nabla \cdot (hu_\alpha)) + \left(\frac{1}{2}z_\alpha^2 - \frac{1}{6}(h^2 - h\eta + \eta^2) \right) \nabla (\nabla \cdot u_\alpha) \right] \right\} = 0 \quad (5.29)$$

$$\begin{aligned} u_{\alpha t} + (u_\alpha \cdot \nabla)u_\alpha + g \nabla \eta + z_\alpha \left(\frac{1}{2}z_\alpha \nabla (\nabla \cdot u_{\alpha t}) + \nabla (\nabla \cdot (hu_{\alpha t})) \right) \\ + \nabla \left(\frac{1}{2}(z_\alpha^2 - \eta^2)(u_\alpha \cdot \nabla)(\nabla \cdot u_\alpha) + \frac{1}{2}[\nabla \cdot (hu_\alpha) + \eta \nabla \cdot u_\alpha]^2 \right) \\ + \left((z_\alpha - \eta)(u_\alpha \cdot \nabla)(\nabla \cdot (hu_\alpha)) - \eta \left[\frac{1}{2}\eta \nabla \cdot u_{\alpha t} + \nabla \cdot (hu_{\alpha t}) \right] \right) = 0 \quad (5.30) \end{aligned}$$

where η is the surface elevation, h is the still water depth, u_α is the horizontal velocity vector at the water depth $z = z_\alpha = -0.531h$, $\nabla = (\partial/\partial x, \partial/\partial y)$ is the horizontal gradient operator, g is the gravitational acceleration, and subscript t is the partial derivative with respect to time.

The first equation represents the conservation of mass and the second one is the momentum equation.

Numerical model

In this model, a different approach of using a higher-order scheme in order to perform computations is considered. FUNWAVE 1.0 uses an unstaggered finite difference formulation for spatial derivatives with an iterated 4th-order Adams-Bashforth-Moulton (ABM) scheme for time stepping. With this composite technique, the fourth-order accurate

centered differences are used for the first derivatives and second-order accurate differences for the third derivatives.

In FUNWAVE-TVD, a high-order MUSCL-TVD scheme is implemented for the flux terms and the first-order derivative terms. The third-order Strong Stability-Preserving (SSP) Runge-Kutta scheme for nonlinear spatial discretization is used for time stepping. The wave breaking is modelled by switching from Boussinesq equations to NSW (nonlinear SWE) with a TVD scheme to model moving hydraulic jumps at cells where the Froude number exceeds a certain threshold.

The wave absorption and generation is improved from the previous versions. Wave makers are implemented with the ability to generate both regular and irregular waves, with an extension that includes alongshore periodicity to account for breaking wave-induced nearshore circulation, i.e. alongshore currents and rip currents. The eddy viscosity model of Zelt (1991) is used to model breaking waves, while a moving shoreline in the swash zone is handled by using a "slot" or a porous-beach method.

FUNWAVE is written in Fortran 90 and can be run on various software platforms. It includes a 1D and 2D model that are separate, but they share the basic structure. In the user's manual (Fengyan, Kirby, Tehranirad, Harris, & Grilli, 2012) one can find a detailed program outline and flow chart of the subroutines and a description of their functions.

Limitations

Numerical solution of Boussinesq equations can be significantly corrupted if truncation errors arising from the differencing of the leading order wave equation terms are allowed to grow in size and become comparable to the terms describing the weak dispersion effects. In FUNWAVE, all errors involved in solving the underlying non-linear SWE are reduced to 4th order in grid spacing and time step size. Due to non-linear interaction in the model, higher harmonic waves will be generated as the program runs. These super harmonic waves could have very short wave length and the classic Boussinesq model is not valid. For this reason, a numerical filter suggested by Shapiro (1970) can be used.

In the previous versions of FUNWAVE there were several important problems. The models were noisy (unstable) for high wavenumbers. At the same time noise was created due to the implementation of the boundary conditions, the staggered grid and the eddy viscosity formulation. In the new version, most of these issues have been successfully resolved.

Applications

There are published applications (Chen, Kirby, Dalrymple, Kennedy, Thornton, & Shi, Boussinesq modeling of waves and longshore currents under field conditions, 2000) of Boussinesq-type equations to include surf zone phenomena for calculation of 1D tests of shoaling, breaking and run up in two horizontal dimensions. The model simulates a shoreline while allowing computations over a regular domain. Bottom friction is included, using a quadratic representation, while the 2D implementation of the model also considers subgrid mixing. From these equations it is possible to investigate surface wave transformation and breaking-induced nearshore circulation.

FUNWAVE has also been utilized to simulate the wave-induced vortices near a breakwater (Hommel, Shi, Kirby, Dalrymple, & Chen, 2000) and in the code the Boussinesq equations have been also altered successfully to describe tsunami propagation (Watts, Grilli, & Kirby, 2002).

5.6 Spectral

5.6.1 WAM

WAM (WAVE prediction Model) was first introduced in 1988 by S. Hasselmann. It was one of the first one proposed third generation models. A third generation wave model is able to explicitly represent all the physics relevant for the development of the sea state in two dimensions, such as wind generation, whitecapping, quadruplet wave-wave interactions and bottom dissipation. In WAM, a two-dimensional ocean wave spectrum $F(f, \lambda, \phi, \theta, t)$ was allowed to develop freely (up to a cut-off frequency) with no constraints on the spectral shape. To achieve this, developers of WAM had to deal with two aspects. First, a transfer source function of the same degree of freedom as the spectrum itself needed to be developed and second the energy balance had to be closed by defining the dissipation source function. Hasselmann's approximation (1985) and Komen's form (1984) were employed to deal with these aspects respectively. The dissipation was selected in order to replicate the observed fetch-limited wave growth and the fully developed Pierson-Moskowitz spectrum (The WAMDI group, 1988).

WAM was verified in six hindcast studies at North Atlantic – North Sea storms, three Gulf of Mexico hurricanes and a global run for the SEASAT period. The wave fields for all six storms were computed using the shallow water, first order propagation model and compared against the wave measurements taken at 11 stations in North Sea. The results were encouraging (The WAMDI group, 1988).

Constant improvements and updates have led to a third-generation WAM model. A third-generation wave model explicitly represents all the physics relevant to the development of the sea state in two dimensions.

Mathematical model

The evolution of the two-dimensional wave spectrum takes the following mathematical formulation for the deep water case:

$$\frac{\partial F}{\partial t} + (\cos \phi)^{-1} \frac{\partial}{\partial \phi} (\dot{\phi} \cos \phi F) + \frac{\partial}{\partial \lambda} (\dot{\lambda} F) + \frac{\partial}{\partial \theta} (\dot{\theta} F) = S \quad (5.31)$$

where θ is the direction (measured clockwise relative to true north); ϕ is the latitude and λ is the longitude on the spherical earth; and where S is the net source function describing the change of energy of propagating wave and represent the rates of the position and propagation direction of a wave packet travelling along a great circle path (The WAMDI group, 1988).

$$\dot{\phi} = \frac{d\phi}{dt} = vR^{-1} \cos \theta \quad \dot{\lambda} = \frac{d\lambda}{dt} = v \sin \theta (R \cos \phi)^{-1} \quad \dot{\theta} = \frac{d\theta}{dt} = v \sin \theta \tan \phi R^{-1} \quad (5.32a, b, c)$$

Numerical model

WAM is an Eulerian phase-averaged model. It is designed as a deep water model and it can be used to predict directional spectra and wave properties (wave height, mean wave direction and frequency, swell wave height). By introducing bottom dissipation source function and refraction, WAM can be used in finite depth as well. There are also three source functions that describe explicitly the wind input, nonlinear transfer and white-capping dissipation. The model runs on a spherical latitude-longitude grid for arbitrary region ocean.

In WAM, different numerical methods have been utilized to integrate the source functions and the advective terms of the transport equation. In this model, in contrast to first and second generation wave models, the energy balance is evaluated up to the high cut-off frequency. The issue at this point is that the time scales for the high frequencies are shorter than those of the energy-containing frequency, where the spectrum changes are slower. To deal with this, in the high-frequency region a quasi-equilibrium level is defined that accounts for the time scale adjustments.

Two propagation schemes are used: a) a first-order upwind scheme and b) a second-order leapfrog scheme. The first-order scheme is characterized by a higher numerical dispersion which is proportional to $\Delta x^2/\Delta t$ and requires the time step to satisfy $\Delta t < \Delta x/u$ for numerical stability. On the other hand, the second-order scheme introduces less numerical dispersion, but suffers from unphysical energy generation in regions of sharp gradients (The WAMDI group, 1988).

Limitations

As an Eulerian model, which is formulated on a grid, and as a phase-averaged model, WAM is able to simulate wave propagation in deep and intermediate waters. The propagation of waves can also be extended to finite depth water by introducing a depth-dependent propagation speed and Eulerian representation of refraction. Nevertheless, the model does not compute all relevant physical processes for finite-depth water, such as depth induced wave breaking and triad wave-wave interactions, which can be important for coastal regions. To account for these processes, the model includes source and sink terms in the basic equations.

However, the drawbacks of this approach in coastal waters are: a) the absence of diffraction, which implies that the area of examination should be at least a few wave lengths away from obstacles and b) the use of linear wave theory for wave propagation. In order to make the model applicable in coastal waters, non-linear corrections to linear wave propagation should be sufficiently represented by triad and quadruplet wave-wave interactions or they should be dominated by generation or dissipation of the waves. Energy dissipation is often the case in shallow waters, where the waves break (N.Booij, 1999).

Applications

An important application of WAM is the wave forecast system of the German Weather Forecast Centre. WAM runs twice a day and provides 7-days forecasts on a global scale and for the Mediterranean, as well as 2-days forecast for the North and Baltic Seas. There is also a comparison of the significant wave height, one obtained at a buoy location near the Coast of Newfoundland, Canada and the other one by the global forecast wave model.

Moreover, WAM was used successfully to predict the wave conditions in Singapore waters and ambient seas. The model was implemented to provide the boundary influence for the circulation and transport models, especially in predicting and assessing the structure of physical parameters in the water column (Sannasiraj & Soon, 2004).

ECMWF (European Centre for Medium-range Weather Forecasts) has employed WAM to create the Integrated Forecast System (IFS) to determine and assemble forecast systems (ECMWF, 2005). WAM has also been coupled with a quasi-3D hydrodynamic model to resolve 3D coastal circulation known as the WAM-POM model (Lin, 2008).

5.6.2 WAVEWATCH III

WAVEWATCH III is a full-spectral third-generation wind-wave model developed at NOAA/NCEP that is based on WAM model's principles. The first version of the model (WAVEWATCH) was developed at TU Delft by Tolman in 1989. WAVEWATCH II followed by NASA's Goddard Space Flight Center in 1992. The latest version is WAVEWATCH III that includes many improvements in the governing equations, model structure, numerical schemes and physical parameterizations. The motive of version 3.14 is to evolve from a wave model to a wave modelling framework.

The model solves the random phase spectral action density balance equation for wavenumber-direction spectra. The medium properties, namely the water depth and current properties, as well as the wave field vary in time and space in scales much larger than a single wave. Version 3.14 has important improvements regarding the surf zone, where new source terms and wet-dry grid method implementations ensure better replication of the shallow water phenomena (NOAA, 2013).

WAVEWATCH is open source freely available software and it has been developed in such a way that allows the users to apply their own numerical and physical approaches. The source code is also well documented (Tolman, User manual and system documentation of WAVEWATCH III version 3.14, 2009).

Mathematical model

In order to describe waves or spectral wave components and currents in finite depth waters, phase and amplitude parameters need to be employed. Phase parameters include the wavenumber vector \mathbf{k} , the wavenumber k , the direction θ and several frequencies. When currents are considered, the frequency of the waves is affected. In this case a frame of reference must be considered either relative or absolute to the moving current. The direction of the wave θ and that of the wavenumber vector coincide and are by definition perpendicular to the crest of the wave.

For the quasi-uniform linear wave theory to be valid locally, the assumption that the scale of depth and currents variations is much greater than that of an individual wave has to be considered. This assumption yields the dispersion relation and Doppler type equation to interrelate the phase parameters:

$$\sigma^2 = gk \tan(kd) \quad (5.33)$$

$$\omega = \sigma + k \cdot U \quad (5.34)$$

where d is the mean water depth and U is the (depth- and time- averaged) current velocity.

The wave spectrum F is generally a function of all phase parameters (i.e. wave number k ; intrinsic frequency σ ; and absolute frequency ω) that vary in space (x) and time (t).

$$F = F(\mathbf{k}, \sigma, \omega; x, t) \quad (5.35)$$

The individual spectral components are usually assumed to satisfy the linear wave theory (locally). Therefore only two independent phase parameters exist and the local and instantaneous spectrum reduces to two dimensions.

The basic spectrum is the wavenumber-direction spectrum $F(k, \theta)$. The reason to select these parameters is that they represent the physical principles of wave growth and decay in variable water depths. However, the output is a frequency-direction spectrum $F(f_r, \theta)$.

The model can run with or without currents. In both cases, the wave action, which is expressed by the total spectral energy over the intrinsic frequency, has to be conserved. In the numerical model an Eulerian form is needed for the balance equation. The balance equation can be written in a transport (with velocities outside the derivatives) or conservation form (with velocities inside the derivatives). The latter form is preferred, because it conserves the total wave energy/action, unlike the first one. The balance equation for the spectrum $N(k, \theta; x, t)$ represents the basic equation of the WAVEWATCH III and it is valid for a Cartesian grid.

$$\frac{\partial N}{\partial t} + \nabla_x \dot{x} N + \frac{\partial}{\partial k} \dot{k} N + \frac{\partial}{\partial \theta} \dot{\theta} N = \frac{S}{\sigma} \quad (5.36)$$

$$\dot{x} = c_g + U \quad (5.37)$$

$$\dot{k} = -\frac{\partial \sigma}{\partial d} \frac{\partial d}{\partial s} - \mathbf{k} \cdot \frac{\partial \mathbf{U}}{\partial s} \quad (5.38)$$

$$\dot{\theta} = -\frac{1}{k} \left[\frac{\partial \sigma}{\partial d} \frac{\partial d}{\partial m} - \mathbf{k} \cdot \frac{\partial \mathbf{U}}{\partial m} \right] \quad (5.39)$$

where c_g is given by c_g and θ ; s is a coordinate in the direction θ and m is a coordinate perpendicular to S .

For large-scale applications, a spherical grid defined by longitude λ and latitude φ is preferable. Moreover, modified versions of these equations are used when a) a variable wavenumber grid is considered, b) certain numerical schemes are selected and the dispersion needs to be properly described and c) sub-grid obstacles are considered (Tolman, User manual and system documentation of WAVEWATCH III version 3.14, 2009).

Numerical model

WWIII has a wave model subroutine as a core, which can be called by either a stand-alone program shell or any other program that requires dynamically updated wave data. The current release of WWIII includes two such programs. There are also other programs provided with WWIII for pre-processing (mesh generation, initial conditions and other input parameters) and for post-processing (Tolman, User manual and system documentation of WAVEWATCH III version 3.14, 2009).

WWIII is programmed in ANSI standard FORTRAN 90. It is structured in order to be fully modular. The internal dynamic data structure exclusively includes use-associated data modules. It is important that the user changes and additions should be made in the incomplete FORTRAN files that require standard WWIII processing and not in the extracted true FORTRAN files. The new routines are expected to be in accordance with the WWIII coding practices and include an interface routine to WWIII (Tolman, WAVEWATCH III development best practices, 2010).

One of the most important implementations in Version 3.14 is the “mosaic” approach for grids. In practice, that means that an arbitrary number of grids can be designed and full two-way interactions between the grids are allowed. This effectively makes a mosaic of grids of variable spatial resolution operational in a single model. For the moment, only static grids are available and relocatable grids are under development. However, in this version, the user can predefine a path for a grid to move along. This has important applications in modelling of hurricanes.

The discretization of the wave energy spectra in all directions is achieved by using a constant directional increment and a spatially varying wavenumber grid, which corresponds to an invariant logarithmic intrinsic frequency. In order to achieve high accuracy, both first order and third order schemes are available for wave propagation. For the integration of source terms in time a semi-implicit scheme is used, similar to the one used in WAM, which includes a dynamically adjusted time stepping algorithm

WWIII can be run in parallel. The model can optionally be compiled to include shared memory parallelisms using OpenMP compiler directives or it can be compiled for a distributed memory environment using Message Passing Interface (MPI) (NOAA, 2013).

Assumptions

As mentioned in the introduction, the properties of medium, namely the water depth and the current, as well as the wave field itself, vary on time and space scales that are much larger than the scales of a single wave. In practice that means that a large-scale bathymetry needs to be considered in order for the depths and the currents to vary slowly and allow the wave diffraction to be ignored. At the same time, the definition of the wave number and angular frequency derived from the phase function of a wave implies that the number of wave crests is conserved (Tolman, User manual and system documentation of WAVEWATCH III version 3.14, 2009).

Moreover, the model assumes that the wave propagation is linear. However, proper source terms account for nonlinear effects, such as resonant interactions.

Limitations

At the current stage of development, WWIII is not able to simulate the strong three-wave interactions that occur in finite-depth and shallow waters. That has led to simplified empirical calculations with large errors, especially for complex wave trains with multi-modal spectra. However, the goal is to develop a three-wave interaction module in the near future (Sheremet & Kaihatu).

Applications

WAVEWATCH III was tested in the Pacific Ocean for the Wave Information Study (WIS). A set of three nested grids was developed to match the coarse and intermediate resolution wind fields from Oceanweather Inc (Tolman, Example of WAVEWATCH III for the NE Pacific, 2008).

The new feature of “mosaic” grids extended the application of WWIII to wind waves generated by tropical cyclones. More specifically, the model was applied to hurricane Lili in the Gulf of Mexico in October 2002 (Tolman & Alves, 2005).

WWIII has been also used as a part of a real-time integrated modelling system for weather, currents, wind-waves coupled with oil spill transport in the Black Sea region (Brovchenko, Kuschan, Maderich, Shliakhtun, Yuschenko, & Zheleznyak, 2003).

5.6.3 SWAN

SWAN (Simulating WAVes Nearshore) is a third-generation wave model developed at the Delft University of Technology for obtaining realistic estimates of wave parameters in coastal areas, lakes and estuaries from given wind, bottom and current conditions (SWAN, 2013). At the same time, SWAN can be used on any scale relevant for wind-generated

surface gravity waves. The model is based on the wave action balance equation with sources and sinks.

SWAN has been developed to simulate coastal wave conditions (with friction, breaking, whitecapping, triad and quadruplet wave-wave interaction). SWAN can be also coupled with other programs such as WAVEWATCH III or WAM, and inherit the boundary conditions, the nesting and sometimes the spectral grid for this model can be extracted from these larger-scale models. SWAN can provide a computational representation of directional and no-directional spectrum at one point and several spectral and time-dependant parameters of waves, such as significant wave height, peak or mean period, direction and direction of energy transport. All the possible wave parameters are documented in the user manual (The SWAN team, 2006).

SWAN is freely available open source software. The source code of SWAN 40.91 can be downloaded from the website. This distribution may be implemented on Microsoft Windows, Linux, Unix and Mac OS/X, provided a Fortran90 compiler is available (SWAN, 2013).

Mathematical model

SWAN is based on the spectral action balance equation, which describes the evolution of the wave spectrum (Ris, Holthuijsen, & Booij, 1999). In Cartesian coordinates the evolution of the action density is governed by the following balance equation:

$$\frac{\partial N}{\partial t} + \frac{\partial(c_x N)}{\partial x} + \frac{\partial(c_y N)}{\partial y} + \frac{\partial(c_\theta N)}{\partial \theta} + \frac{\partial(c_\sigma N)}{\partial \sigma} = \frac{S_{total}(x, y, t, \theta, \sigma)}{\sigma} \quad (5.40)$$

where σ is the intrinsic frequency; θ denotes the direction of the spectral component; t is the time; x and y are coordinates in the geographic space; N is the wave action density spectrum with $N(t, x, y, \sigma, \theta) = E(k, \theta, x, y, t)/\sigma$ where E is the wave energy density spectrum; S_{total} is the source term; $c_x, c_y, c_\sigma, c_\theta$ are the wave propagation velocities in the geographic and wavenumber space, respectively, and are given by

$$c_x = c_g \cos \theta + U_x \quad \text{and} \quad c_y = c_g \sin \theta + U_y \quad (5.41a, b)$$

$$c_\sigma = -\frac{\partial \sigma}{\partial h} \frac{\partial h}{\partial s} - K \cdot \frac{\partial U}{\partial s} \quad \text{and} \quad c_\theta = -\frac{1}{k} \frac{\partial \sigma}{\partial h} \frac{\partial h}{\partial m} - K \cdot \frac{\partial U}{\partial m} \quad (5.41c, d)$$

where k is the wavenumber; $c_g = \partial \sigma / \partial k$ is the group velocity; s , a coordinate in the θ direction; m , a coordinate perpendicular to s ; h , the mean water depth; $K = (k \cos \theta, k \sin \theta)$, the wavenumber vector.

The left hand side of the action balance equations is the kinematic terms. Terms with derivatives with respect to x and y account for the propagation in space; c_x and c_y are the propagation velocities. The term with the derivative with respect to θ is the refraction term, which changes the propagation direction. The term with respect to σ causes a change of frequency. This term is equal to zero if the depth is stationary and the current is zero. c_θ depends on the spatial derivatives of the current velocity and on the bottom slope. The right hand side is the source term. It contains the effects of wind generation, whitecapping dissipation, bottom friction, surf breaking and nonlinear wave-wave interaction.

This balance equation is implemented with finite difference schemes in all directions: time, geographic space (x, y) , and spectral space $S(\sigma, \theta)$. For the discretization of time, a simple backward finite difference method is used.

The whole set of the governing equations regarding the spectral description of wind waves, the propagation of wave energy, the source and sinks, the wave damping due to vegetation, the influence of ambient current on waves, the modelling of obstacles and the wave-induced set-up can be found at SWAN's website (SWAN, 2013).

Numerical Model

The essential input data to run the model comprise of the bathymetry for a sufficiently large area, the incident wave field and the wind field. Various grids (included nested grids) can be optionally selected. This choice mainly depends on the availability of high resolution data and the computational efficiency. Nesting is a very important implementation that can save computational time and increase accuracy. The concept of nesting is that the computations are performed first on a coarse grid for a larger region and the results are used as boundary conditions for a finer grid in the region of interest. The same types of coordinates (Cartesian or spherical) have to be used in order to apply nesting. It is important to mention that curvilinear grids can be used for nested computations, but the boundaries should always be rectangular (The SWAN team, 2006).

Since the computations are performed on a grid, SWAN is an Eulerian model that accounts for refractive propagation over arbitrary bathymetry and current fields by solving the discrete balance equation. SWAN is designed to reproduce triad and four wave-wave interactions and depth-induced wave breaking. An important numerical feature of SWAN is that in contrast to other third-generation wave models, the propagation scheme is implicit, which results in more economical computations in shallow waters. The model is validated with analytical solutions, field observations and experimental measurements and has shown good agreement (N.Booij, 1999). Another scheme, which is proven to be relatively cheap, accurate and fully monotone and can be applied for nearshore applications, is an implicit first-order upwind scheme used for the fluxes in the geographical space (Zijlema & J. van der Westhuysen, 2005).

Moreover, SWAN can operate with unstructured grids as well. A method of vertex-based, fully implicit, finite differences presented by (Zijlema M. , 2010) is designed for unstructured meshes with high variability in geographic resolution. It is useful for complex bottom topographies in shallow areas and irregular shorelines. A Gauss-Seidel iteration scheme is employed that requires a number of sweeps through the grid. This method achieves stability for any time step and allows local mesh refinement.

Furthermore, a cut-off frequency, which is formulated analogous to WAM is used. The difference in SWAN is that the mean frequency of the wind input term is used for the scaling. An important amount of time should be dedicated to the pre-processing of the simulation, in order to run the model efficiently.

The output quantities of SWAN are organized in tables, maps and time series and they comprise of one- and two-dimensional spectra, significant wave height and wave periods, average wave direction and directional spreading, one- and two-dimensional spectral source terms, root-mean-square of the orbital near-bottom motion, dissipation, wave-induced force (based on the radiation-stress gradients), set-up, diffraction parameter, etc. (SWAN, 2013).

Assumptions

One of the most important assumptions of SWAN lies in the boundary conditions. In the model, the boundaries are defined either as dry land, where no generation of waves occurs and absorption of the waves is implemented, or as water boundaries. On the latter boundaries, the wave conditions are not always known and SWAN assumes that no waves enter this area and that waves can radiate freely through the boundary. Such assumptions contain errors that propagate in the domain and it is recommended that water boundaries are chosen to be sufficiently far from the area where reliable computations are needed (The SWAN team, 2006).

Limitations

SWAN is basically designed for applications in coastal scale. Ocean scale simulations are not recommended from an efficiency point of view and other models especially designed for that should be employed, like WAVEWATCH III and WAM. However, SWAN can run on much larger scales than coastal scales, but there is need to employ nesting in spherical coordinates. Regarding the nesting, it must be pointed out that curvilinear grids can be used for nested computations but the boundaries should always be rectangular.

Diffraction is a complicated case that in SWAN is modelled in a restricted sense. That means that the model should be used in areas where variations in wave height are large within a horizontal scale of a few wave lengths. For cases with arbitrary geophysical conditions a phase-decoupled approach is adopted, so the same qualitative behaviour of spatial redistribution and changes in wave direction is achieved.

Another aspect not modelled by SWAN is wave-induced current. Such currents should be included in the input, for example from a circulation model.

Regarding the triad and four wave-wave interactions, LTA and DIA approximations are considered for each case respectively. Both the LTA and DIA approximations depend on the width of the directional distribution of the wave spectrum. SWAN is tuned according to observations made in narrow wave flume (long-crested waves). For many applications this seems to provide reasonable results. However, DIA appears to be a poor approximation for long-crested waves and it also depends on the frequency resolution (The SWAN team, 2006).

Applications

SWAN has been employed successfully for many applications worldwide.

In the work of Zhang *et al.* 2003, two common testing cases were simulated by using SWAN: the first is the refraction of a monochromatic wave propagating from deep to shallow waters and the second is the generation of wind waves by a constant wind field of fixed fetch and unlimited duration. The results of the test cases showed that the significant wave heights and periods match to theoretical solutions and empirical equations. At the last part of the study, SWAN simulated a realistic case of wave generation and propagation during a tropical storm and the storm-induced surge (Dan, Huanwen, & Pengzhi, 2003).

SWAN was used to simulate the significant wave height and the change of wave height. The model was verified with the measurements from Petchburi and Ko Srichang buoy station. SWAN was used to simulate the significant wave height at Bangkhuntien shoreline from 1981 to 2004 and the findings of this study are useful for further calculations regarding erosion, shoreline protection and coastal zone management (Ekphisitsuntorn, Wongwises, Chinnarasri, Vongvisessomjai, & Zhu, 2010).

In another study regarding sediment transport, SWAN was employed together with EBED model to simulate transport patterns and their implications for topographic changes due to waves and currents in the Ystad Bay, Skåne, Sweden. (Sadabadi , 2011)

In the literature many other examples can be found. One of them is the energy dissipation induced by the vegetation, which became a module of SWAN, named SWAN-VEG (de Oude, 2010).

6. Numerical Models: Overview and Applicability

6.1 Introduction

In chapter 5, a list of typical numerical models is presented. Although, these are some of the most commonly used numerical models for ocean engineering applications, the list is not exhaustive and there is an even greater list of models that are not included in this report. One is advised to refer to other examples of comparisons between numerical models for marine applications, such as the SuperGen Marine report, where hydrodynamic and CFD software packages are presented and compared (McCabe, 2004) or to general guidance for numerical modelling in wave and tidal energy (Topper, 2010).

In order to extend the purpose of this report and make it useful for a wider group of potential users, in this chapter the applicability of the models is presented according to the equations solved. As a result, a potential modeller will be able to choose the most appropriate model according to the physical processes it can replicate. Moreover, there is an indicative assessment of the computational cost and the skills required for each model, related to the equations that it solves.

However, this kind of inter-comparison between models is quite general and might be misleading in certain cases as usually, the modelling process is case specific. The performance of individual models should be assessed by the same means, such as grid resolution, level of detail required etc. Therefore, this comparative analysis can be used as a first guidance, mostly to eliminate some choices, rather than to take the final decision.

At the end of the chapter, the modelling requirements for a marine renewable energy project are discussed. A sketch helps the user to realise the complexity of the problem and to see the areas of the project where numerical modelling is essential. For each process mentioned, a different numerical model is suggested as the most suitable to use.

Last but not least, it is important to note that the numerical models tend to evolve in modelling platforms that can be used for many different cases with modules switched “on and off”. At the same time, the developers constantly update their models and expand their applicability and therefore the potential user should keep updated.

6.2 Numerical models and physical processes

The scope of this paragraph is to show which of the physical processes can be described by the equations used in numerical modelling. Table 6.2 shows, in a rating system format, which set of equations is more appropriate to use for each physical process. The user, according to the problem that needs to be modelled, should identify the dominating physical processes and eliminate the equations that are incapable to replicate it or those that describe it poorly.

To facilitate the connection with chapter 5 and to provide some suggestions for particular software, Table 6.1 shows which equations are solved in the models listed in Chapter 5.

Table 6.2 can be sourced in (Lin, 2008). The Quasi-3D model in Lin’s table has been replaced with Hydrostatic model for the sake of consistency with the previous naming system.

Table 6.1: Models presented in chapter 5 classified according to the equations solved

	Navier-Stokes (CFD)	Hydrostatic	Potential flow	Shallow Water Equations	Boussinesq	Spectral
OpenFOAM	✓			✓		
ANSYS CFX	✓					
DualSPHysics	✓					
SHYFEM				✓		
TELEMAC-MASCARET		✓				
FUNWAVE					✓	
Delft3D		✓		✓		✓
ANSYS AQWA			✓			
QALE-FEM			✓			
OrcaFlex			✓			
POM		✓				
COHERENS		✓				
WAM						✓
WAVEWATCH III						✓
SWAN						✓
MIKE 21		✓				✓
WAMIT			✓			

It can be seen from Table 6.2 that the suitability of the numerical model depends both on the equations solved, as well as on the different formulations and numerical methods employed. It is clear that the Navier-Stokes equations can describe any process more accurately than any other model. The trade for accuracy is the high computational cost and the level of user expertise that is required for CFD models, as seen from Table 6.3. These two factors make CFD less suitable for large-scale modelling or long runs. However, as the processing computer power increases, the computational cost will have a lower weighting factor in the decision making process. Table 6.3 is a combination of Lin's (Lin, 2008) and Folley's, et al (Folley, et al., 2012) summary tables.

Table 6.2: Suitability of wave models for simulation of different physical processes

Physical process Numerical models	Formulation/ Numerical Methods	Wave Diffraction	Wave Refraction	Wave Dispersion	Wave Non- linearity	Wave Breaking	Wave Run-up	Over- topping	Turbulence	Wave- Structure Interaction	Wave- Current Interaction
Navier-Stokes (CFD)	FVM or FEM FDM SPH	**** **** ****	**** **** ****	**** **** ****	**** **** ****	**** **** ****	**** **** ****	**** **** ****	**** **** ****	**** *** ⁽¹⁾ ****	**** **** ****
Hydrostatic	FDM or FVM	****	****		**				***		** ⁽²⁾
Potential flow	BEM FEM FDM	**** **** ****	**** **** ****	**** **** ****	*** *** ***	* ^(3a) (^{3c}) (^{3d})	*** *** ***	* *		*** ^(3b) *** **	
Shallow Water Equations	FDM or FEM	****	****		***	**	***	*+	*+	*+	*+ ⁽⁴⁾
Boussinesq	Standard High-order	**** ****	**** ****	** ***	**+ ***	**+ ***	*** ***	*+ *+	*+ *+	*+ *+	** ** ⁽⁵⁾
Mild Slope Equations	Elliptic ^(6a) Hyperbolic ^(6b) Parabolic ^(6c)	**** **** ***	**** **** **	**** **** ***+	* * *	* * *			+ + +	*+ *+ +	** ** *
Spectral	Wave Energy Wave Action	+ +	**** ****	**** ****	** **	** **+			** **		***

Comments: ⁽¹⁾ Cut-cell, Virtual Boundary Force, or their kinds used; ⁽²⁾Mainly for current simulation only and solved in the σ -coordinate; ^(3a) For initiation of wave breaking only; ^(3b) For large structures only; ^(3c) Adaptive mesh or σ -coordinate; ^(3d) σ -coordinate; ⁽⁴⁾ Current module only in a coupled model; ⁽⁵⁾For coupled wave-current simulation; ^(6a)For steady wave field only; ^(6b)For transient wave field; ^(6c)Waves with primary propagation direction.

Notes: 1) The number of stars represents the level of suitability of a particular model for the corresponding wave phenomenon; + represents half star .
**** highly suitable; *** moderate suitability; ** poorly suitable; * not suitable; no star indicates incapability of the model to replicate the physical process.

Table 6.3: Efficiency of the numerical models

	Required Skill	Computational Cost	Solver	
			Complexity	Stability
Navier-Stokes (CFD)	High	****	Complex	Possibly unstable
Hydrostatic	Medium	**	Simple	Stable
Potential Flow	Low – High ¹	**	Simple ³	Stable ⁴
Shallow Water Equations	Medium	*	Simple	Stable
Boussinesq	Medium	**	Simple	Possible unstable
Mild Slope Equations	Low	**	Simple	Stable
Spectral	Low – High ²	*	Simple	Stable

¹There are four types of potential flow models which require different level of skills: a) linear BEM, b) semi-analytical techniques, c) time-domain formulation and d) non-Linear BEM, requiring low, high, medium and high skills respectively.

²Low corresponds to “supra-grid” models and High corresponds to “sub-grid” spectral models

³Potential flow models with nonlinear BEM are characterized as complex.

⁴Time-domain potential flow models can be unstable.

Note: The rating of cost does not correspond to units of cost associated with the simulation time, grid resolution etc. It is a qualitative comparison only.

6.3 Numerical modelling for a MRE project

The sector of Marine Renewable Energy is still in its infancy and more experience, especially from practical applications, needs to be built in order to help the emergence of detailed protocols and guidelines. However, there is important work that has been already done, even at this early stage.

The design of marine renewable energy projects is even more demanding and challenging than classic offshore engineering. The complexity of the problem covers many fields including device description, environmental guidance, loading and fatigue guidance, design of foundations and mooring, grid connection, deployment, maintenance and monitoring, etc. Guidelines regarding the design basis for MRE have been published by HMRC (HMRC, 2003). A more specific discussion about the MRE development, mainly focusing on the Wave Hub site for demonstration and testing of marine renewable energy devices, confirms the integrated character of a MRE project (Greaves, et al., 2009).

Figure 6.1 demonstrates the different designing processes involved in a MRE that require the use of numerical modelling techniques. MRE projects are subject to economic analysis

and interfere with other sectors as well, but this discussion falls out of the purpose of this document.

It should be noted that this figure is quite simplified and in a MRE project almost all the processes are bonded together. For example, the design of the moorings is crucial for the survivability of the device in extreme conditions, but it also affects the performance of a moored floating body and its interaction with the surrounding devices. At the same time, different mooring systems result in different levels of environmental impact on the seabed. Similar examples can show that none of these technical aspects should be examined separately and that the modelling process is integrated, requiring many different models and techniques.

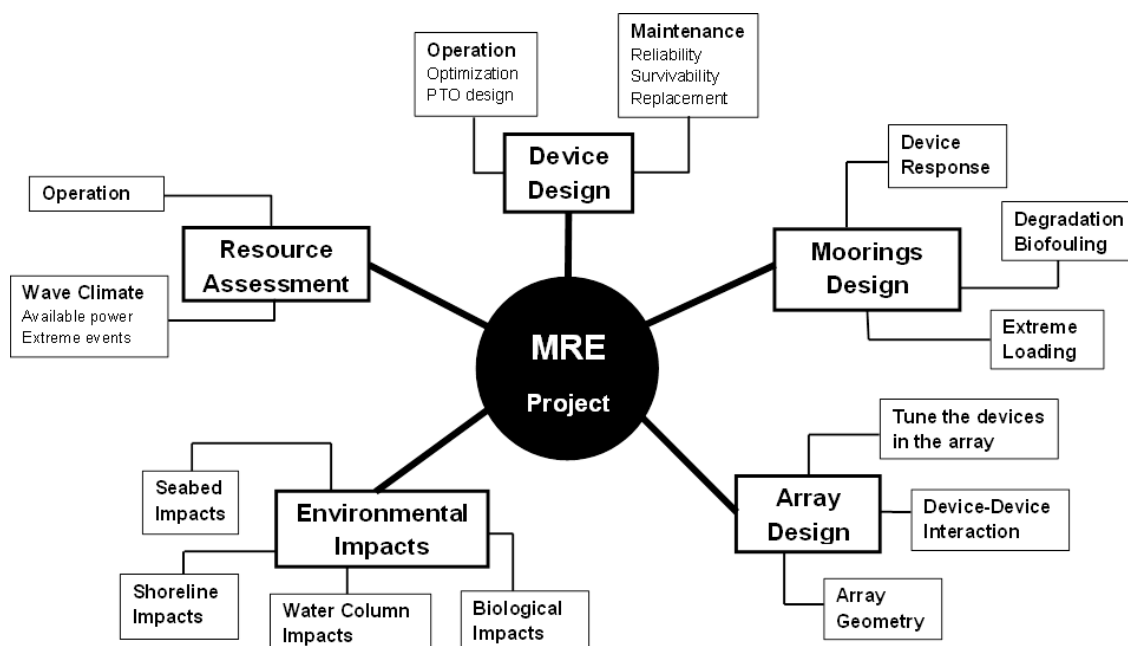


Figure 6.1: Technical aspects for a MRE project examined with numerical modelling.

Probably, the most significant proportion of studies until now focuses on the resource assessment for an MRE. Regional models are employed for the prediction of the available wave or tidal energy. General guidelines regarding the assessment of the wave energy resource, which describe the different techniques that can be used, have already emerged (EMEC, 2009). More detailed protocols for wave and tidal resource assessment include guidelines for the numerical modelling processes, the assessment of the extreme conditions and the identification of the constraints on the development of the MRE project (Davey, et al., 2010). There are also examples of inter-comparison of numerical models, such as SWAN, TOMAWAC and MIKE 21 for resource assessment (Venugopal, et al., EquiMar D2.4: Wave Model Intercomparison, 2011).

Table 6.4, although very general, gives a good indication of the importance of the different physical processes according to the sea area considered (Venugopal, et al., EquiMar D2.3: Application of Numerical Models, 2010). It can be useful for identifying the governing

physical phenomena in the area of deployment of a MRE farm and for choosing the regional wave model for resource assessment.

Table 6.4: Physical processes according to the depth of the sea

Physical Process	Deep Oceans	Shelf Seas	Shoaling Zone	Harbours
Diffraction	*	*	**	****
Depth refraction/shoaling	*	***	****	***
Current refraction	*	**	***	*
Quad Wave Interactions	****	****	**	*
Triad Wave Interactions	*	**	***	**
Atmospheric Input	****	****	**	*
White-capping	****	****	**	*
Depth Breaking	*	**	****	*
Bottom Friction	*	****	**	*

Table 6.5 shows the suitability of different models according to the process of a MRE project examined. This table is linked to Figure 6.1 and Table 6.2. The elements of the device-device interaction, operation and annual energy production is taken from (Folley, et al., 2012), where they are referred as localised effects, dynamic control and AEP respectively.

6.4 Conclusion

To sum up, a potential modeller can use the tables included in this chapter in order to identify the relevant physical processes included in the engineering project; then, according to physical processes (Table 6.2) and the available resources (Table 6.3), to select the set of equations that need to be solved in the model. Finally, the user can choose the software package from the models listed in Table 6.1 or from other available open-source or commercial models.

In any case, the authors recommend the users to always read the software manual and to contact the developers of the software for further clarifications. Review of the literature is useful to identify the areas of prior applications of the models. Last but not least, there are online user groups and for most numerical models, where the applicability and limitations of the models can be found within the discussions of experienced users.

Table 6.5: Suitability of numerical models for different aspects of MRE projects

	Device Design				Array Design				
	Operation	Maintenance	Mooring		Resource	Device-Device Interaction	Array Geometry Optimization	Annual Energy Production	Environmental Impacts
			Response	Extreme					
Navier-Stokes (CFD)	***	****	****	****	*	****	*	**	**
Hydrostatic	*	**	**	**	***	***	***	**	****
Potential Flow	* to **** ¹	***	****	**	*	***	****	**	*
Shallow Water Equations	*	*	*	*	***	**	**	***	****
Boussinesq	*	*	**	*	***	**	**	***	***
Mild Slope Equations	*	*	*	*	***	**	**	***	***
Spectral	*	*	*	*	****	*	***	***	****

¹Rating according to the different discretization methods, i.e.: a) linear BEM, b) semi-analytical techniques, c) time-domain formulation and d) non-Linear BEM.

7. Bibliography

- Abundo, M., Nerves, A., Paringit, E., & Villanoy, C. (2012). A Combined Multi-Site and Multi-Device Decision Support System for Tidal In-Stream Energy. *Energy Procedia*, 14, 812-817.
- Adcock, T. A., Taylor, P. H., Yan, S., Ma, Q. W., & Janssen, P. A. (2011). Did the Draupner wave occur in a crossing sea? *Proceedings of the Royal Society A*.
- Anderson, J. D. (1995). *Computational Fluid Dynamics, The basics with applications*. Singapore: McGraw-Hill International Editions.
- ANSYS. (2009). *ANSYS CFX -Solver Theory Guide*. Canonsburg: ANSYS Inc.
- ANSYS. (2013, December). *www.ansys.com*.
- ANSYS Inc. (2010). *ANSYS Release 13.0*. Retrieved from *www.ansys.com*.
- Bergsma, E. (2012). *Process-based modelling of the Maumusson inlet: Interaction between inlet, ebb-delta and adjacent shoreline*. Delft University of Technology.
- Berkhoff, J. C. (1972). Computation of combined refraction-diffraction. *13th International Conference on Coastal Engineering*, (pp. 471-490). ASCE.
- Bosma, B. (2013). *On the Design, Modeling, and Testing of Ocean Wave Energy Converters*. Oregon State University.
- Brocchini, M. (2013). A reasoned overview on Boussinesq-type models: the interplay between physics, mathematics and numerics. *Proceedings of the Royal Society A*, 469.
- Brovchenko, I., Kuschan, A., Maderich, V., Shliakhtun, M., Yuschenko, S., & Zheleznyak, M. (2003). The modelling system for simulation of the oil spills in the Black Sea. *Elsevier Oceanography Series*, 69, 586-591.
- Campbell, J. C., Vignjevic, R., & Patel, M. (2008). A Coupled FE-SPH approach for Simulation of Structural Response to Extreme Wave and Green Water Loading. *Offshore Technology Conference*. Houston, Texas, USA.
- Carballo, R., Iglesias, G., & Castro, A. (2008). Numerical model evaluation of tidal stream energy resources in the Ria de Muros (NW Spain). *Renewable Energy*, 34(6), 1517-1524.
- CEM. (2002). *Coastal Engineering Manual*. US Army Corps of Engineers.
- CFD Online. (2013). *CFD Online Wiki*. Retrieved November 2013, from http://www.cfd-online.com/Wiki/Main_Page
- Chen, Q., Kirby, J., Dalrymple, R., Kennedy, A., Thornton, E., & Shi, F. (2000). Boussinesq modeling of waves and longshore currents under field conditions. *27th International Conference of Coastal Engineering*, (pp. 651-663). Sydney.
- Cheng, A. H.-D., & Cheng, D. T. (2005). Heritage and early history of the boundary element method. *Engineering Analysis with Boundary Elements*, 29, 268-302.

- Clauss, S. T. (2009). Motion behaviour of a new offshore LNG transfer system at harsh operational conditions. *28th International Confernece on Ocean, Offshore and Arctic Engineering* (pp. 1-9). Honolulu: ASME.
- Crespo, A., Domínguez, J., Gesteira, M., Barreiro, A., Rogers, B., Longshaw, S., et al. (2013). *User Guide for DualSPHysics code: DualSPHysics_v3.0*.
- Dalrymple, R., & Rogers, B. (2006). Numerical modeling of water waves with the SPH method. *Coastal Engineering*, 53(2-3), 141-147.
- Dan, Z., Huanwen, L., & Pengzhi, L. (2003). The application of SWAN to the simulation of a storm surge. *International Conference on Estuaries and Coasts*, (pp. 756-762). Hangzhou, China.
- Davey, T., Venugopal, V., Smith, H., Smith, G., Lawrence, J., Cavaleri, L., et al. (2010). *EquiMar D2.7: Protocols for wave and tidal resource assessment*.
- de Oude, R. (2010). *Modelling wave attenuation by vegetation with SWAN-VEG, Model evaluation and application to the Noordwaard polder*. Univeristy of Twente, Deltares.
- Dean, R. G., & Dalrymple, R. A. (1991). *Water wave mechanics for engineers and scientists* (Vols. Advanced series on ocean engineering - Volume 2). Singapore: World Scientific Publishing.
- Deltares. (2011). *User Manual, Delft3D- FLOW version 3.15*. Deltares.
- Deltares. (2013). *Delft3D Open Source Community*. Retrieved December 10, 2013, from <http://oss.deltares.nl/web/delft3d/home>
- DHI. (2011). *Modelling the world of water*. Retrieved September 18, 2012, from MIKE by DHI: <http://www.dhisoftware.com/>
- DHI Software. (2007). *MIKE 21 Flow Model, Hydrodynamic Module User Guide*.
- DHI webpage. (2011). *MIKE by DHI*. Retrieved December 15, 2013, from <http://www.mikebydhi.com/Products/CoastAndSea/MIKE21.aspx>
- Dingemans, M. (1997). Waterwave propagation over uneven bottoms. *Advanced Series on Ocean Engineering*, 13(2), 967.
- Douglas, J. F., Gasiorek, J. M., Swaffield, J. A., & Jack, L. B. (2005). *Fluid Mechanics Fifth edition*. Essex: Pearson Education Limited.
- DualSPHysics. (2013). *DualSPHysics Homepage*. Retrieved December 2013, from <http://www.dual.sphysics.org/>
- DualSPHysics. (2013). *DualSPHysics References*. Retrieved December 2013, from <http://www.dual.sphysics.org/index.php/references/>
- ECMWF. (2005, November 15). *ECMWF*. Retrieved September 19, 2012, from European Centre for Medium-Range Weather Forecasts: <http://www.ecmwf.int/>

- Ekphisitsuntorn, P., Wongwises, P., Chinnarasri, C., Vongvisessomjai, S., & Zhu, J. (2010). The Application of Simulating WAVes Nearshore Model for Wave Height Simulation at Bangkhuntien Shoreline. *American Journal of Environmental Sciences*, 6(3), 299-307.
- EMEC. (2009). *Assesment of Wave Eeneegy Resource: Marine Renewable Energy Guides*. London: BSI.
- ERCOFTAC. (2013). *SPHERIC Home Page*. Retrieved December 15, 2013, from https://wiki.manchester.ac.uk/spheric/index.php/Main_Page
- Fengyan, S., Kirby, J. T., Tehranirad, B., Harris, J. C., & Grilli, S. (2012). *FUNWAVE-TVD: Fully Nonlinear Boussinesq Wave Model with TVD Solver. Documentation and User's Manual (Version 2.0)*. University of Delaware. Center for Applied Coastal Research,.
- Fenton, J. D. (1985). A fifth-order Stokes theory for steady waves. *Journal of Waterway Port Coastal and Ocean Engineering*, 111, 216-234.
- Ferziger, J. H., & Peric, M. (2002). *Computational Methods for Fluid Dynamics*. Berlin: Springer.
- Finnegan, W. (2013). *PhD Thesis: Wave-structure interaction of offshore wave energy converters*. National University of Ireland.
- Finnegan, W., & Goggins, J. (2012). The Structural Dynamics of a Two-Body Wave Energy Converters. *4th International Conference on Ocean Energy*. Dublin.
- Fletcher, C. A. (2006). *Computaional Techniques for Fluid Dynamics 1, Fundamental and General Techniques* (Second ed.). Springer-Verlag.
- Folley, M., Babarit, A., Child, B., Forehand, D., O'Boyle, L., Silverthorne, K., et al. (2012). A Review of Numerical Modeling of Wave Energy Converter Arrays. *International Conference on Ocean, Offshore and Arctic Engineering*. ASME.
- Garrison , C. J., & Berklite, R. B. (1973). Impulsive Hydrodynamics of Submerged Rigid Bodies. *Journal of the Engineering Mechanics Division*, 99(1), 99-120.
- Garrison, C. J., & Chow, P. Y. (1972). Wave Forces on Submerged Bodies. *Journal of the Waterways, Harbors and Coastal Engineering Division*, 98(3), 375-392.
- Garrison, C. J., & Rao, V. S. (1971). Interaction of Waves with Submerged Bodies. *Journal of the Waterways, Harbors and Coastal Engineering Division*, 97(2), 259-277.
- Gesteira, M., Rogers, B., Dalrymple, R., Crespo, A., & Narayanaswamy, M. (2010). *User Guide for the SPHysics code*.
- Gotoh, H., Shao, S., & Memita, T. (2004). SPH-LES model for numerical investigation of wave interaction with partially immersed breakwater. *Coastal Engineering Journal*, 46(1), 39-63.
- Goundar, J., & Ahmed, M. (2013). Design of a horizontal axis tidal current turbine. *Applied Energy*, 111, Pages 161-174.

- Greaves, D. (2009). *Application of the Finite Volume Method to the Simulation of Nonlinear Water Waves*. The world Scientific Publishing Co.
- Greaves, D., Attrill, M., Chadwick, A., Conley, D., Eccleston, A., Hosegood, P., et al. (2009). Marine renewable energy development – research, design, install. *Proceedings of the ICE - Maritime Engineering*, 162(4), 187-196.
- Heller, V., & Spinneken, J. (2013). Improved landslide-tsunami prediction: Effects of block model parameters and slide model. *Journal of Geophysical Research*, 118, 1489-1507.
- Higuera, P., Lara, L. J., & Losada, J. I. (2012). Realistic wave generation and active wave absorption for Navier-Stokes Models Application to OpenFOAM.
- HMRC. (2003). *Development & Evaluation Protocol, Part 1: Wave Power*.
- Holthuijsen, L. (2007). *Waves in Oceanic and Coastal Waters*. Cambridge University Press.
- Hommel, L., Shi, F., Kirby, J., Dalrymple, R., & Chen, Q. (2000). Modelling of a wave-induced vortex near a breakwater. *27th International Conference of Coastal Engineering*, (pp. 2318-2330). Sydney.
- Isobe, M. (1994). Time-dependent mild-slope equations for random waves. *Coastal engineering conference*, (pp. 1-15).
- Iwasaki, S., Isobe, A., & Kako, S. (2014). Atmosphere–Ocean Coupled Process along Coastal Areas of the Yellow and East China Seas in Winter. *Journal of Climate*, 27, 155-167.
- Jacobsen, N. G., Fuhrman, D. R., & Fredsøe, J. (2012). A wave generation toolbox for the open-source CFD library: OpenFoam®. *International Journal for Numerical Methods in Fluids*(70), 1073-1088.
- Johanning, L., Smith, G. H., & Wolfram, J. (2007). Measurements of static and dynamic mooring line damping and their importance for floating WEC devices. *Ocean Engineering*, 34, 1918-1934.
- Kirby, J. T, W. G. (1998). *FUNWAVE 1.0: Fully Nonlinear Boussinesq Wave Model Documentation and user's Manual*. Newark: Centre for Applied Coastal Research.
- Koutitas, C. G. (1988). *Mathematical models in coastal engineering*.
- Krivtsov, V., & Linfoot, B. (2012). Disruption to benthic habitats by moorings of wave energy installations: A modelling case study and implications for overall ecosystem functioning. *Ecological Modelling*, 245, 121-124.
- Lawrence, J., Kofoed-Hansen, H., & Chevalier, C. (2009). High-resolution metocean modelling at EMEC's (UK) marine energy test sites. *8th European Wave and Tidal Energy Conference*. Uppsala, Sweden .
- Lesser, G. R. (2009). *An Approach to Medium-term Coastal Morphological Modelling*, PhD Dissertation. Delft.

- Lesser, G. R., Roelvink, J. A., van Kester, J. A., & Stelling, G. H. (2004). Development and validation of a three-dimensional morphological model. *Coastal Engineering*, 51(8-9), 883-915.
- Lin, P. (2008). *Numerical modeling of water waves* (1st ed.). New York: Taylor and Francis.
- López, A., Somolinos, J. A., Núñez, L. R., & Santamaría, M. (2011). Modelling and simulation of moored devices for ocean currents energy harnessing. *Journal of Maritime Research*, VIII(1), 19-34.
- Luyten, P. (2000). *COHERENS Home Page*. Retrieved August 29, 2012, from www.mumm.ac.be/~patrick/mast/coherens.html
- Luyten, P. J., Jones, J. E., Proctor, R., Tabor, A., Tett, P., & Wild-Allen, K. (1999). *COHERENS – A Coupled Hydrodynamical-Ecological Model for Regional and Shelf Seas: User Documentation*. Management Unit of the Mathematical Models of the North Sea.
- Ma, Q. W., & Yan, S. (2006). Quasi ALE finite element method for nonlinear water waves. *Journal of Computational Physics*(212), 52–72.
- Magar, V., Joshi, C. R., Williams, B. G., & Conley, D. (2013). Wave Energy Resource Characterisation for Guernsey Island (UK). *European Wave and Tidal Energy Conference* . Aalborg, Denmark.
- Manenti, S., & Ruol, P. (2008). Fluid-Structure Interaction in Design of Offshore Wind Turbines: SPH Modeling of Basic Aspects. *Handling Exceptions in Structural Engineering: Robustezza Strutturale, Scenari Accidentali, Complessità di Progetto*. Rome, Italy.
- Marshall, J., Hill, C., Perelman, L., & Adcroft, A. (1997). Hydrostatic, quasi-hydrostatic, and nonhydrostatic ocean modeling. *Journal of Geophysical Research*, 102, 5733-5752.
- McCabe, A. P. (2004). *Work package 2, T2.3.4: An Appraisal of a Range of Fluid Modelling Software*. SuperGen Marine.
- McComb, C., Lawson, M., & Yu, Y.-H. (2013). Combining multi-body dynamics and potential flow simulation methods to model a wave energy converter. *1st Marine Energy Technology Symposium* . Washington DC.
- Mellor, G. L. (2004). *Users guide for a three-dimensional, primitive equation, numerical ocean model*. Princeton University.
- MIKE 21. (2011). *MIKE 21 Wave Modelling Spectral Waves*. Horsholm: DHI.
- Monaghan, J. J. (1992). Smoothed Particle Hydrodynamics. *Annu. Rev. Astron. Astrophys.*, 30, 543-74.
- Monaghan, J. J. (2005). Smoothed particle hydrodynamics. *Reports on progress in Physics*, 68, 1703–1759.
- N.Booij, R. R. (1999). A third-generation wave model for coastal regions: 1.Model description and validation. *Journal of Geophysical Research*, 104(4), 7667-7681.

- NOAA. (2013, December). *Centre, National Weather Service - Environmental Modeling*. Retrieved from <http://polar.ncep.noaa.gov/>:
<http://polar.ncep.noaa.gov/waves/wavewatch/wavewatch.shtml>
- O'Rourke, F., Boyle, F., & Reynolds, A. (2010). Tidal current energy resource assessment in Ireland: Current status and future update. *Renewable and Sustainable Energy Reviews*, 14(9), 3206-3212.
- Oey, L. (2008). *The Princeton Ocean Model*. Retrieved August 17, 2012, from <http://www.aos.princeton.edu/WWWPUBLIC/htdocs.pom/index.html>
- OpenFOAM. (2012). *OpenFOAM, The Open Source CFD Toolbox, User Guide Version 2.1.1*.
- OpenFOAM Foundation. (2011-2013). *OpenFOAM: The OpenFOAM Foundation*. Retrieved December 2013, from <http://www.openfoam.org/>
- Orcina Limited. (2013). *OrcaFlex version 9.7: Technical Specification*. Ulverston, UK.
- Orcina Ltd. (2013). *Orcina Orcaflex website*. Retrieved December 2013, from <http://www.orcina.com/SoftwareProducts/OrcaFlex/index.php>
- Orcina Ltd. (2013). *OrcaFlex Manual: Version 9.7a*. Ulverston, UK.
- Payne, G. (2008). *Guidance for the experimental tank testing of wave energy converters*. The University of Edinburgh. SUPERGEN MARINE.
- Peregrine, D. H. (1976). Interaction of water waves and currents. In *Advances in Applied Mechanics* (Vol. 16, pp. 9-117). Academic Press.
- POM. (2013). *The Princeton Ocean Model*. Retrieved December 2013, from <http://www.ccpo.odu.edu/POMWEB/index.html>
- Ransley, E., Hann, M., Greaves, D., Raby, A., & Simmonds, D. (2013). Numerical and Physical Modelling of Extreme Wave Impacts on a Stationary Truncated Circular Cylinder. *10th European Wave and Tidal Conference (EWTEC)*. Aalborg.
- Ricci, S., Piacentini, A., Weaver, A., Ata, R., & Goutal, N. (2013). A Variational Data Assimilation Algorithm to Estimate Salinity in the Berre Lagoon with TELEMAC-3D. *XXth TELEMAC-MASCARET User Conference*, (pp. 19-24).
- Ris, R. C., Holthuijsen, L. H., & Booij, N. (1999). A third-generation wave model for coastal regions: 2. Verification. *Journal of Geophysical Research*, 104, 7667-7681.
- Roelvink, D., & Reniers, A. (2012). *A guide to modelling coastal morphology*. Singapore: World Scientific Publishing.
- Ruiz-Minguela, J. P., Rodriguez, R., Ricci, P., Maron, A., Prieto, M. E., & Taboada, M. (2008). Design and testing of the mooring system for a new offshore wave energy converter. *2nd International Conference on Ocean Energy*. Brest, France.
- S. Yan, Q. W. (2010). QALE-FEM for modelling 3D overturning waves. *International journal for numerical methods in fluid*(63), 743–768.

- Sadabadi, S. A. (2011). *Modeling Wave, Currents, and Sediment Transport in Ystad Bay*. Lund, Sweden: Division of Water Resources Engineering, Lund University.
- Sannasiraj, A. S., & Soon, E. C. (2004). *Application of Ocean Wave Prediction Model to China Sea*. Beijing: The Sixth OMISAR Workshop on Ocean Models.
- Sheremet, A., & Kaihatu, J. M. (n.d.). *Development of numerical 3-wave interactions module for operational wave forecasts in intermediate-depth and shallow water*.
- SHYFEM. (2013). *S.HY.F.E.M.* Retrieved December 2013, from <https://sites.google.com/site/shyfem/home>
- Smith, G. (2009). *Harnessing the Power of Ocean Waves*. Aberdeen, Scotland: Green Ocean Energy Ltd.
- Sutherland, J., & Barfuss, S. L. (2011). Composite Modelling: Combining Physical and Numerical Models. *34th IAHR World Congress*. Brisbane, Australia: HR Wallingford.
- SWAN. (2013). *SWAN home page*. Retrieved from <http://swanmodel.sourceforge.net/>
- TELEMAC-3D Software. (March 2013). *TELEMAC Modelling System, Operating Manual, Release 6.2*.
- TELEMAC-MASCARET. (2013). *open Telemac-Mascaret - Home*. Retrieved September 3, 2013, from www.opentelemac.org
- The SHYFEM Group. (2009). *SHYFEM Finite Element Model for Coastal Seas - User Manual*. Venezia: The SHYFEM Group.
- The SWAN team. (2006). *SWAN User Manual, SWAN Cycle III version 40.51*. Delft University of Technology.
- The WAMDI group. (1988). The WAM Model - A Third Generation Ocean Wave Prediction Model. *Journal of physical oceanography*, 18, 1775-1810.
- Thies, P. R., Johanning, L., & Smith, G. H. (2011). Assessing mechanical loading regimes and fatigue life of marine power cables in marine energy applications. *Proceedings of the Institution of Mechanical Engineers, Part O: Journal of Risk and Reliability*, 226.
- Tolman. (2008, March 13). Example of WAVEWATCH III for the NE Pacific. Camp Springs.
- Tolman. (2009, May). User manual and system documentation of WAVEWATCH III version 3.14. Camp Springs.
- Tolman. (2010, May). WAVEWATCH III development best practices. Camp Springs.
- Tolman, H. L., & Alves, J.-H. G. (2005). Numerical modeling of wind waves generated by tropical cyclones using moving grids. *Ocean Modelling*, 9(4), 305-323.
- Topper, M. B. (2010). *Guidance for Numerical Modelling in Wave and Tidal Energy*. SuperGen.
- Venugopal, V., & Smith, G. H. (2007). Wave climate investigation for an array of wave power devices. *7th European Wave and Tidal Energy Conference*. Porto, Portugal.

- Venugopal, V., Davey, T., Girard, F., Smith, H., Cavaleri, L., Bertotti, L., et al. (2011). *EquiMar D2.4: Wave Model Intercomparison*.
- Venugopal, V., Davey, T., Girard, F., Smith, H., Smith, G., Cavaleri, L., et al. (2010). *EquiMar D2.3: Application of Numerical Models*.
- Versteeg, H. K., & Malalasekera, W. (2007). *An Introduction to Computational Fluid Dynamics, The Finite Volume Method* (Second edition ed.). Essex, England: Pearson Education Limited.
- Vyzikas, T., Ransley, E., Hann, M., Magagna, D., Greaves, D., Simmonds, D., et al. (2013). Integrated Numerical Modelling System for Extreme Wave Events at the Wave Hub Site. *ICE: Coasts, Marine Structures and Breakwaters 2013*. Edinburgh.
- WAMIT. (2008). *Examples of structures*. Retrieved September 18th, 2012, from WAMIT inc: <http://www.wamit.com/index.htm>
- WAMIT INC. (2012, April 18). User manual version 7.0. Massachusetts.
- Watts, P., Grilli, S., & Kirby, J. (2002). Coupling 3D tsunami generation with Boussinesq tsunami propagation. *27th European Geophysical Society General Assembly*. Nice.
- Wendt, J. (2009). *Computational Fluid Dynamics, An introduction* (3rd ed.). Springer.
- WS Atkins Consultants , & NSC. (2002). *Best practice Guidelines for Marine Applications of Computational Fluid Dynamics*. MARNET CFD.
- Zheng, J.-h., Soe, M. M., Zhang, C., & Hsu, T.-W. (December 2010). Numerical wave flume with improved smoothed particle hydrodynamics. *Journal of Hydrodynamics*, 22(6), 773-781.
- Zijlema, M. (2010). Computation of wind-wave spectra in coastal waters with SWAN on unstructured grids. *Coastal Engineering*, 57(3), 267-277.
- Zijlema, M., & J. van der Westhuysen, A. (2005). On convergence behaviour and numerical accuracy in stationary SWAN simulations of nearshore wind wave spectra. *Coastal Engineering*, 52(3), 237-256.



www.merific.eu



European Regional Development Fund
The European Union, investing in your future



Fonds européen de développement régional.
L'union Européenne investit dans votre avenir

MERiFIC was selected under the European Cross-Border Cooperation Programme INTERREG IV A France (Channel) – England, co-funded by the ERDF.

MERiFIC a été sélectionnée dans le cadre du programme européen de coopération transfrontalière INTERREG IV A France (Manche) Angleterre, cofinancé par le FEDER.